Description and Validation of a MATLAB - Simulink Single Family House Energy Model with Furniture and Phase Change Materials (Update)

Johra, Hicham; Heiselberg, Per Kvols

Publication date:
2018

Document Version
Publisher's PDF, also known as Version of record

DEPARTMENT OF CIVIL ENGINEERING
AALBORG UNIVERSITY

Description and Validation of a MATLAB - Simulink Single Family House Energy Model with Furniture and Phase Change Materials (Update)

Hicham Johra
Per Heiselberg

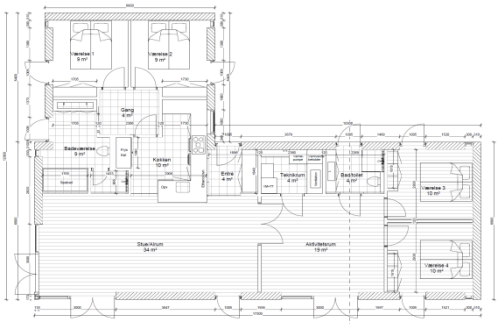

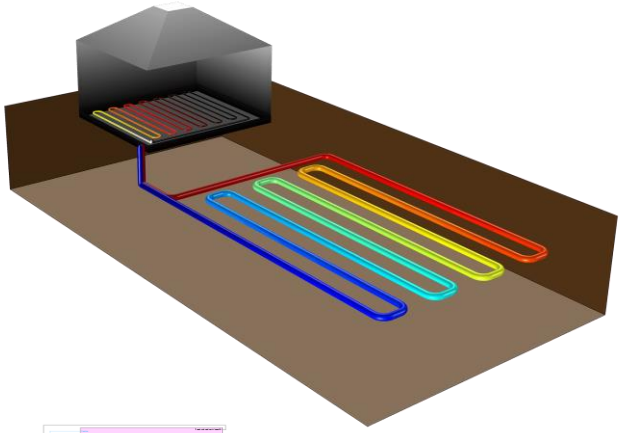

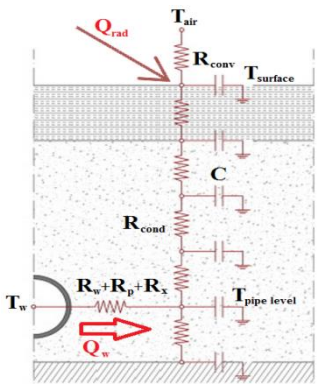

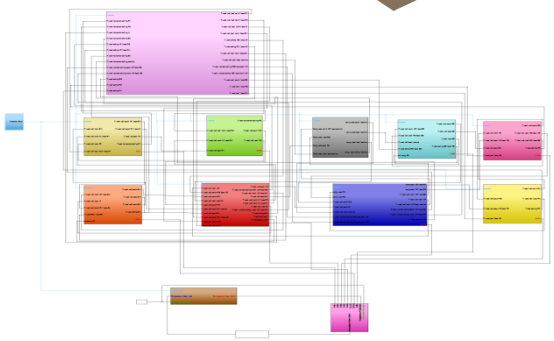

ISSN 1901-726X
DCE Technical Report No 238

Aalborg University
Department of Civil Engineering
Architectural Engineering

DCE Technical Report No. 238

Description and Validation of a MATLAB - Simulink Single Family House Energy Model (Update)

by

Hicham Johra
Per Heiselberg

February 2018

Scientific Publications at the Department of Civil Engineering

Technical Reports are published for timely dissemination of research results and scientific work carried out at the Department of Civil Engineering (DCE) at Aalborg University. This medium allows publication of more detailed explanations and results than typically allowed in scientific journals.

Technical Memoranda are produced to enable the preliminary dissemination of scientific work by the personnel of the DCE where such release is deemed to be appropriate. Documents of this kind may be incomplete or temporary versions of papers—or part of continuing work. This should be kept in mind when references are given to publications of this kind.

Contract Reports are produced to report scientific work carried out under contract. Publications of this kind contain confidential matter and are reserved for the sponsors and the DCE. Therefore, Contract Reports are generally not available for public circulation.

Lecture Notes contain material produced by the lecturers at the DCE for educational purposes. This may be scientific notes, lecture books, example problems or manuals for laboratory work, or computer programs developed at the DCE.

Theses are monograms or collections of papers published to report the scientific work carried out at the DCE to obtain a degree as either PhD or Doctor of Technology. The thesis is publicly available after the defence of the degree.

Latest News is published to enable rapid communication of information about scientific work carried out at the DCE. This includes the status of research projects, developments in the laboratories, information about collaborative work and recent research results.

Published 2018 by
Aalborg University
Department of Civil Engineering
Thomas Manns Vej 23
DK-9220 Aalborg Øst, Denmark

Printed in Aalborg at Aalborg University

ISSN 1901-726X
DCE Technical Report No. 238

Contents

Introduction

In recent years, significant efforts have been made to decrease the energy consumption of our societies. In heating dominated climates such as in Denmark, in Germany or in the U.K, individual heat pumps have been found to be the most efficient heat supply for buildings detached from district heating network [1][2][3]. This flexible technology can also improve the integration of intermittent renewable energy sources (RES). Heat pumps thus became a key component for the energy development policy of many countries, leading to a substantial increase of the market demand [4]. It is therefore important to bring new and cost effective technical solutions.

The “EnovHeat” project aims to develop an innovative magnetocaloric heat pump based on the active magnetic regenerator technology with a higher coefficient of performance (COP) than conventional vapour-compression heat pumps. It should be able to provide for the indoor space heating needs of a recently built single family house in Denmark [5].

The main task of the work package conducted at Aalborg University is to investigate how to integrate a magnetocaloric heat pump into a residential building, and assess its performance and impact on the overall system [6]. The objective is to demonstrate the feasibility and the advantages of using such magnetocaloric device compared to conventional solutions and develop an efficient control strategy for it.

A typical Danish single family house is used as case study. The magnetocaloric heat pump model has been developed within the MATLAB software environment. It must be tested in a versatile environment with the possibility for implementation of complex controller and small simulation time step resolution. A MATLAB - Simulink multi-zone model is therefore created for the dwelling with water-based under floor heating (UFH) system and two different types of ground source heat exchangers (GSHE): horizontal and vertical.

Passive heat accumulation or thermal energy storage (TES) in the indoor space is an efficient way to modulate house heating power usage [7]. Flexible demand side management was found to improve the operation of a smart energy grid systems with a large share of intermittent RES [8]. This building energy flexibility potential can also be employed to optimize the operation of the magnetocaloric heat pump. For that reason, the building model is also used to assess the impact of additional indoor content thermal mass on the house energy flexibility capacity [9]. A simplified model of furniture / indoor content is implemented together with a phase change material (PCM) model based on finite volume method and enthalpy formulation.

This report aims to present in details the numerical building model and each of its elements. In the second part, the results of different validation tests are presented to certify the reliability of the model and thus the results of numerical analyses using it.

1. Presentation of the Case Study Buildings

1.1. EnovHeat Case Study Building

The EnovHeat project aims to create a magnetocaloric heat pump which is able to provide 2 kW of heating power for a single family house with a temperature span of around 20 °C - 30 °C between the ground source and the heating emitter [5]. These objectives are only reachable for a well-insulated building.

The “iLiving Project” single storey house is chosen to be the case study of the EnovHeat project. It is a typical newly built low energy single family house located in Løkken, Denmark.

Figure 1: *Location of the building case study in Denmark.*

This house has been designed according to the Danish building regulation “BR10” [10] with the goal of achieving very low energy consumption . It is equipped with a heat recovery ventilation system and has a radiant under floor heating system connected to a ground source heat pump. The details about the building case study parameters are presented in **Table 1 - 3** and **Figure 2 - 5**.

Table 1: *EnovHeat building parameters.*

Total ground floor area including walls [m²]	150
Heated floor area [m²]	126
Heated net volume [m³]	309
Building envelope area including ground [m²]	545
Number of occupants	4
External walls U-value [W/m².K]	0,11
Floor U-value [W/m².K]	0,071
Roof U-value [W/m².K]	0,081
Doors and windows U-value [W/m².K]	1
Glazing transmittance [%]	0,63
Infiltration rate [h^{-1}]	0,1
Ventilation [m³/s]	0,103
Air change rate (without infiltration) [h^{-1}]	1,2
Ventilation heat recovery [%]	85
Design heat loss [kW]	3,78
Heating system max power [kW]	2,93
Heating temperature set point [C]	22
Heating energy need (SP = 20°C) [kWh/m².year]	16

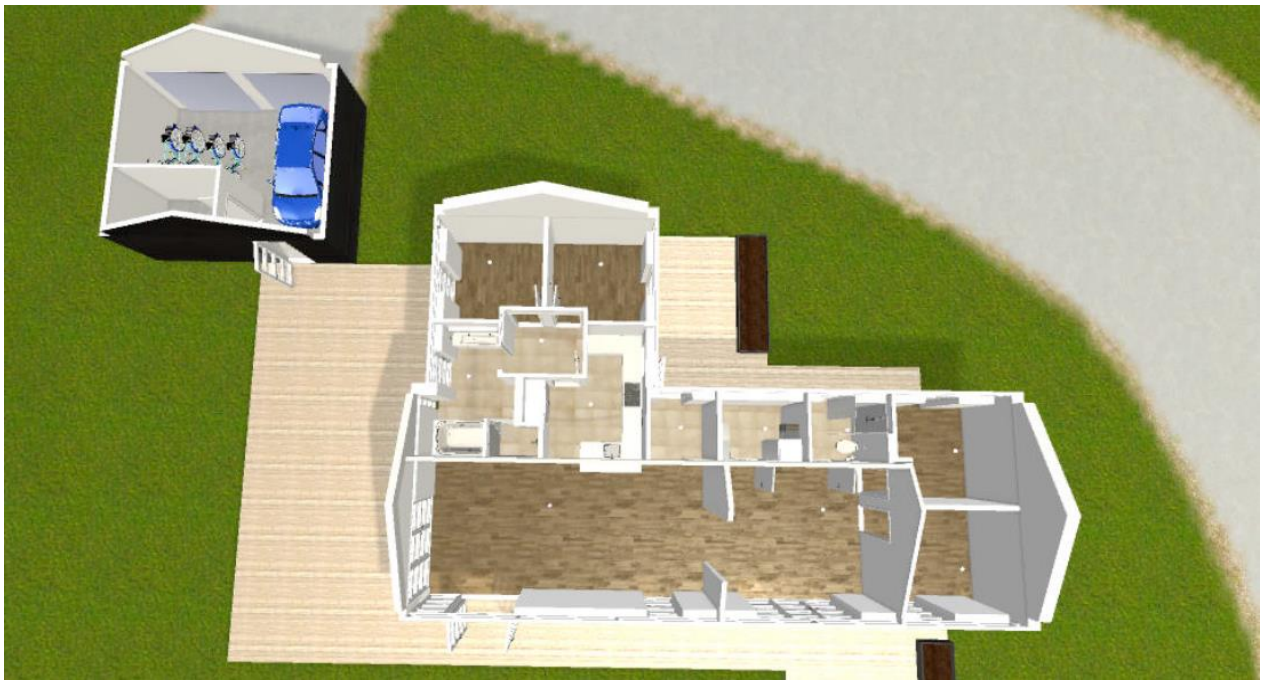

Figure 2: *View of the EnovHeat house case study.*

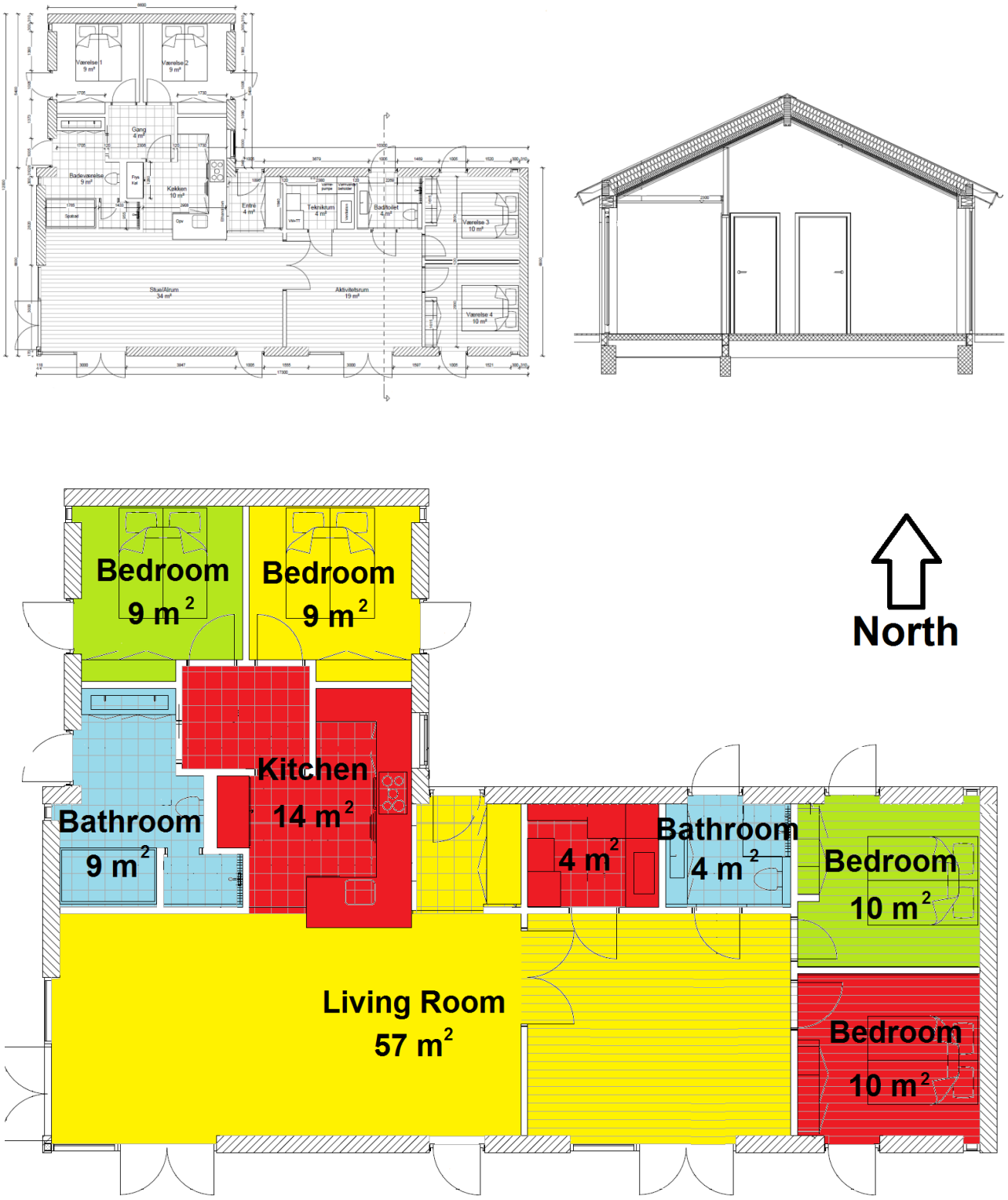

Figure 3: *Plan view of the house case study.*

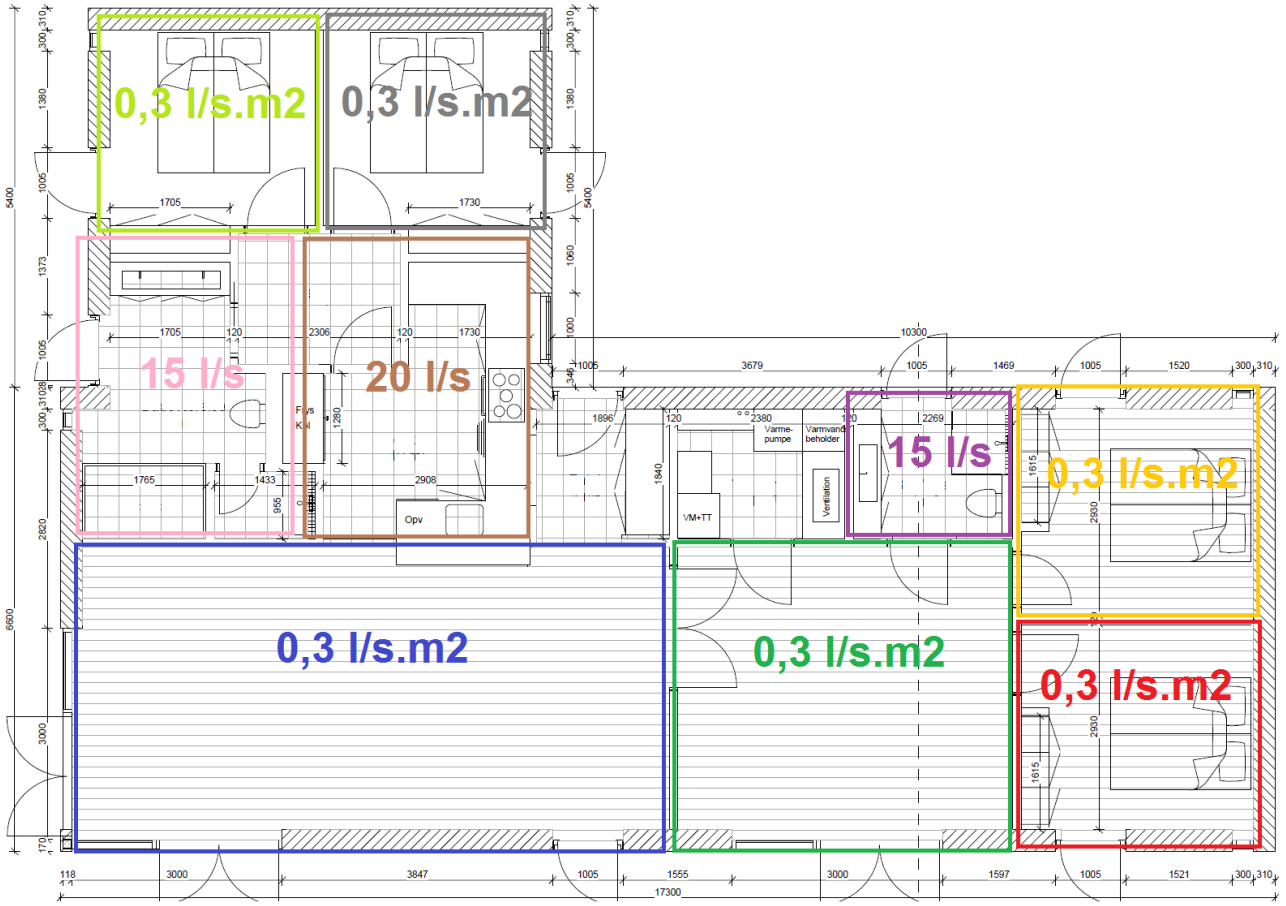

Figure 4: *Ventilation rate of each thermal zone.*

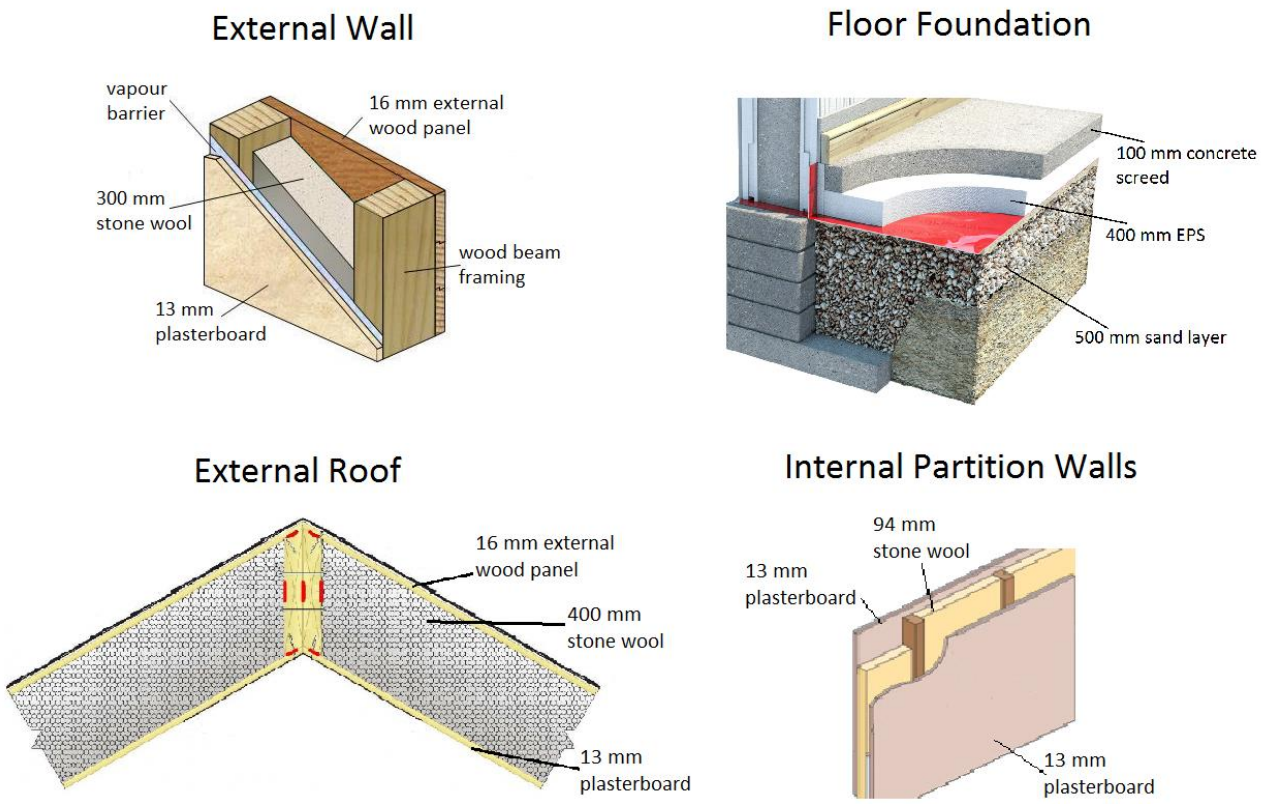

Figure 5: *Description of the construction elements.*

Table 2: *Thermal properties of the construction materials.*

	External Wood Panel	Plasterboard	Stone Wool	Concrete	EPS Insulation	Sand (house underground)	Brick
Thermal Conductivity [W/m.K]	0,12	0,2	0,033	2,1	0,03	0,68	0,68
Density [kg/m3]	500	900	45	2400	17	800	1840
Heat Capacity [J/kg.K]	1800	1000	800	800	750	1600	800

Table 3: *Radiation surface properties of the building elements.*

	Light Grey Painting (internal surfaces/floor)	Wood (external surfaces)	Grass (outdoor surrounding)
Emissivity	0,9	0,9	0,9
Solar Absorptance	0,4	0,55	0,8
Reflectance	0,6	0,45	0,2
Albedo			0,25

One can see on **Figure 6 - 7** that the EnovHeat house case study has a very efficient thermal envelope which lies between “class 2020” and “Passive House” level according to the Danish building regulation [10] [11].

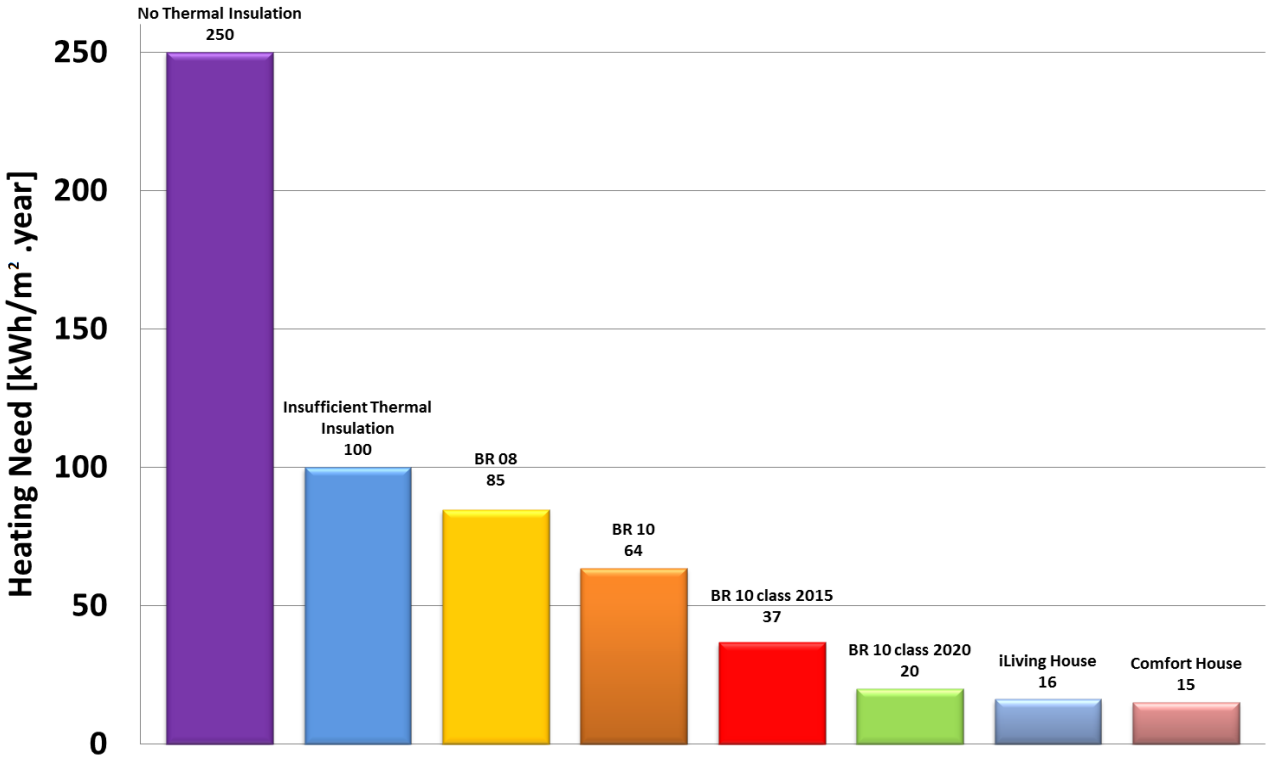

Figure 6: *Total yearly heating need of detached residential houses in Denmark (Indoor temperature set point = 20 °C). Results from the iLiving project are obtained from a BSim model of the house.*

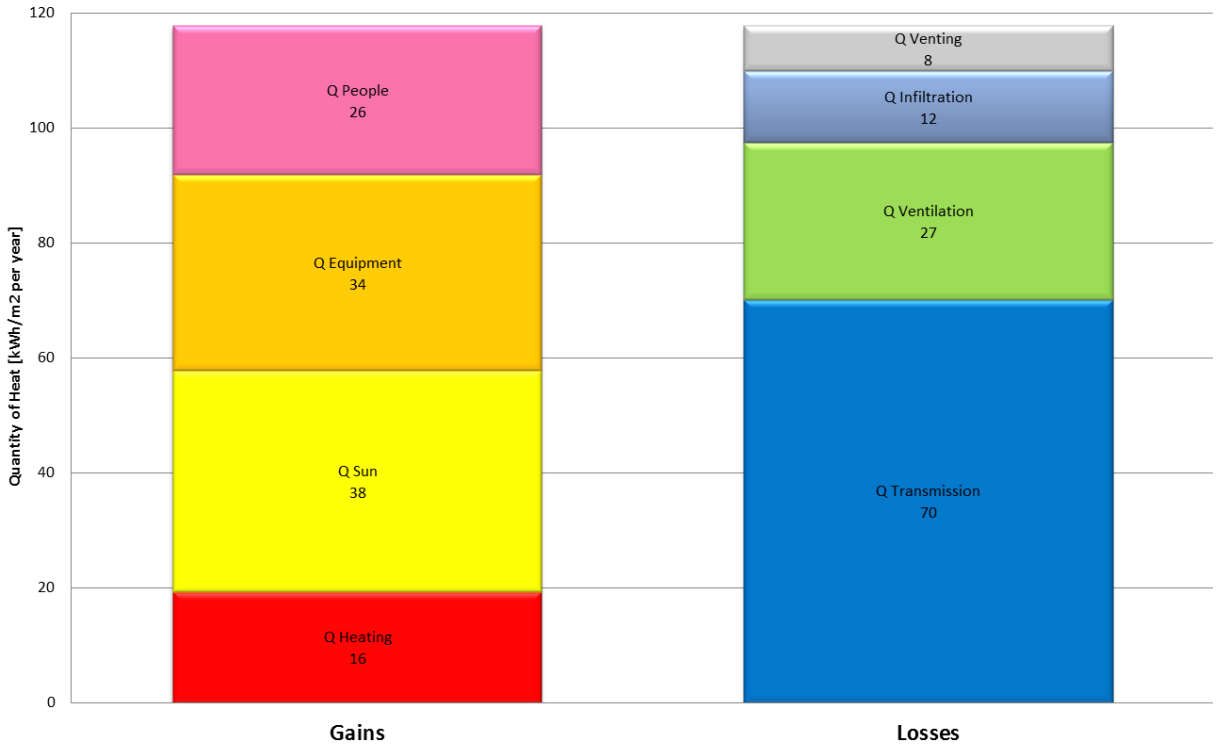

Figure 7: *Yearly energy balance of the iLiving project house (Indoor temperature set point = 20 °C). Results are obtained from a BSim model of the house under Danish weather conditions.*

1.2.Energy Flexibility Case Study Buildings

The EnovHeat case study building parameters are changed in order to generate different thermal mass and insulation level categories for further numerical investigations on the impact of thermal mass on the energy flexibility capacity of dwellings.

The insulation layer of the roof, external walls and floor, the infiltration, the windows and HVAC systems' performance are varied accordingly. The low insulation house category corresponds to the typical insulation level of a 1980's house in Denmark. The high insulation house category corresponds to the typical insulation level of a Passive House or "Komforthus" in Denmark. The original design of the EnovHeat house has a medium effective thermal capacity. The materials of the internal and external surfaces of the walls, roofs and floors are changed in order to vary the total thermal inertia of the building. 3 different building structure thermal mass categories are generated [12] with 3 different case variations in each categories (9 different building structure thermal mass cases in total):

- Light-weight structure house: 30 Wh/K.m², 40 Wh/K.m² and 45 Wh/K.m²
- Medium-weight structure house: 50 Wh/K.m², 60 Wh/K.m² and 70 Wh/K.m²
- Heavy-weight structure house: 90 Wh/K.m², 100 Wh/K.m² and 110 Wh/K.m².

The details of the construction elements of each thermal mass category are presented in **Figure 8**. Details of the different building parameters of the house study cases are presented in **Table 4**.

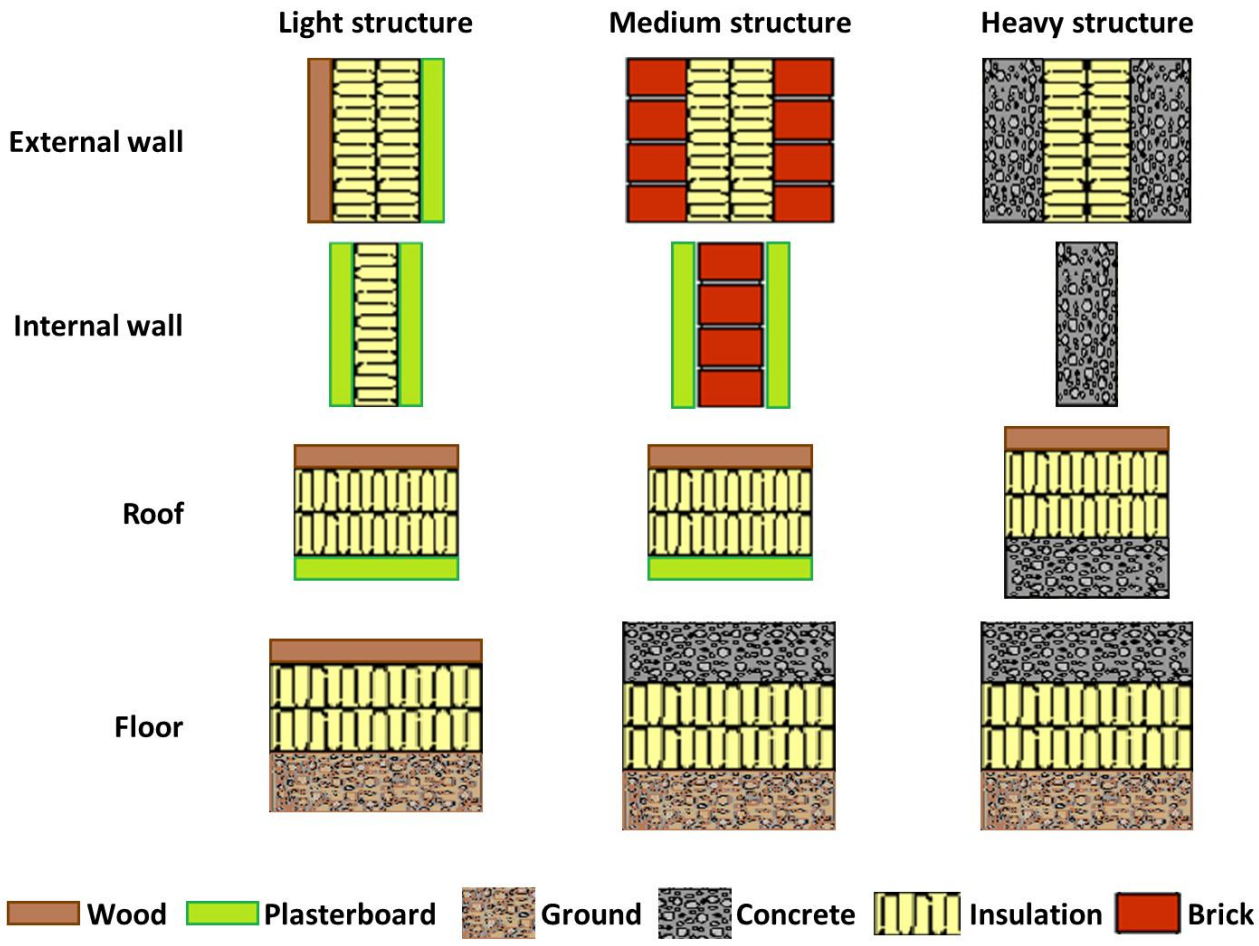

Figure 8: *Details of the construction elements for each thermal mass category.*

Table 4: *Building parameters.*

Building envelope category	House 1980's			Passive House		
Structural thermal inertia category	**Light**	**Medium**	**Heavy**	**Light**	**Medium**	**Heavy**
Building thermal inertia (Wh/K.m²)	30 - 40 - 45	50 - 60 - 70	90 - 100 - 110	30 - 40 - 45	50 - 60 - 70	90 - 100 - 110
Building envelope heat losses (W/K.m² gross floor)	1.12	1.13	1.13	0.37	0.37	0.37
U-value windows (W/m².K)	1.70			0.78		
g-value windows (-)	0.63			0.50		
Ratio windows / gross floor area (%)	16.7 %			26.9 %		
Windows area (m²)	25.10			40.39		
Air infiltration (ACH)	0.2			0.07		
Ventilation (ACH)	0.4			0.4		
Heat recovery (-)	0			0.8		
Air flow heat losses (W/K)	64			15.6		
Air flow heat losses (W/K.m² gross floor)	0.43			0.10		
Yearly radiator heating need with set-point at 22°C (kWh/m² net floor)	164	160	155	14	13	12
Maximum radiator heating power (W/m²)	75			25		
Under-floor heating type	Type G wood floor	Concrete screed	Concrete screed	Type G wood floor	Concrete screed	Concrete screed
Yearly under-floor heating need with set-point at 22 °C (kWh/m² net floor)	160	151	157	15	13.5	13
Nominal water flow per UFH loop (l/h)	170			125		
UFH maximum inlet water temperature (°C)	47	43	43	35	30	30

1.3.Conventional Heat Pump System

The reference heat generation system of the building case study is a conventional vapor-compression water-to-water heat pump with characteristics similar to the model TWM036 of ClimateMaster® [13]. When running at nominal fluid volumetric flow rate of 2052 L/h in both heat source and heat sink loops, this heat pump delivers 8.28 kW of heating power with a COP of 4.51. The heat pump is coupled with a ground source heat exchanger and a hydronic low-temperature radiant under-floor heating system (see **Figure 9**). The hot water storage tank has a capacity of 250 L (cylindric shape tank with radius of 29 cm and and height of 95 cm) with 5 cm of polyurethane insulation (heat losses to the ambient U-value of 1.356 W/K).

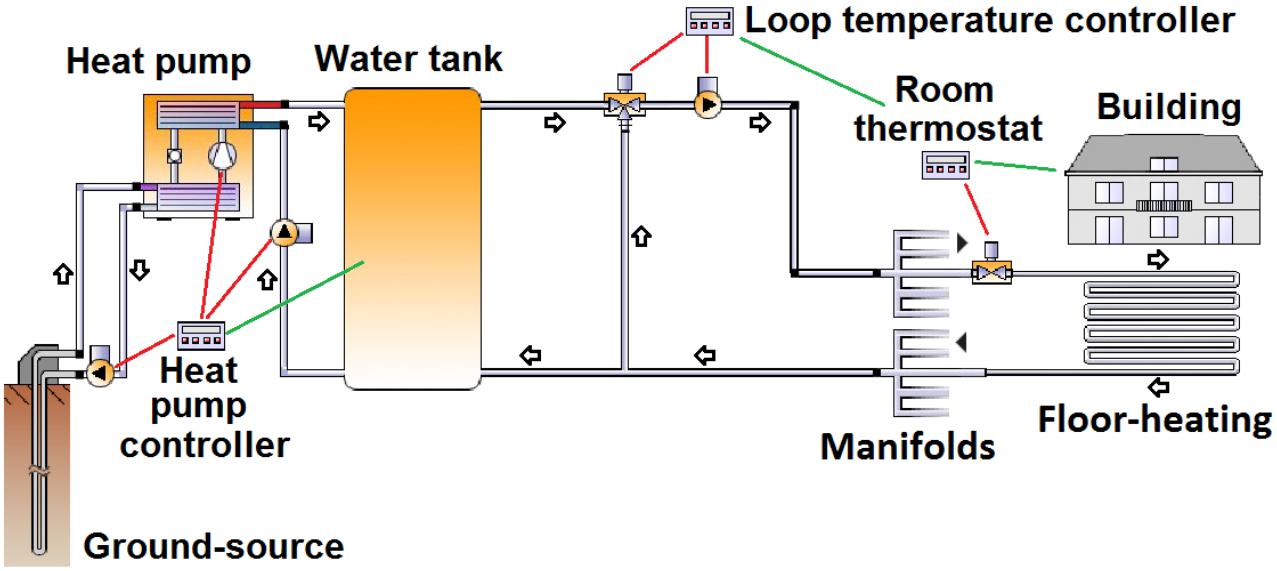

Figure 9: *Schematic of the heating system implementation for the conventional heat pump.*

Hydraulic circulation pumps are placed on the different sections or loops of the water/brine-based heating system in order to carry the heat-transfer fluid from the ground heat source to the under-floor manifolds and the different loops in each room.

To choose an appropriate hydraulic pump for that system, the pressure drop of the critical loop is calculated for the nominal mass flow and a water-brine with 20%vol ethylene glycol and 80%vol water. It is found that the critical loop on the side of the heat sink (under-floor heating) has a total pressure drop which is always below 15 kPa at nominal mass flow rate. It is therefore chosen to use an hydraulic circulation pumps Grundfos ALPHA2 L 15-40 [14]. These circulator pumps can operate with variable flow rate and constant pressure difference. It is therefore chosen to use the lowest constant pressure regulation (CP1) at 23 000 Pa. Similarly, the maximum pressure drop in ground source heat exchanger loop is always below 15 kPa at nominal mass flow. It is therefore also chosen to use an hydraulic circulation pumps Grundfos ALPHA2 L 15-40. The hot water storage tank circuit circulation pump is also a Grundfos ALPHA2 L 15-40.

1.4.Magnetocaloric Heat Pump System

The magnetocaloric heat pump is coupled with the ground source heat exchanger and the under floor heating system within a single hydronic loop without an intermediate heat exchanger or hot water storage tank (see **Figure 10**).

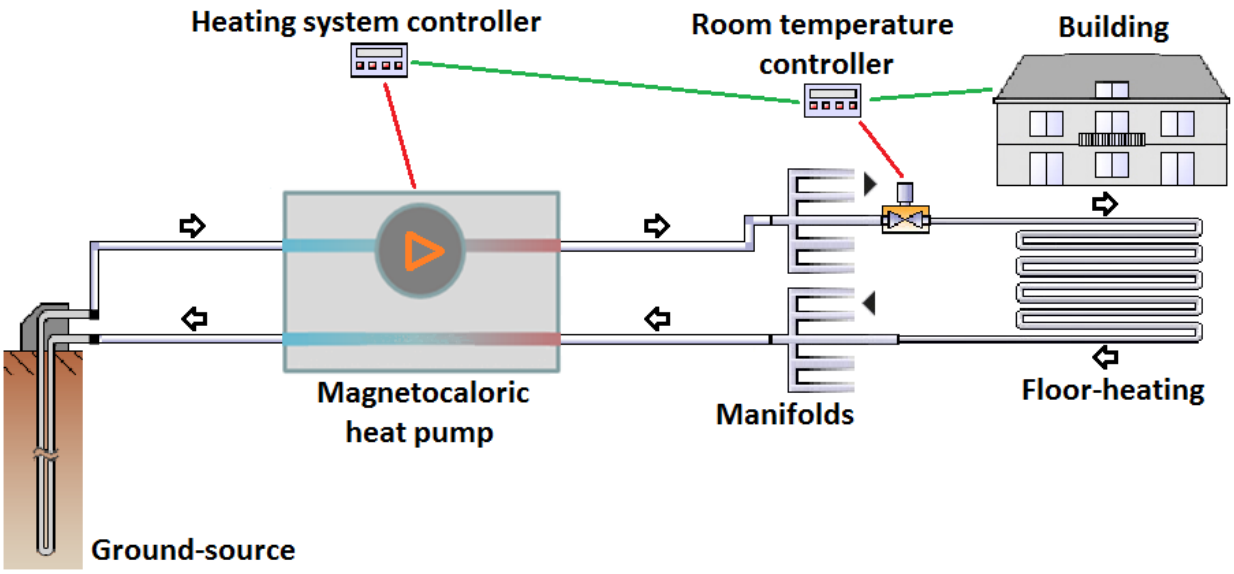

Figure 10: *Schematic of the heating system implementation for the magnetocaloric heat pump.*

The pressure drop in the packed bed sphere regenerator of the magnetocaloric heat pump is significantly higher than the pressure drop in the under floor heating loops or in the ground source heat exchanger loop. Consequently, an hydraulic pump able to generate enough pressure difference is chosen to circulate the heat transfer fluid in the single hydronic loop. The circulation pump is a Grundfos CR 1-9 A-FGJ-A-E-HQQE – 96478872 operating on the power curve P2 [15].

1.5.Under Floor Heating Systems

Two different types of water-based under floor heating systems are implemented in the building study cases. Light structure buildings are equipped with a “type G” wooden floor embedded pipe under floor heating (See **Figure 11**). Medium and heavy structure buildings are equipped with a concrete screed embedded pipe under floor heating (See **Figure 12**).

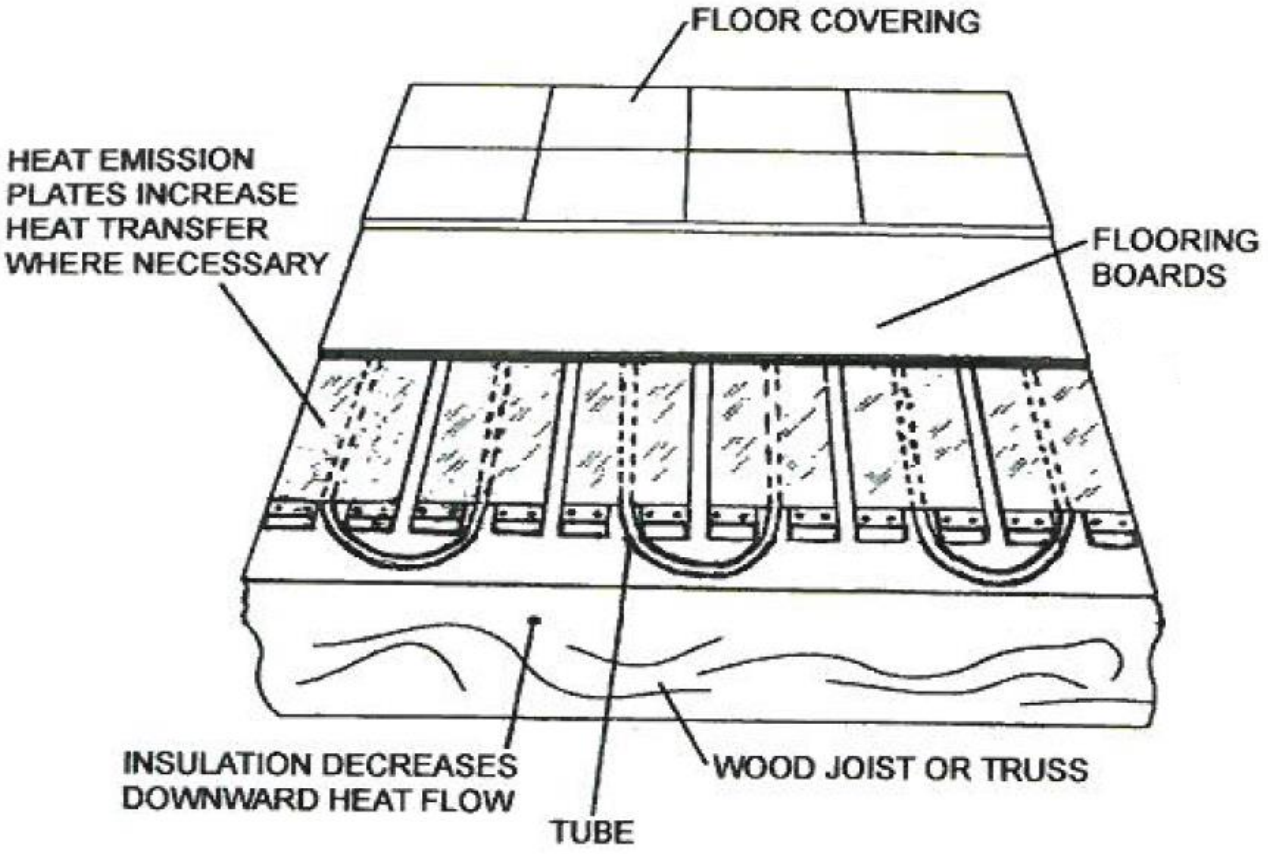

Figure 11: *Type G under floor heating system with pipe embedded in wooden floor.*

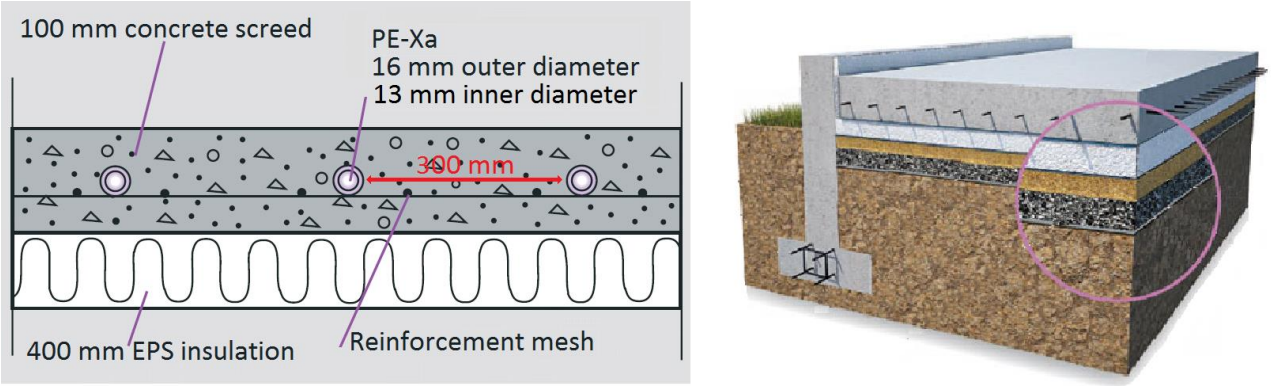

Figure 12: *Concrete screed embedded pipe under floor heating (EnovHeat case study house).*

The design and sizing of the under-floor heating systems are performed according to manufacturer's technical guidelines (Uponor) and international standards [16] [17] [18] [19] [20].

For concrete screed under floor heating system, the total thickness of the concrete layer is 100 mm. The center of the pipes network embedded in the concrete screed is 60 mm from the upper surface of the

concrete slab. The hydronic network is made of PE-Xa pipes with external diameter of 16 mm, internal diameter of 13 mm (wall thickness of 1.5 mm), thermal conductivity of 0.45 W/m.K, and inner surface pipe roughness (according to Prandtl and Colebrook) of 0.007 mm/m. The spacing in between the center of each pipe is of 200 mm for the houses of 1980's and 300 mm for the passive houses.

For the type G under floor heating system with pipe embedded in wooden floor, the total thickness of the wooden layer is 30 mm. The center of the pipes network embedded in the wooden floor is 12 mm from the upper surface of the wooden slab. The hydronic network is made of PE-Xa pipes with external diameter of 16 mm, internal diameter of 13 mm (wall thickness of 1.5 mm), thermal conductivity of 0.45 W/m.K, and inner surface pipe roughness (according to Prandtl and Colebrook) of 0.007 mm/m. The spacing in between the center of each pipe is of 200 mm for the houses of 1980's and 300 mm for the passive houses. The heat emission plates are made of aluminum. They are 1 mm thick with a thermal conductivity of 300 W/m.K. The gap between each plate is 5 mm.

1.6.Ground Source Heat Exchangers

The space heating needs of the case study buildings are provided by a water-to-water heat pump connected to a ground source heat exchanger (domestic hot water production is not in the scope of the study). Two types of ground source heat exchangers are therefore designed to insure enough heat supply to the building: a vertical borehole heat exchanger and a horizontal ground source heat exchanger.

First of all, representative characteristics of the ground properties in Denmark are evaluated from numerous measurement campaigns gathered into publically available database [21] [22] [23] [24] [25]. The soil parameters chosen for the case study are the ones of a humid clayey sand (humid winter conditions in Denmark) with a thermal conductivity of 1.5 W/m.K, a density of 1900 kg/m³ and a specific heat capacity of 1400 J/kg.K. The grouting material is chosen to be with a thermal conductivity of 1.4 W/m.K, a density of 1500 kg/m³ and a specific heat capacity of 1670 J/kg.K.

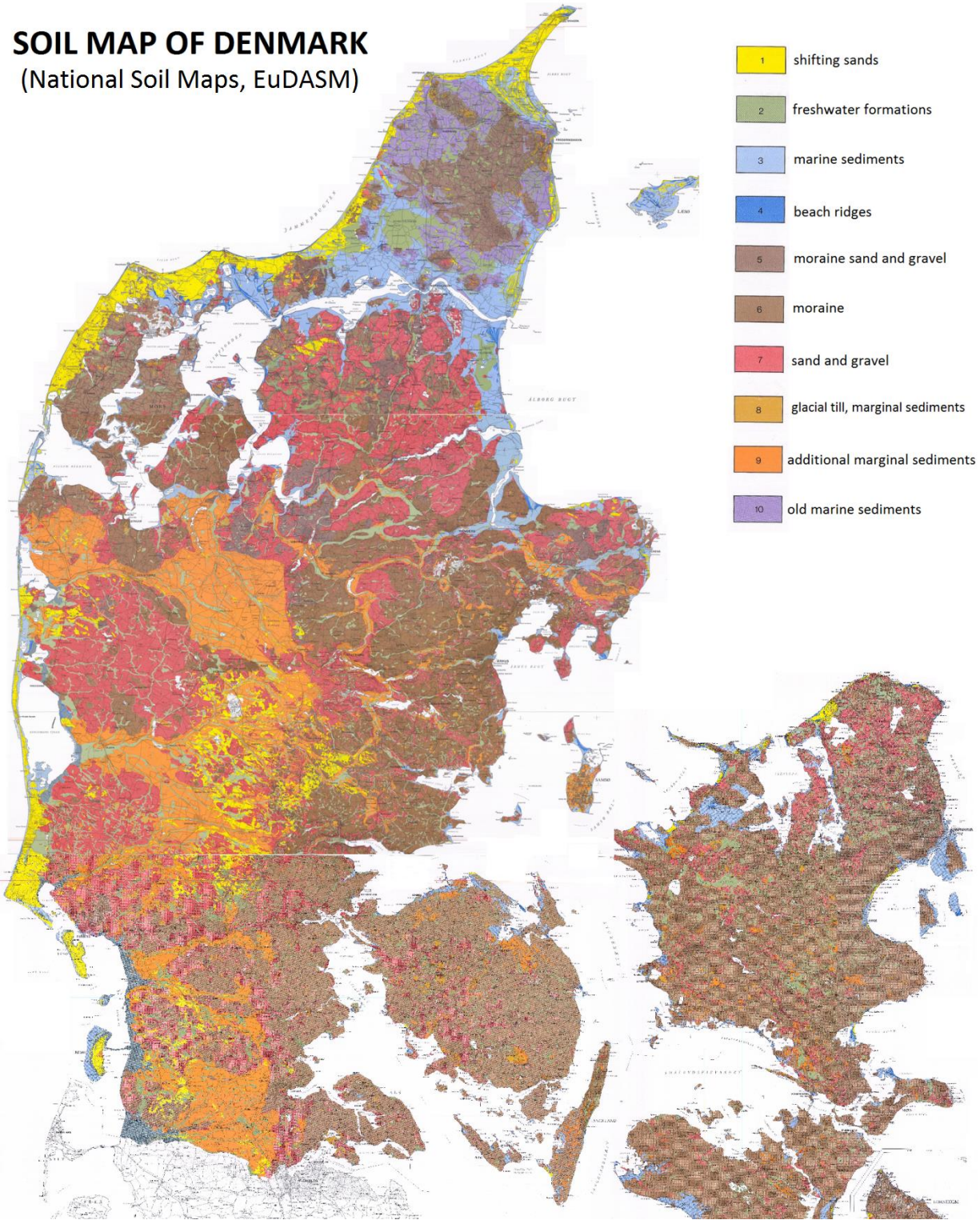

Figure 13: *Soil map of Denmak.*

The horizontal ground source heat exchanger is designed according to the VDI 4640 standard and the recommendations of manufacturers [26] [27] [28]. The hydronic network is made of PEX pipes with outer

diameter of 40 mm, wall thickness of 3.5 mm, inner diameter of 33 mm, thermal conductivity of 0.45 W/m.K and Inner roughness (according to Prandtl-Colebrook) of 0.007 mm/m. They are placed at a depth of 1.5 m from the ground surface according to a serpentine layout (See **Figure 14**). The spacing in between each pipe's leg is 1.5 m. The total length of the pipe collector is 194 m and it covers 291 m² of soil surface area.

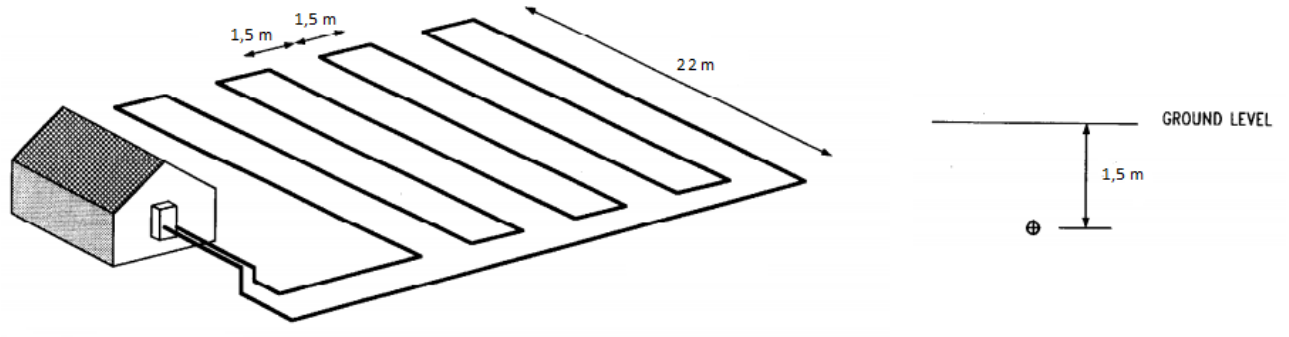

Figure 14: *Serpentine layout of the horizontal ground source heat exchanger.*

The vertical borehole ground source heat exchanger is designed according to the VDI 4640 standard and the recommendations of manufacturers [26] [27] [28]. The hydronic loop is made of single double U-tube PEX pipe with outer diameter of 44 mm, wall thickness of 3.5 mm, inner diameter of 37 mm, thermal conductivity of 0.45 W/m.K and Inner roughness (according to Prandtl-Colebrook) of 0.007 mm/m. The borehole has a depth of 100 m (see **Figure 15**) with a diameter of 160 mm. The spacing between the centers of the two legs of the U-pipe is 80 mm (see **Figure 16**). The total length of the pipe collector is 200 m.

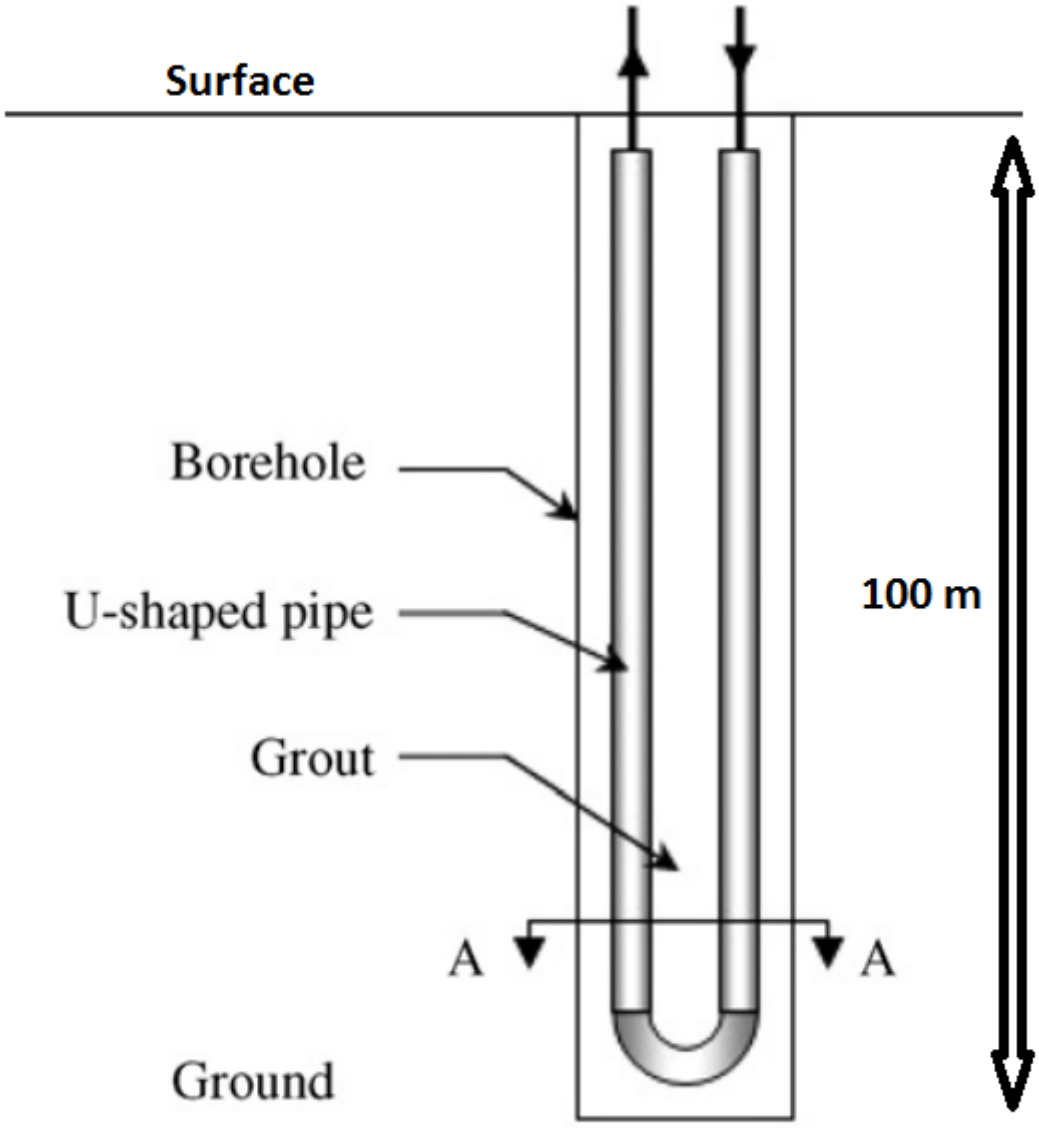

Figure 15: *Schematic of a vertical borehole ground source heat exchanger with U-pipe.*

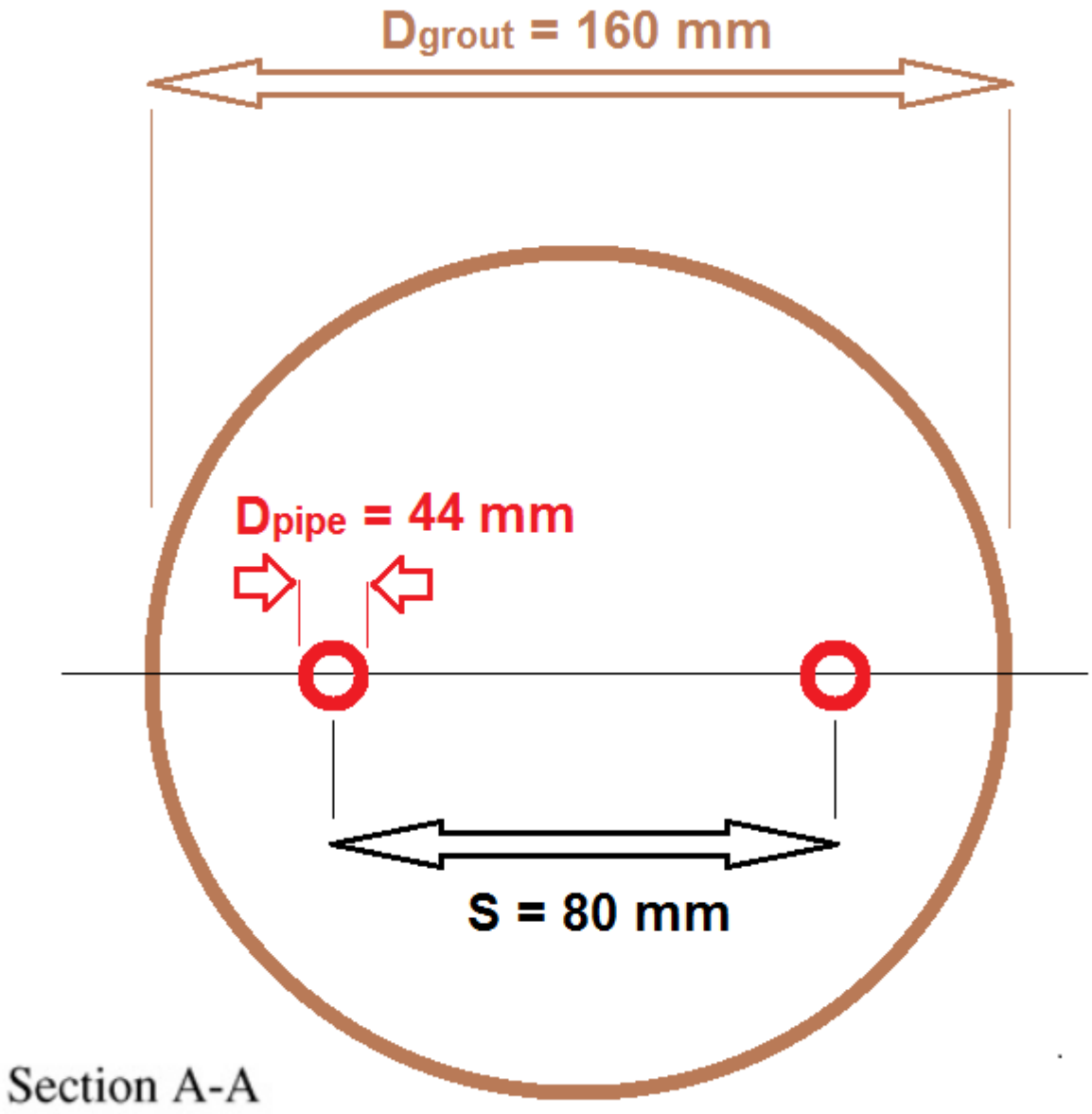

Figure 16: *horizontal cross section of the vertical borehole heat exchanger.*

1.7.Phase Change Material

The thermal storage capacity of a building can be enhanced by the integration of phase change materials. Concerning passive latent heat storage in the indoor environment, studies found that the most efficient location for PCM is on the inner surfaces of the indoor space for a maximum thermal activation [29]. Consequently, some of the case study buildings are equipped with PCM panels fixed on the inner surfaces of the thermal zones: external walls, internal walls, ceiling and furniture surfaces.

The PCM wallboards used in the study are similar to the Energain® [30]. This is a common commercial product made of 60%mass micro-encapsulated paraffin incorporated into 40%mass polyethylene matrix.

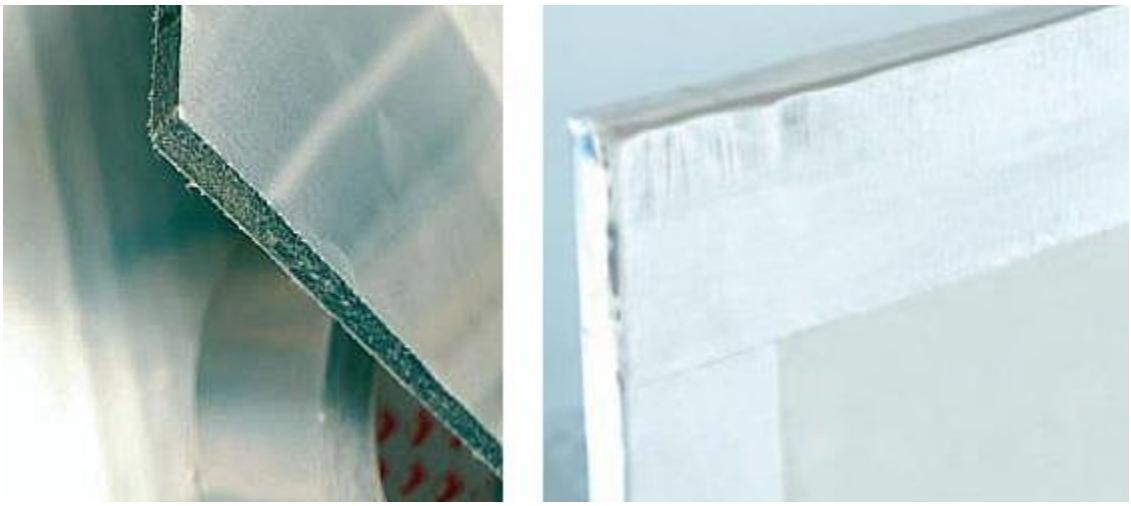

Figure 17: *Energain® PCM wallboards (DuPont).*

Experimental tests have been conducted at Aalborg University Laboratory in order to measure the thermal characteristics of this PCM. These characteristics are used in the numerical models of the study and presented hereafter.

The melting and solidification temperatures of the PCM are 22 °C and 21.8 °C respectively. The latent heat of fusion for the pure paraffin is 200 kJ/kg. This is a very common value compared to other products used for ambient temperature applications [29]. Therefore the latent heat of fusion for the 60 %mass paraffin stable form PCM is 120 kJ/kg.

The global thermal conductivity is assumed to follow the results found by Kuznik et al. in a previous study [31]. The PCM has a constant thermal conductivity of 0.22 W/m.K and 0.18 W/m.K below 16 °C and above 28 °C, respectively. It is assumed that the thermal conductivity varies linearly from 0.22 to 0.18 W/m.K in between 16 °C and 28 °C. These results have been confirmed by Guarded Hot Plate Apparatus measurements on Energain® test samples with different thicknesses (see **Figure 18**).

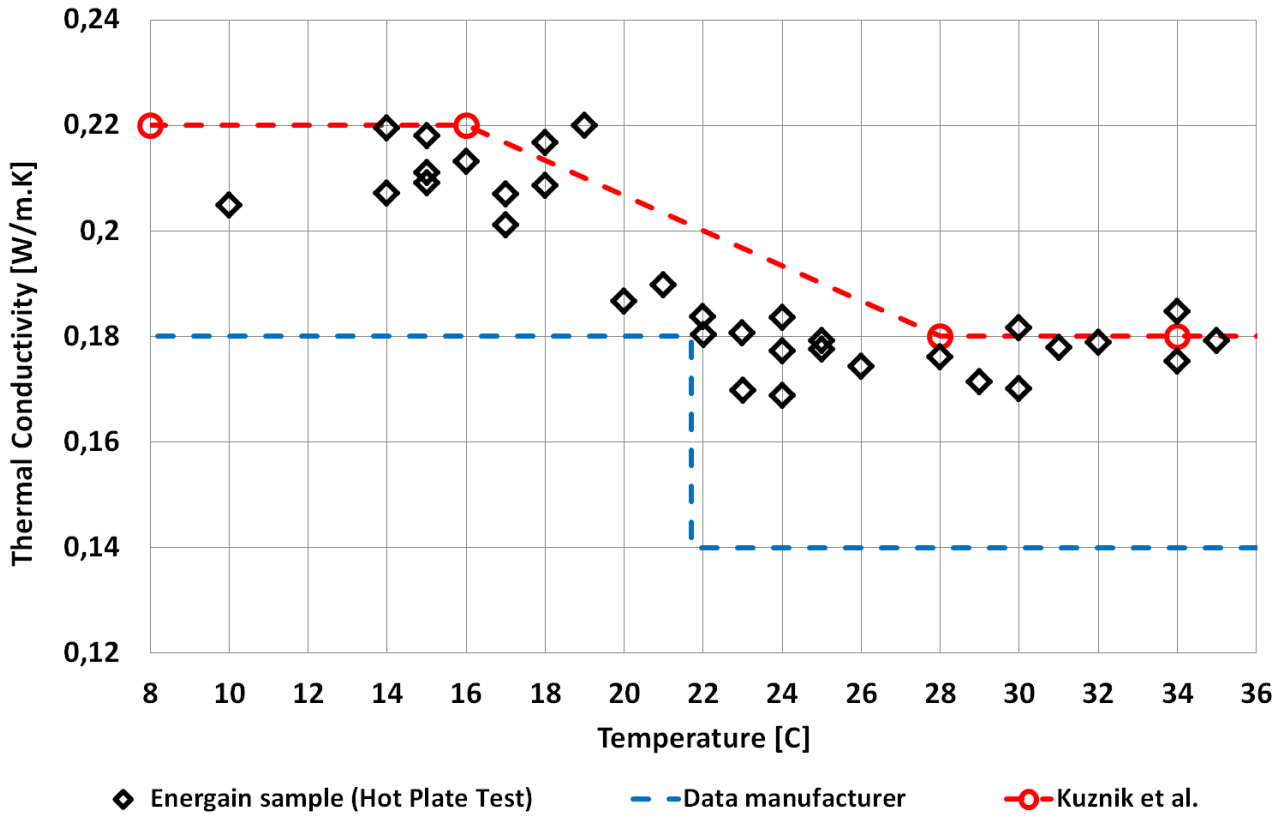

Figure 18: *Guarded Hot Plate thermal conductivity measurements.*

The specific heat capacity of the stable form PCM is 2000 J/kg.K. This value corresponds to the mass percentage content weighted sum of the specific heat capacity of paraffin and polyethylene. It fits very well with Differential Scanning Calorimetry (DSC) measurements of Energain® test samples above the melting temperature when no phase transition occurs (experimental tests performed at Aalborg University laboratory with temperature change of 2 K/min). One can see on **Figure 19** that there is a noticeable difference between the measurements of Kuznik et al. and the ones of Aalborg University. This dissimilarity could be due to the variability of the Energain® manufacturing process. Moreover, one can notice that the increase of apparent heat capacity forms a rather wide dome instead of a sharp peak. It seems that the phase transition occurs marginally all along the 0 °C to 30 °C temperature interval. This might be due to the fact that the micro-encapsulated paraffin of the PCM product is composed of different grades of hydrocarbon chains with different individual melting temperature. However, the main phase transition is at 22 °C.

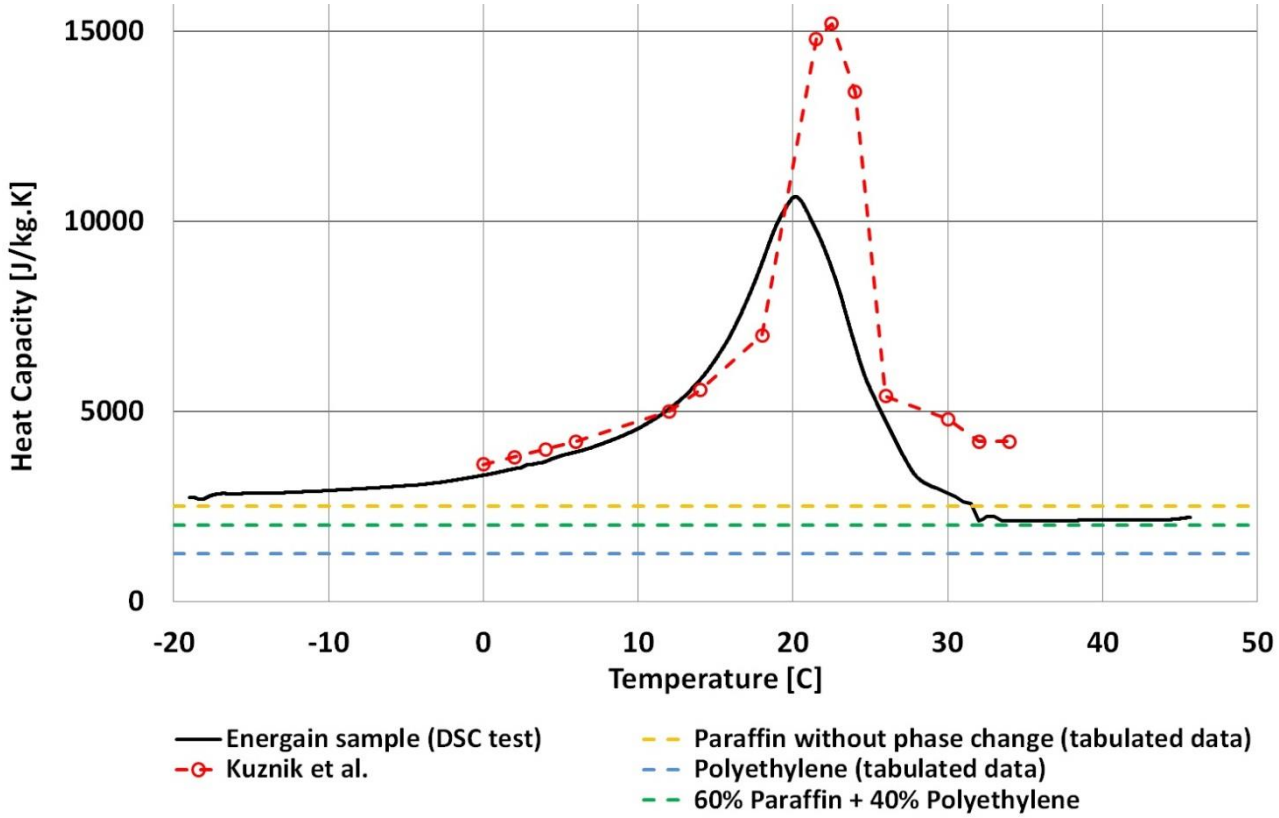

Figure 19: *Differential Scanning Calorimetry heat capacity measurements.*

The average density measured for the stable form PCM is 1000 kg/m³, which is close to the density of paraffin and polyethylene and in agreement with measurements of Kuznik et al. Moreover, the DSC test shows that the total heat storage capacity is 144 kJ/kg (temperature rising from 10 °C to 40 °C). This result is in very good agreement with the technical documentation provided by the manufacturer [30].

All parameters of the PCM used in the study are summarized in **Table 5**.

	PCM model	Measurements (current study)	Energain® (data manufacturer)	Kuznik et al.
Paraffin mass content (%)	**60**	**-**	**60**	**60**
Paraffin latent heat of fusion (kJ/kg)	**200**	**-**	**-**	**-**
Melting temperature (°C)*	**22**	**20**	**21,7**	**22**
Thermal conductivity (W/m.K)*	**0.22 - 0,18**	**0.22 – 0.17**	**0.18 – 0.14**	**0,.22 – 0.18**
Density (kg/m³)*	**1000**	**900**	**800**	**1019**
Specific heat capacity (J/kg.K)*	**2000**	**2000**	**-**	**-**
Latent heat of fusion (kJ/kg)*	**120**	**-**	**> 70**	**-**
Total heat storage for $\Delta\theta$ = 30 K (kJ/kg)*	**180**	**170**	**140**	**200**

* For stable form PCM product: 60 %mass paraffin in polyethylene matrix

Table 5: *Phase change material thermal properties.*

1.8.Phase Change Material Wallboard

The stable form PCM boards are implemented in the case study buildings as passive latent heat thermal energy storage (LHTES) systems. These systems have to be sized to the optimum thickness to maximize the additional thermal inertia with the minimum amount of PCM possible. The effective energy storage capacity is proportional to the PCM volume which melted and solidified during a complete TES cycle. If the material amount is overestimated, the time needed for the heat to penetrate the PCM layer could become larger than the charging period, and the melting process cannot be completed.

The effective heat capacity optimization for normal material without phase transition is rather simple to perform. The daily effective heat capacity can be calcualted with the detailed matrix method described in the standard EN ISO 13786 [32] with a 24 hour period of variations. This method is straightforward, robust and easy to implement for multilayer materials. Dynamic boundary conditions are restricted to sinusoidal variations, which is a common way to model indoor and outdoor temperature change over time.

As indicated by Ma and Wang [33], the change of effective thermal storage capacity of a normal material as function of its layer thickness presents a maximum. Increasing further the thickness of the material layer does not improve its effective thermal capacity and actually decreases it slightly.

However, this methodology is based on the analytical solution of one-dimensional heat transfers through solids with constant thermal properties. Therefore it cannot be used for materials presenting phase transition. In order to assess the effective thermal inertia of elements including PCM, a numerical model (described later in this report) is used for the calculation of internal energy variations. A similar approach is used by Kuznik et al. [31] for the optimization of a PCM wallboard. The areal effective thermal inertia κ on one side of a plane element is its ability to store energy when temperature varies periodically [32]. It is equal to the maximum variation of internal energy ΔE (Joule) of a half element divided by the maximum boundary temperature change ΔΘ (K) and the surface area A (m²):

$$\kappa = \frac{\Delta E}{\Delta \theta \times A}$$

Similarly to the matrix method, the temperature boundary conditions are changing as a 24 hour period sinusoidal function. After 10 cycles, the system reaches a periodic steady state and the effective heat capacity is calculated. This method has been compared to the detailed matrix one and presents very good agreement for normal materials: average deviation of 0.09% for concrete wall modeled with 100 control volumes (see **Figure 20**).

The **Figure 20** shows the evolution of the effective heat capacity of an internal wall element made of mineral wool and covered by a PCM layer with variable thickness. These results are coherent with the investigations of Kuznik et al. [31]. However no clear maximum effective thermal capacitance can be observed. The amplitude of boundary temperature variation does not influence the areal effective thermal inertia of material with constant thermal properties. However, one can see that it induces noticeable deviations of 4% in average for the PCM elements. Larger temperature swing increases non-linearly the maximum amount of melted PCM and stored energy because of latent heat and temperature dependent thermal conductivity. Nevertheless, the optimum PCM thickness with maximum heat capacity remains the about same.

The thickness of the PCM layer for the wallboard of the study case is chosen to be 1.5 cm. This value seems to be a reasonable choice to insure a maximum thermal heat capacity for daily temperature variations and it is in agreement with the results of Kuznik et al.

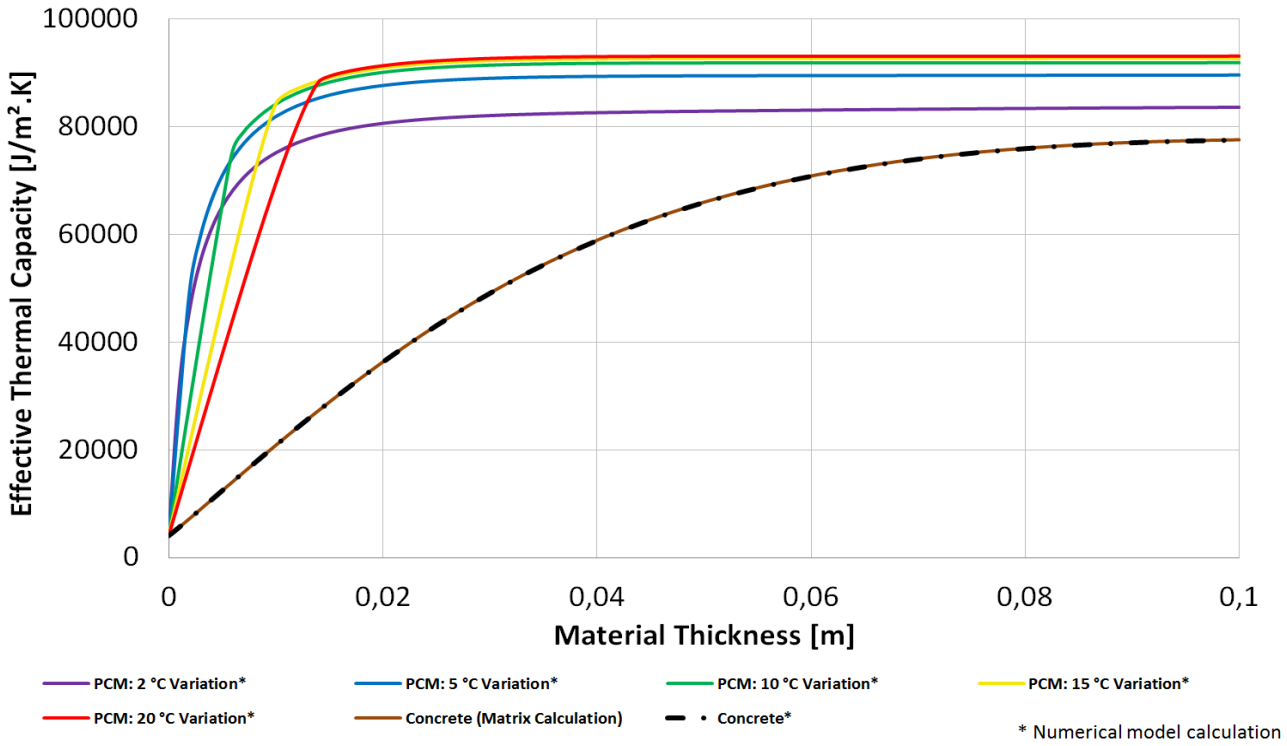

Figure 20: *Phase change material effective thermal capacity in function of layer thickness.*

The PCM wallboards are attached to the inner surface of the building's thermal zones: external walls, internal walls and ceiling. The average amount of PCM in the building is therefore about 40 kg/m² of floor surface area.

1.9.Additional Indoor Thermal Mass / Furniture

One of the aims of this study is to assess the influence of additional thermal mass in the indoor environment such as internal thermal mass or furniture. This additional indoor thermal mass is here considered to be representative of a house with a significant amount of items inside. The total mass of indoor thermal mass / furniture in the case study building is 60 kg/m² of floor surface area [29].

1.8.Phase Change Material Integrated into Furniture Elements

Another additional indoor thermal mass to be tested is the integration of PCM into furniture elements. The same PCM element used as wallboard is here placed on one surface of the furnishing directly exposed to the indoor space. The thickness of the PCM elements is also 1.5 cm.

2. Presentation of the Building Model

Similarly to the HAM-tools [34], the MATLAB - Simulink building model used in this study is based on an one-dimensional explicit finite volume method (FVM) formulation with a limited number of control volumes (also known as Resistance-Capacitance network or RC thermal network. The water-based under-floor heating system and the horizontal ground source heat exchanger are modeled with a MATLAB function. They couple a dynamic fluid "plug flow" model in a pipe with a ε-NTU method which accounts for the equivalent interaction thermal resistance in the layer of the slab where the heat exchanger is laid. The vertical borehole heat exchanger is modeled with a MATLAB function coupling two fluid plug flow pipes in a Resistance-Capacitance network. Both ground sources are integrated in a Simulink state space block function representing the soil surrounding the collector as a 1-D finite domain. The fluid of the hydronic systems can be chosen among 5 different brines. All flow regimes are taken into account for the calculation of the convective heat transfer and the pressure loss. Concerning additional indoor thermal mass, the furniture elements are modeled as an equivalent planar element. A PCM enthalpy model accounts for the LHTES system. The following section presents in details each part of the building model used in the study.

2.1. Construction Elements

The basic blocks of this building model are simulating the heat transfer through the construction elements: external walls, internal walls, internal ceiling, external roof, floor and ground. The building envelope and internal partitions are subdivided into a collection of planar elements. The thickness of these planar elements is considered very small in comparison to their length and width. Therefore it is possible to assume that all heat transfers occur in only one direction normal to the main plan surface of the element (See **Figure 21**).

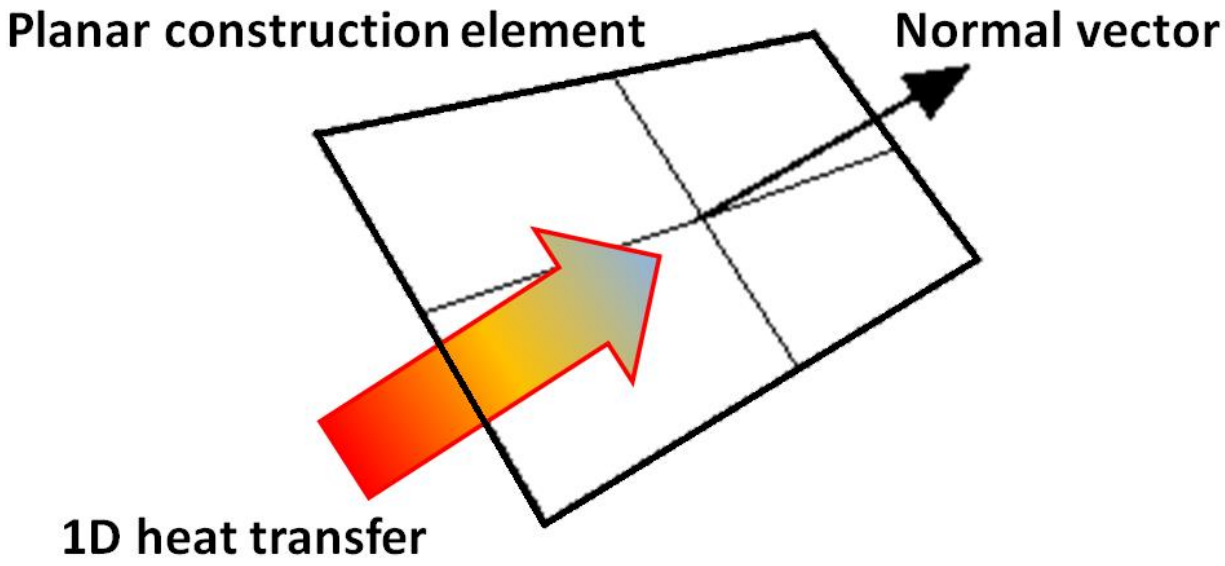

Figure 21: *One-directional heat transfer through planar construction element.*

Each construction element is then subdivided into finite control volumes (See **Figure 22**). It is assumed that within each time step, the temperature of each control volume is constant and homogeneous. Therefore the heat transfers are calculated based on the temperature in the center node of each control volume.

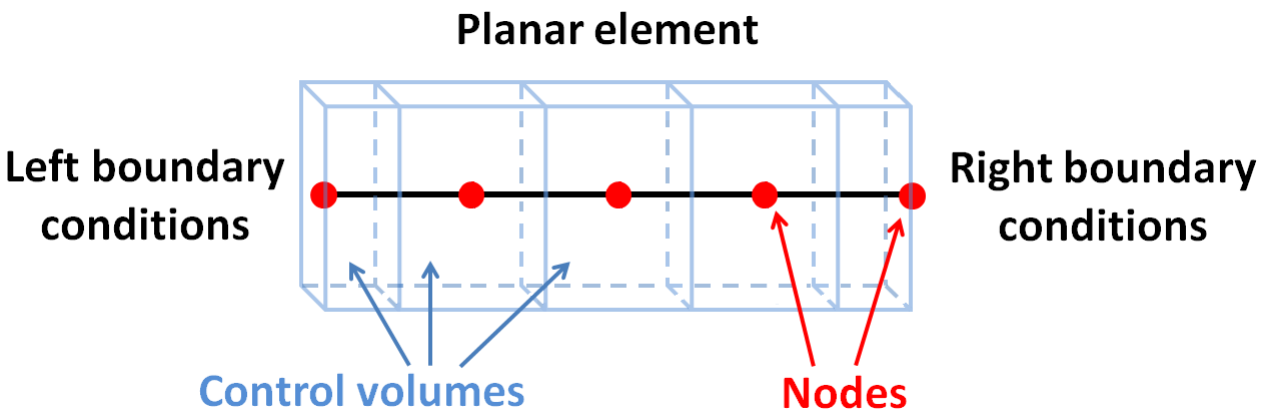

Figure 22: *Space discretization of the planar construction element domain.*

The heat transfers are calculated by solving the heat equation in each thermal node with an explicit finite volume formulation or Resistance-Capacitance network (See **Figure 23**).

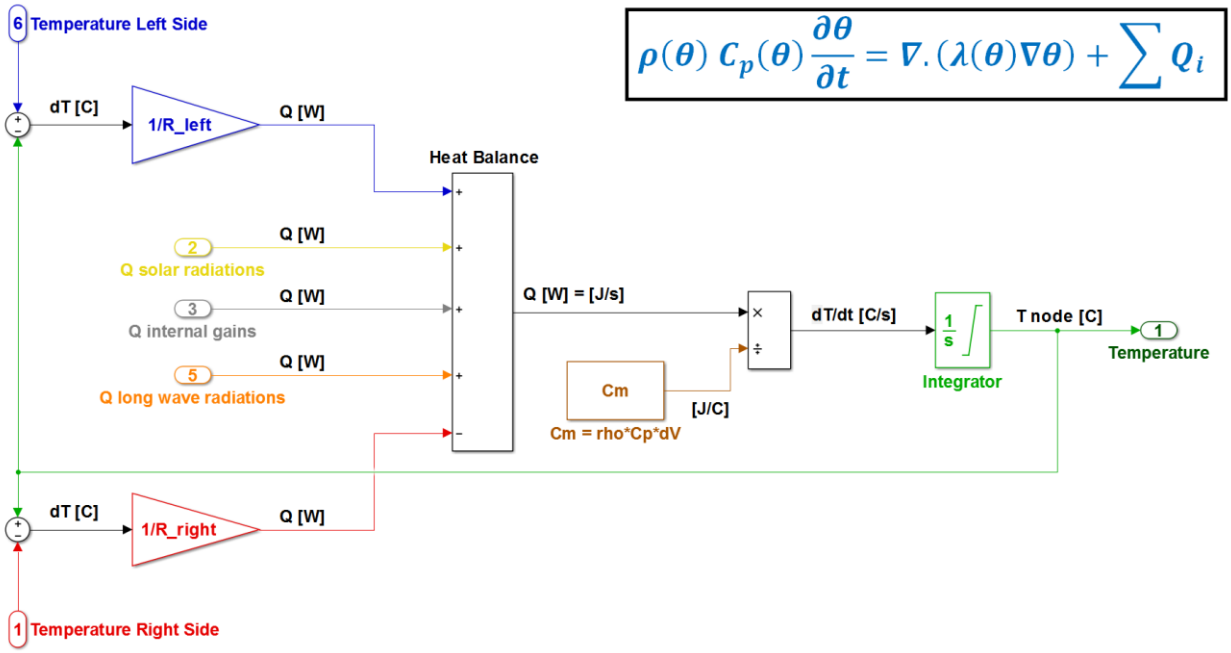

Figure 23: *Explicit finite volume* formulation (RC network) of *the heat equation with Simulink.*

The Simulink formulation for each thermal node is coupled together in order to solve the heat transfer of the whole construction element (See **Figure 24 -25**).

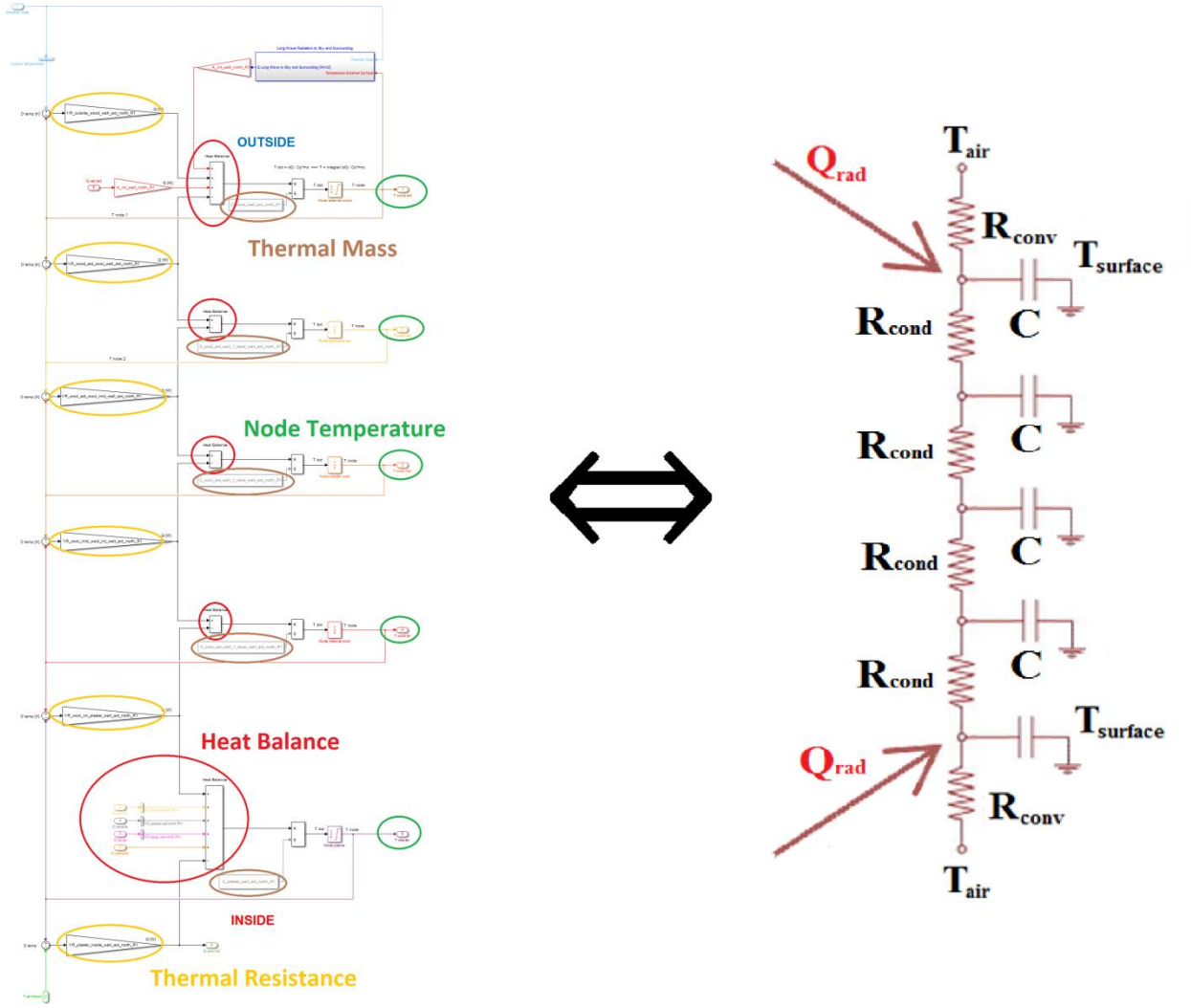

Figure 24: *Implementation of a RC network into a Simulink explicit finite volume formulation.*

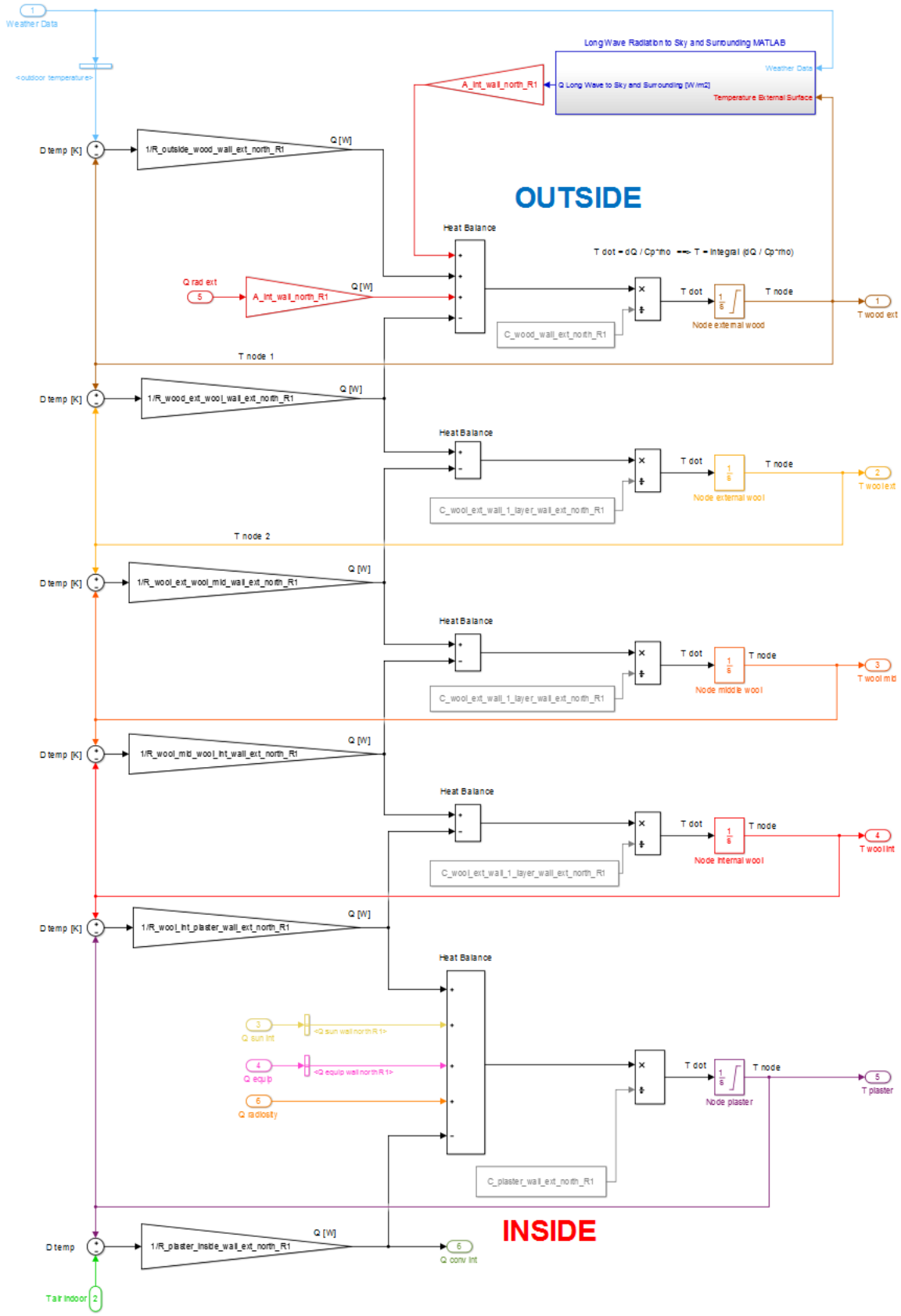

Figure 25*: Finite volume formulation of an external wall element.*

External walls, internal walls, ceiling and roof elements are subdivided into 5 thermal nodes: 1 node on the left hand side and 1 node on the right hand side for the external panels (plaster, wood, brick, concrete). 3 nodes in the middle of the domain for the insulation layer (stone wool). Floor elements are subdivided into 9 nodes. They include the soil layer under the house and the layers of the water-based under floor heating system.

Because the heat equation is solved in this model with an explicit formulation, the time step size of the simulation has to be chosen with great care so that there is no numerical instability. Therefore the time step size is chosen to be 60 seconds. This time step size is small enough to respect the stability criteria for every thermal node in the model:

$$\Delta t \leq \frac{1}{2} \times \frac{\rho \cdot C_p \cdot \Delta x^2}{\lambda}$$

Where Δt is the time step size and Δx, λ, ρ, and Cp are the thickness, the thermal conductivity, the density and the specific heat capacity of a finite control volume, respectively.

For the construction elements of the envelope, the long wave radiation to the sky and to the surrounding are calculated according to the tilt angle of the surface, the surface emissivity, the sky temperature, the surrounding temperature, the outdoor air temperature, cloud cover, atmospheric pressure, outdoor relative humidity and the position of the sun in the sky. The difuse and direct short wave solar radiation reaching the external surfaces are directly extracted from a BSim reference model of the study case building.

For the nodes of the construction elements facing the indoor environment, the short wave radiations of the solar loads and the radiative part of the other internal gains are taken into account. The Surface nodes of each construction element is connected to the outdoor air node or to the appropriate thermal zone air node within a star network configuration with constant mixed convection/radiation surface thermal resistance coefficients (See **Table 6** and **Figure 26**) [35].

Name		Value	Unit
Internal, combined surface resistance	upward heat flow vertical heat flow downward heat flow	0.10 0.13 0.17	m²K/W
External, combined surface resistance	upward heat flow vertical heat flow downward heat flow	0.04 0.04 0.04	m²K/W
External, combined surface resistance for constructions facing ground		1,50	m²K/W
Internal convective resistance	floors ceilings walls	0.40 0.50 0.33	m²K/W

Table 6: *Mixed convection / radiation surface thermal resistance coefficient [35].*

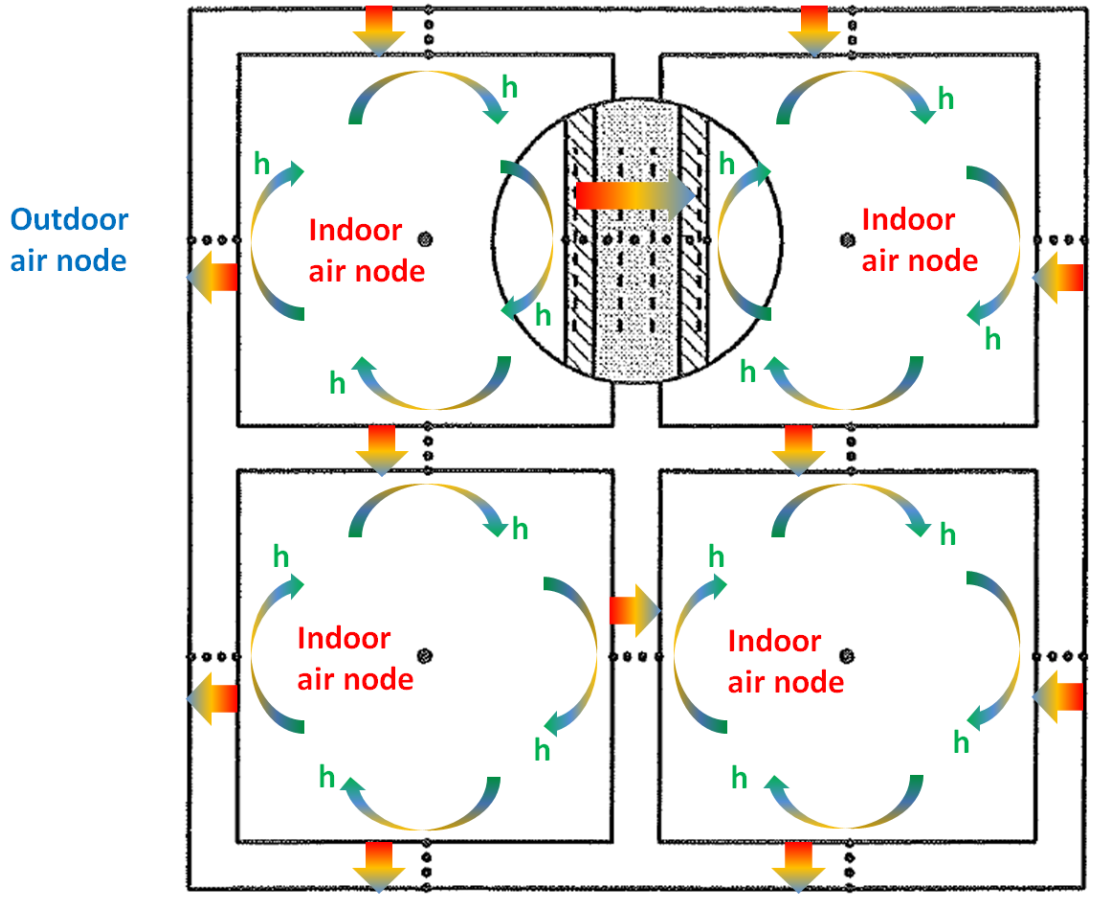

Figure 26: *Coupling of thermal nodes in start network.*

2.2.Windows, Thermal Bridges, Ventilation and Infiltration Losses

Heat losses through windows, thermal bridges, ventilation and air infiltration are modeled in a simple way. A constant U-value is used for windows and thermal bridges heat losses. It is assumed that there is no thermal mass in these elements.

Heat losses due to air infiltrations are also treated in a simple way with the following formula:

$$\boldsymbol{Q_{infiltr\,air} = \dot{V}_{infiltr\,rate} \times \rho_{air} \times C_{p\,air} \times (\theta_{outdoor} - \theta_{indoor})}$$

Ventilation heat losses are calculated with the same formula but taking into account the heat recovery (if any):

$$\boldsymbol{Q_{ventilation} = \dot{V}_{ventilation} \times \rho_{air} \times C_{p\,air} \times (\theta_{inlet} - \theta_{indoor})}$$

with

$$\theta_{inlet} = \eta_{heat\,recov} \times (\theta_{exhaust} - \theta_{outdoor})$$

The inlet air temperature from the heat recovery ventilation unit is limited to 24 °C. Above that temperature, the heat recovery is turned off. Natural ventilation during summer period is simulated by increasing the ventilation rate without any heat recovery process.

2.3.Zone Air Node

All the element blocks of the different building systems are connected together to the air node of the thermal zone. One can see on the **Figure 27** that the thermal zone air node heat balance is made with the heat fluxes coming from the different elements interacting with it: building elements, solar gains, internal gains, convective heating system, ventilation, infiltration, windows and thermal bridges.

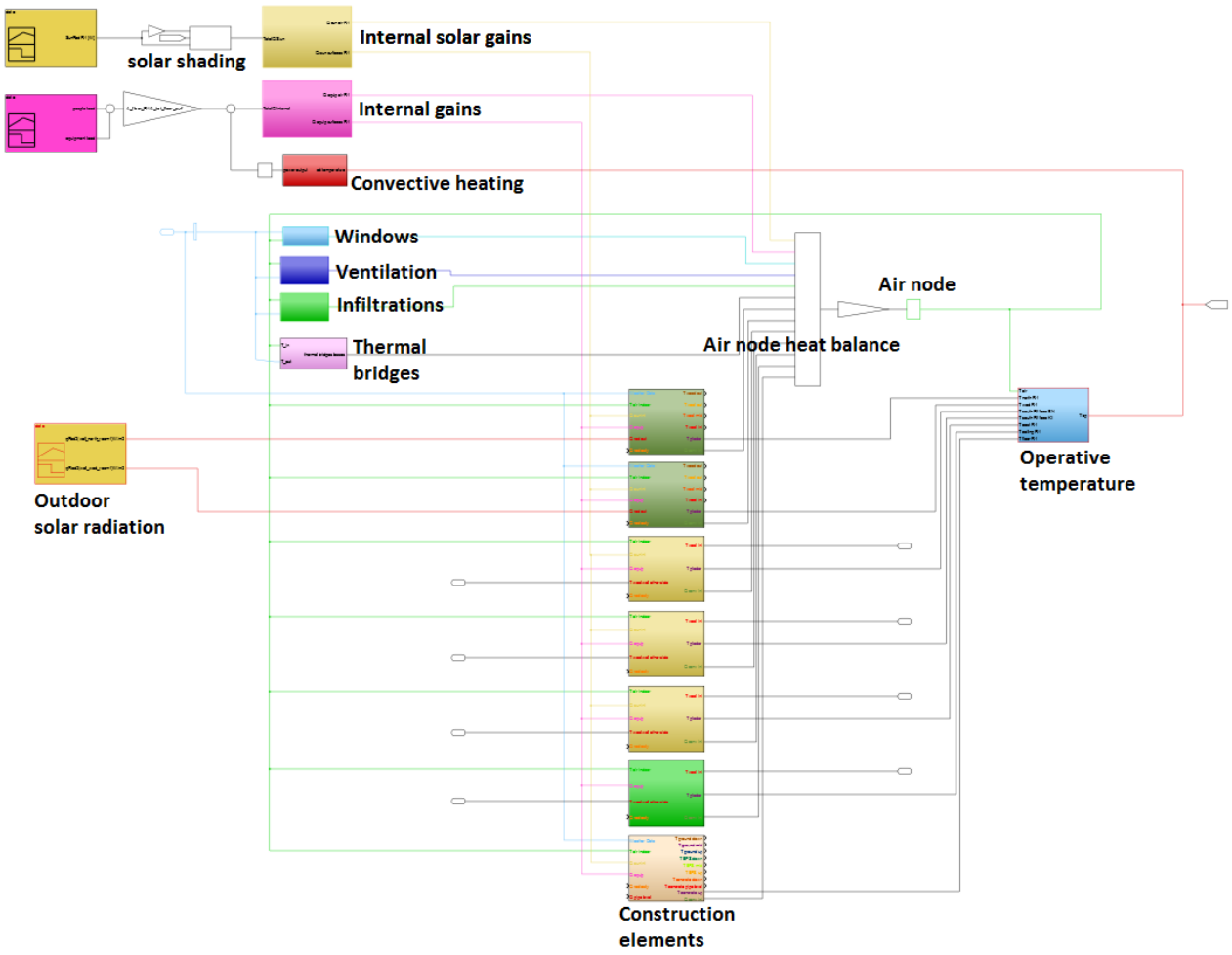

Figure 27: *Thermal zone model – all element blocks connected to the air node of the zone.*

The air temperature and the temperature of all thermal zone surface elements are taken into account for the calculation of the operative temperature. The latter is then used as process variable for the controller of the heating system.

2.4.Multi-Zone Building Model

The different thermal zones of the building model are connected together to form the multi-zone model of the building (See **Figure 28**). The temperature in the middle of a internal partition walls is used as boundary condition for the wall element adjacent to the thermal zone.

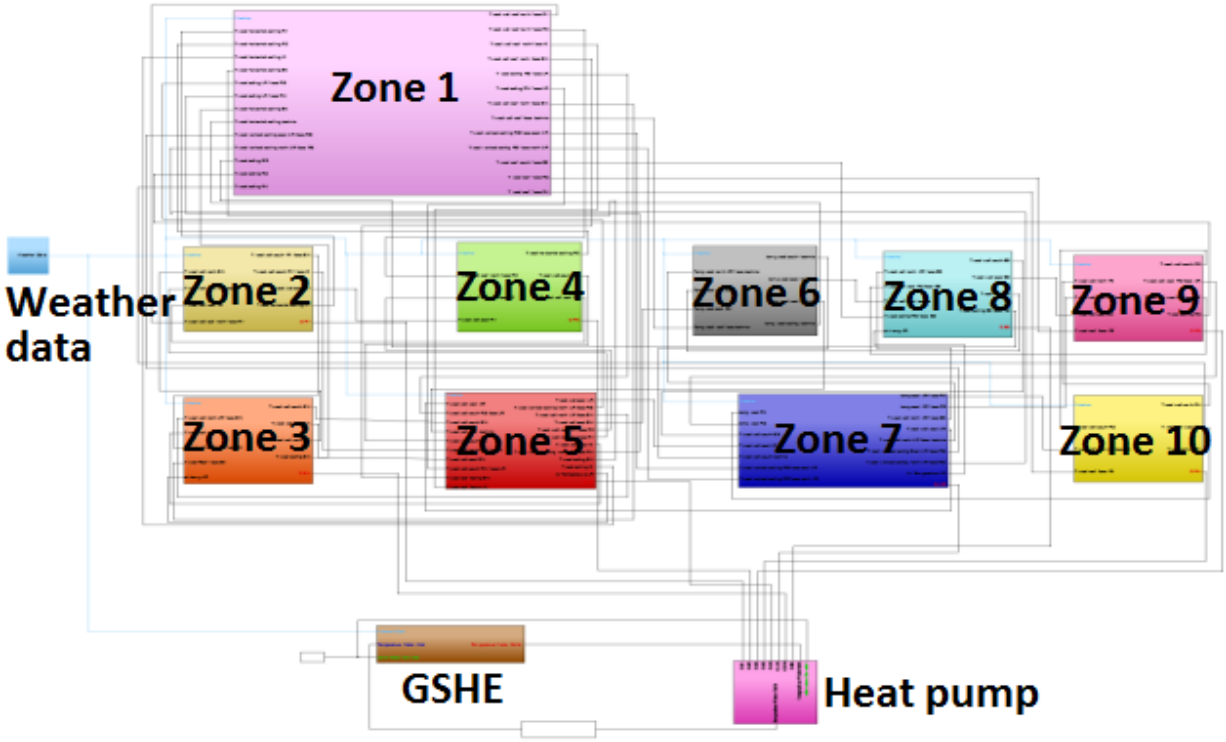

Figure 28: *Overview of the multi-zone building model.*

2.5.Weather Data

The weather data is taken from the national Danish Reference Year (DRY 2013) based on weather station measurements from 2001 to 2010 and updated in 2013 by the Danish Building Research Institute (SBi). These data has been selected to be used for energy performance calculations and building simulations in Denmark [36].

The parameters included in the dataset are temperature, relative humidity, wind speed and direction, atmospheric pressure, global radiation, cloud cover, soil temperature, sea temperature, diffuse irradiance and illuminance. The time resolution is hourly except for soil temperature where the resolution is daily values.

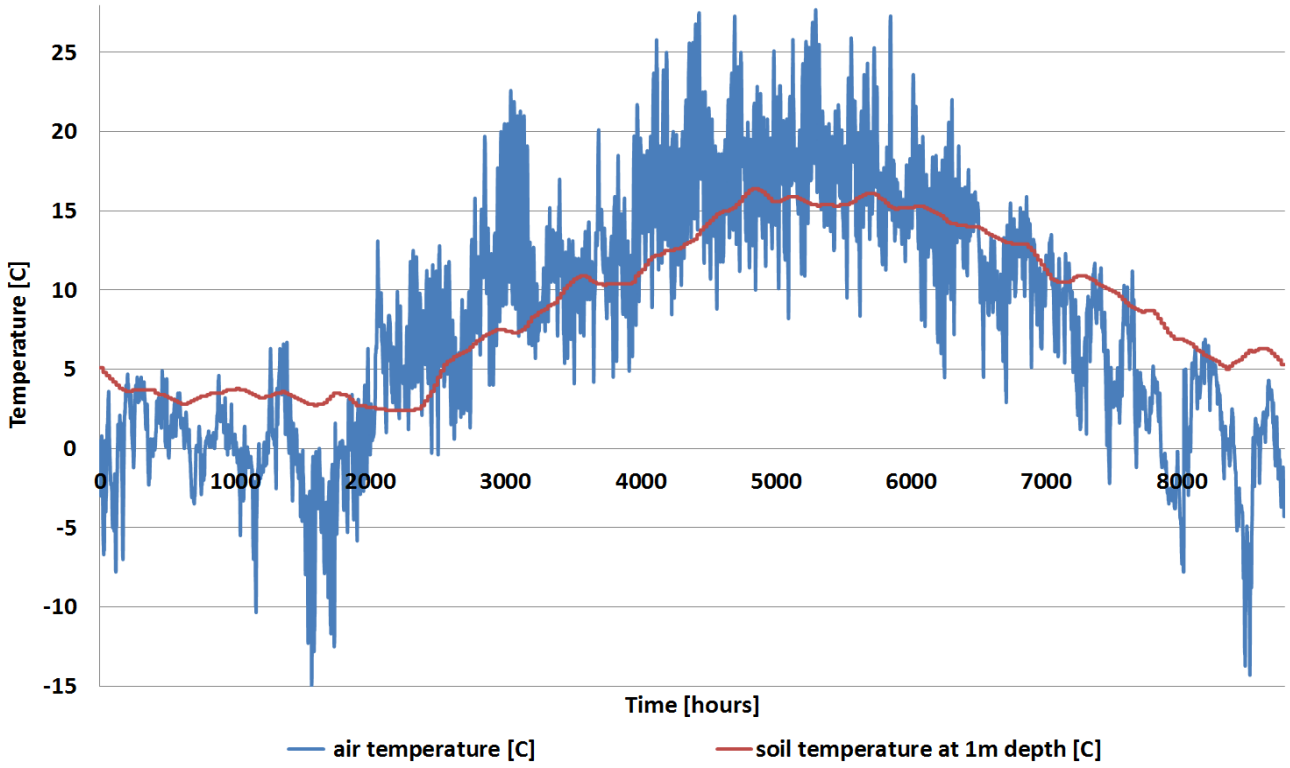

Figure 29: *Outdoor air and ground temperature for the reference year in Denmark (DRY 2013).*

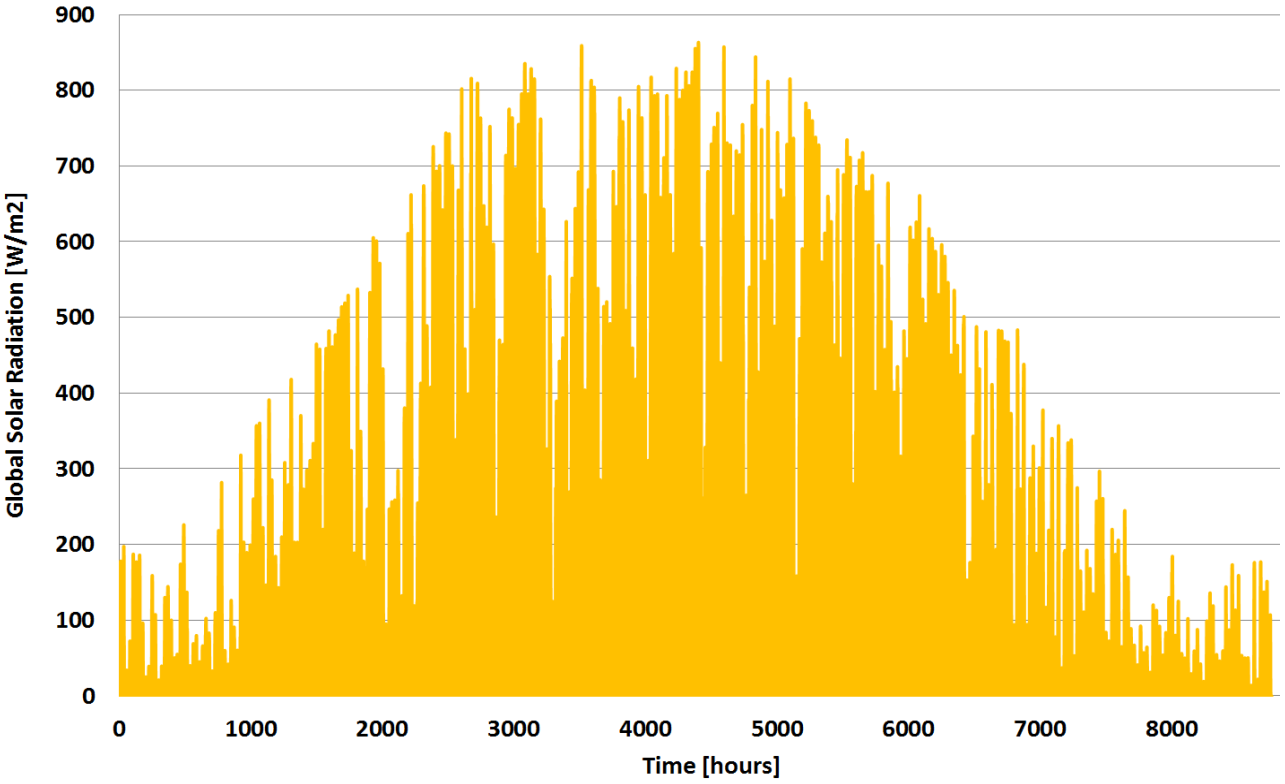

Figure 30: *Global outdoor sun radiation for the reference year in Denmark (DRY 2013).*

2.6.Solar Gains and Internal Gains

Internal thermal gains (excluding the heating system's load) originate from the heat released by the occupants during occupying time and the heat released from the house equipment such as computers, lightning, oven, TV, etc. A standard person has heating power of around 100 W and generates 0,06 kg of moisture and 17 L of CO2 per hour.

The equipment and people load schedules are based on typical Danish equipment use and people schedule for a residential house [37]. The overall internal gains time profile of the house is presented in **Table 7** and **Figure 31**. Each type of room (living room, bedroom, bathroom) has a specific people/equipment loads weekly schedule accounting for realistic average internal loads to these rooms.

4 People Schedule							
Time \ Day	Monday	Tuesday	Wednesday	Thursday	Friday	Saturday	Sunday
1	4	4	4	4	4	4	4
2	4	4	4	4	4	4	4
3	4	4	4	4	4	4	4
4	4	4	4	4	4	4	4
5	4	4	4	4	4	4	4
6	4	4	4	4	4	4	4
7	2	2	2	2	2	4	4
8	2	2	2	2	2	4	4
9	0	0	0	0	0	2	2
10	0	0	0	0	0	2	2
11	0	0	0	0	0	2	2
12	0	0	0	0	0	2	2
13	0	0	0	0	0	2	2
14	0	0	0	0	0	2	2
15	0	0	0	0	2	2	2
16	0	0	0	0	2	2	2
17	2	2	2	2	4	4	4
18	4	4	4	4	4	4	4
19	4	4	4	4	4	4	4
20	4	4	4	4	4	4	4
21	4	4	4	4	4	4	4
22	4	4	4	4	4	4	4
23	4	4	4	4	4	4	4
24	4	4	4	4	4	4	4

Table 7: *Schedule of the people load for a typical single family house in Denmark.*

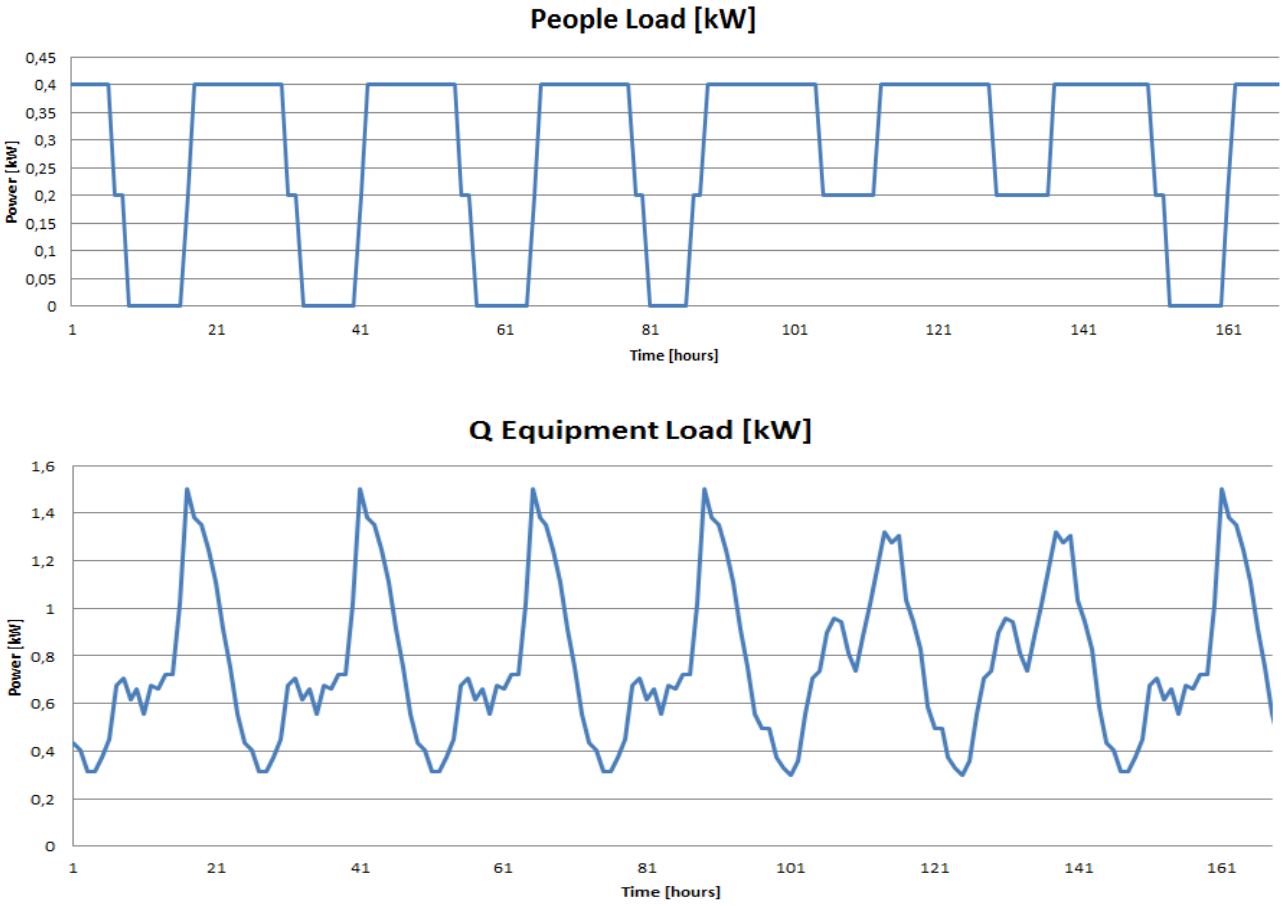

Figure 31: *Time profile of the internal gains of a typical single family house in Denmark.*

The internal solar gains (the direct, diffuse and reflected solar radiation entering the indoor environment and not leaving it) are directly extracted from the BSim reference model of the study case building for each thermal zone and for each hour of the year.

The distribution of the equipment, people and radiator heat load is as follow: 70% goes directly to the air node of the thermal zone; 30% goes to the internal surfaces of the thermal zone (long wave radiation share). The radiative share is equally distributed over all surfaces in function of their surface area weighing [35].

The distribution of the internal solar gain is as follow: 15% goes directly to the air node of the thermal zone; 55% goes to the floor; 30% goes to the vertical walls of the thermal zone and is equally distributed over these surfaces in function of their surface area weighing; no solar radiation goes to the ceiling [35].

In the case of additional indoor thermal mass / furniture in the indoor space, 50% of the radiative share of the equipment, people, solar and radiator heating loads is distributed on the surfaces of the equivalent planar element modeling the furniture.

2.7.Radiator Heating System

Two types of heating emitters are investigated in this study: radiator and water-based under floor heating system.

The radiator heating system is modeled in a simple way with a first order transfer function which has a time constant of 10 minutes [38]. The radiator is regulated with a PI controller. 30% of its heat output is transferred to the indoor environment by radiation and 70% by convection.

2.8.Hydronic Under-Floor Heating Systems

In most building energy software tools, the conductive heat transfer through the building construction is evaluated assuming a one-dimensional heat flow and homogenous surface temperature. For a hydronic radiant floor terminal, the correct modeling of the conductive flow is more difficult due to the three-dimensional heat transfers at the pipe level. The conductive flow at the activated surface (embedded pipe level) is mainly influenced by the type of pipe (diameter, wall thickness and material), the pipe spacing, the water flow (water velocity) and the resistance of the conducting layers. Different calculation methods have been developed to model the conductive flow from the pipe level to the surface with the objective of either calculating the heating/cooling capacity of the radiant systems or of simulating their dynamic behavior in building energy software tools:

- Glück B [39] [40] has developed an analytical solution of the thermal field due to the presence of pipes embedded in an infinitely long slab under steady-state conditions. However the consequent analytical solution is very complex, needs a significant computer calculation time to be obtained, does not take into account the different material layers (pipe, insulation, concrete screed) and therefore cannot be widely applied.

- Most of the models are based on a one-dimensional Resistance - Capacitance network, similar to the technique described in the standard EN 15377-1 [17]. The principle of this calculation method is to determine an equivalent resistance between the heating or cooling medium to the fictive core (or heat conduction layer) where the pipes are located. The variation of fluid temperature along the circuit is modeled considering the pipe circuit as a heat exchanger. The three-dimensional domain collapses into a simpler 1D problem and the efficiency of such heat exchanger is computed via the ε-NTU (effectiveness-Number of Transfer Units) method. Koschenz and Lehmann [41] [42] have developed the calculation procedure for TABS and this model has been extended for other systems by De Carli, Koschenz, Olesen and Scarpa in the standard EN 15377-1. Scarpa et al. [43] developed and validated the RC model for different geometries of radiant systems. It has to be noted that the accuracy of these RC models is greatly affected by the determination the thermal properties of the different RC components.

- Other methods have been developed such as the conduction transfer function method from Strand and Pedersen [44], the response factors technique from De Carli et al. or the universal single power function of the standard EN 1264-2 [16]. More detailed models, which are evaluating the conductive heat transfer based on two-dimensional calculations (FEM, FVM), are also available.

The modeling of the hydronic components in this study is based on the ε-NTU method developed by Scarpa et al. [43] to represent the complex interaction between the embedded pipes and the conductive slab, and a "plug-flow" principle model, similar to the Type 31 model from TRNSYS 17 software [45], in order to account for dynamics of the fluid pushed into the pipes.

For high fluid flow in hydronic system, the time needed for a fluid cell to go through the whole pipe's length is smaller than the time step size of the model. In that case, it is assumed that the fluid subsystem in the pipe reaches a pseudo-steady state within the time step. Therefore the calculation of the fluid temperature profile is performed according to the ε-NTU method.

On the other hand, for low fluid flow, a fluid cell can take several simulation time steps before reaching the outlet of the hydronic loop. In that case, the calculation of the fluid temperature profile is performed according to the "plug flow" principle [45]. As shown on **Figure 32**, at each time step, one fluid cell is added at the beginning of the pipe (queuing in). The new fluid control volume "Ti" pushes all the other control volumes towards the exit of the pipe without any mixing in between adjacent cells (plug flow principle). Heat transfer in between adjacent cells could be considered if there would be some correlation of mixing and heat transfer in between these cells for a pipe, but this is not the case here. This no-mixing assumption is reasonable if the fluid is circulating with a fairly high velocity and if the temperature difference in between each cell is not too important.

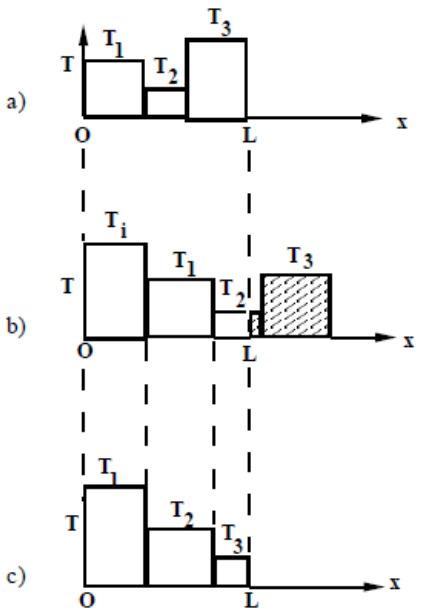

Figure 32: *Plug flow principle.*

The outlet temperature is calculated as volume weighted average temperature of the fluid cells exiting the hydronic system. If the pipe is very long and the flow is very small, a lot of small fluid cells will get stacked into the model queue. To avoid memory issues, the maximum number or fluid cells in the systems is limited

to 100. When the maximum number of fluid cells is reached, the 2 neighboring cells with the smallest temperature difference are merged together and assigned an appropriate new average temperature. The heat exchanger between the fictitious pipe level slab and each fluid cell is performed according to the ε-NTU method.

The water temperature change along the pipe is considered following an exponential decay function. The logarithmic mean fluid temperature along the pipe circuit may be assumed as a reference for the estimation of the heat exchange between the fluid and the inner surface of the pipe. The temperature of the pipe is assumed constant with respect of its length. The ε-NTU calculation is performed with the effectiveness of the equivalent heat exchanger formed by the embedded pipe in the conductive slab of the under-floor heating system. This effectiveness is determined by the thermal resistance of the fluid in the pipe, the thermal resistance of the pipe itself, the thermal resistance of the different layers of the slab and an equivalent thermal resistance. The latter accounts for the complex three-dimensional interactions between the different sections of the serpentine pipe layout network with the rest of the conductive slab where it is positioned [43] (See **Figure 33**).

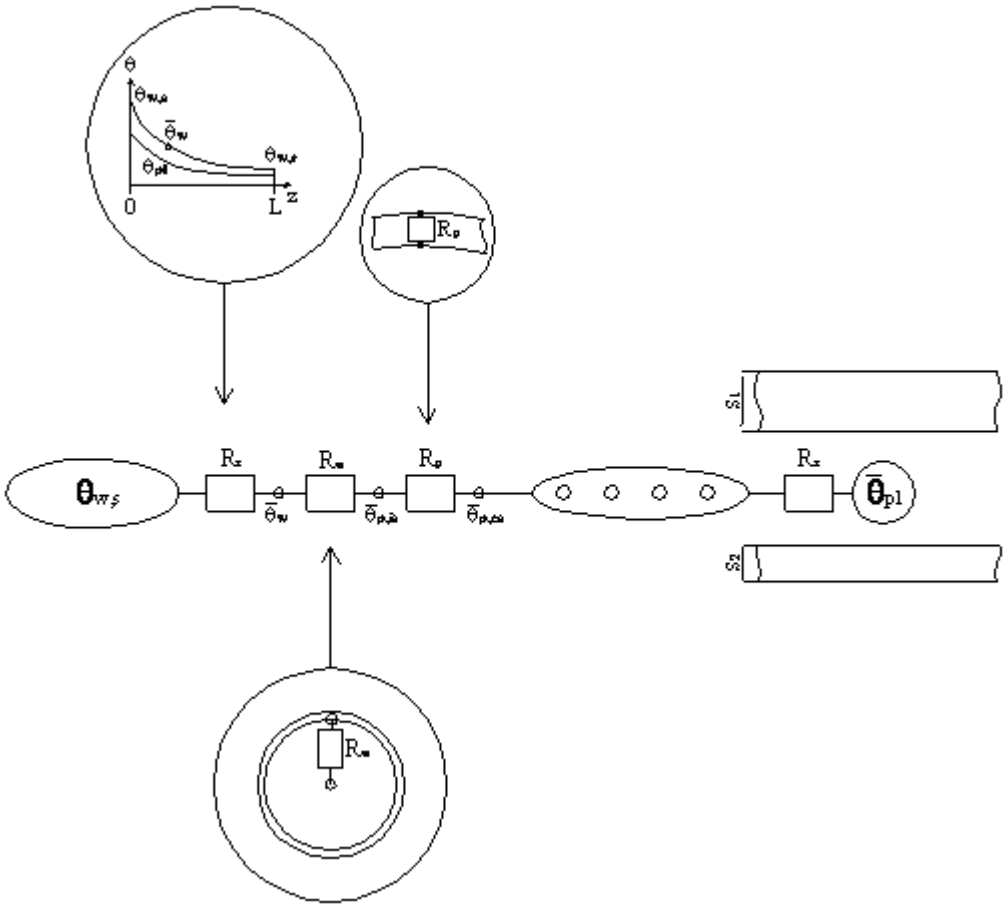

Figure 33: *Schematic of the equivalent RC network of the hydronic floor heating system.*

The convective thermal resistance of the fluid in the pipe is calculated precisely, taking into account the nature and concentration of the brine additive product, its temperature, density, thermal conductivity, specific heat capacity, dynamic viscosity and Reynolds number.

The whole hydronic system model is implemented as a MATLAB function nested into a Simulink block function.

The study case buildings include two types of under floor heating system. The type A concrete screed floor heating is modeled as a concrete slab subdivided in 3 layers: upper concrete layer, pipe level layer and bottom concrete layer. The interaction thermal resistance of the pipe level layer is calculated according to the method detailed by Scarpa et al. [43]. Similarly, the type G wooden floor heating system is also subdivided in 3 wood layers. The interaction thermal resistance between the carrier fluid, the emission plates and the pipe level layer is calculated according to the method detailed in the standard EN 15377 Annex C (see **Figure 34**) [17].

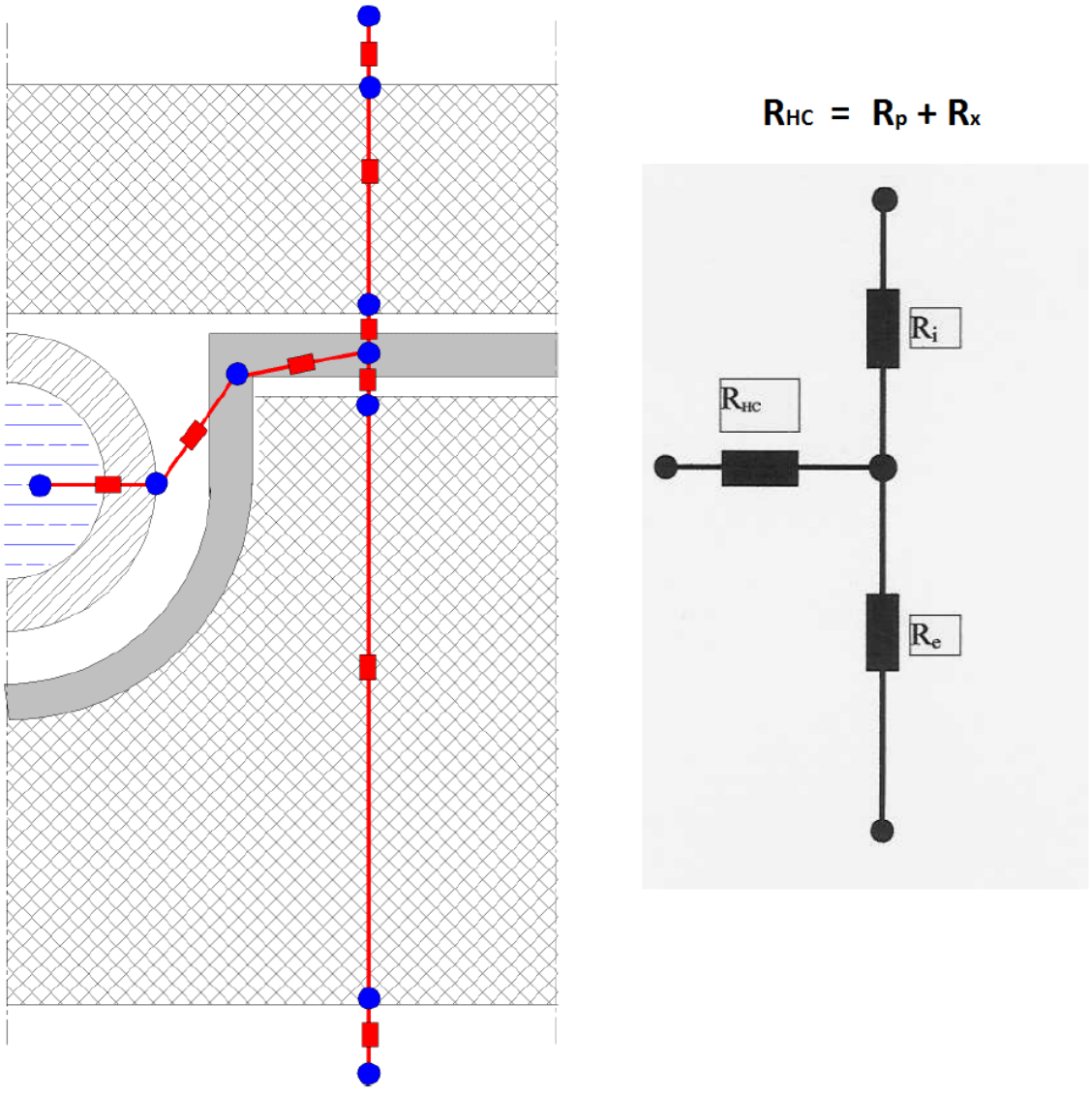

Figure 34: *RC network of a type G wooden floor heating system [17].*

2.9.Horizontal Ground Source Heat Exchanger

Horizontal ground source heat exchangers are buried at depths ranging between 0.8 and 2 m and their performances are also influenced by weather conditions at the soil surface (See **Figure 35**).

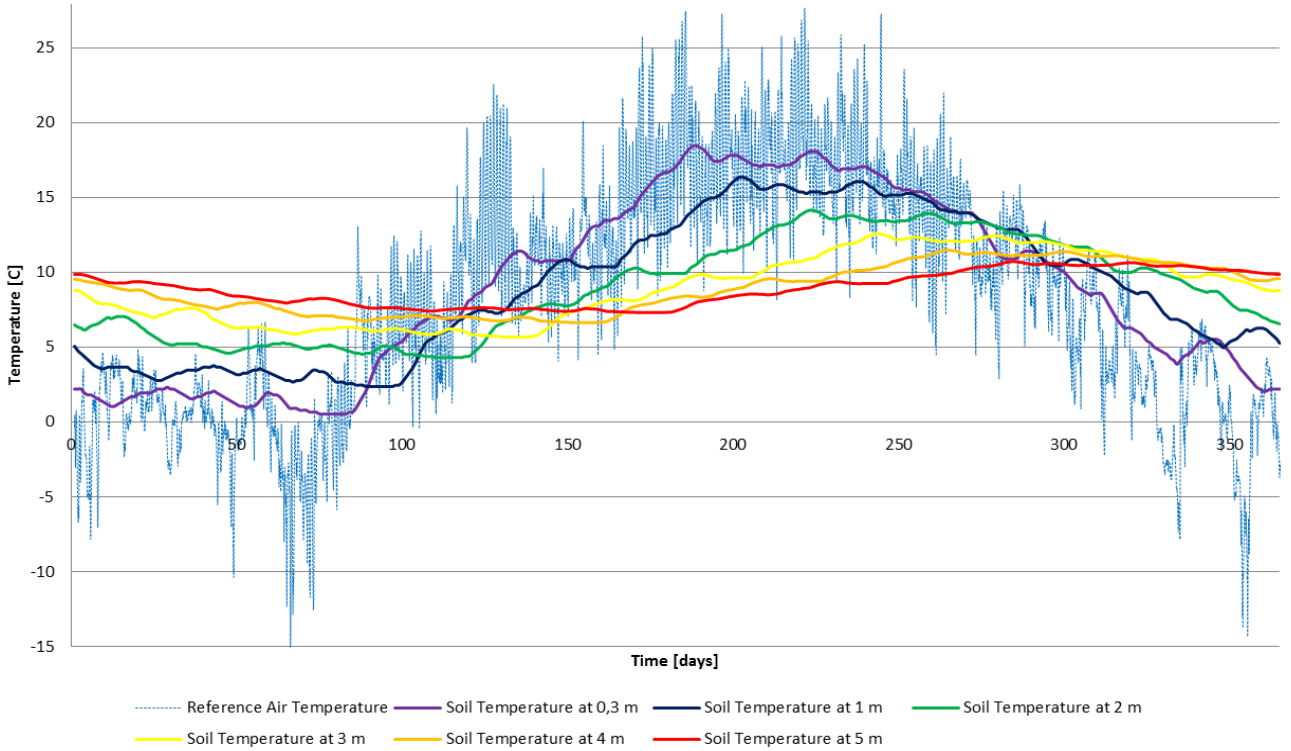

Figure 35: *Ground temperature in Denmark.*

Similarly to the under-floor heating system, the horizontal ground source heat exchanged is modeled with the plug flow / ε-NTU method function. The ground domain is modeled with a state-space function (See **Figure 36**) which represents a soil cube of 12 x 25 m with a depth of 30 m. The bottom boundary conditions of the ground domain are set as constant temperature of 9.4 °C. The boundary conditions of the top surface of the ground domain are determined by the weather data: outdoor air temperature, wind speed and global solar radiations. The temperature boundary conditions on the sides of the domain are following the temperature time variation of the undisturbed ground temperature in Denmark.

$$\{\dot{\theta}\} = [A] \cdot \{\theta\} + [B] \cdot \{u\}$$

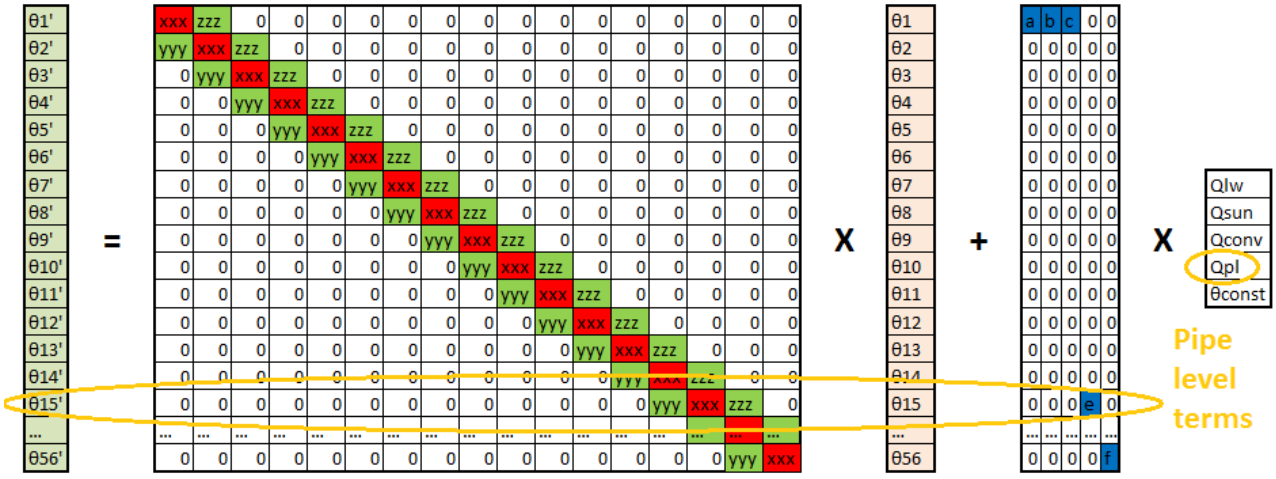

Figure 36: *State space representation of the ground domain.*

The soil domain reduced into a one-dimensional heat transfer system. It is discretized into ground 29 slices of 10 cm (on the top half), 27 slices of 1 m (on the bottom half) and slice of 20 cm for the fictitious pipe level.

2.10. Vertical Borehole Ground Source Heat Exchanger

The vertical borehole ground source heat exchanger is modeled with two plug flow / ε-NTU method MATLAB functions coupled together. The inlet section of the U-pipe is modeled with the first function and the outlet section of the U-pipe is modeled with the second function. The two pipe models are connected to the surrounding ground represented by a state-space model function with concentric cylindrical slices of ground. The ground slice subsystems are 100 m deep and 10 cm or 1 m thick. The ground domain is therefore discretized into 16 volumes accounting for the ground which is 10 m apart from the center of the GSHE.

The complex thermal interaction between the U-pipe of the heat exchanger, the grout and the ground is modeled with a triangular thermal network (RC network) (See **Figure 37**). This thermal network modeling is presented in details in a journal paper of Diersch et al. [46].

The initial temperature conditions for the ground domain are set as the yearly average temperature profile of an undisturbed soil in Denmark (See **Figure 38**). The bottom boundary conditions of the ground domain are set as constant temperature of 10.1 °C, while the boundary conditions of the top surface of the ground domain are determined by the weather data: outdoor air temperature, wind speed and global solar radiations.

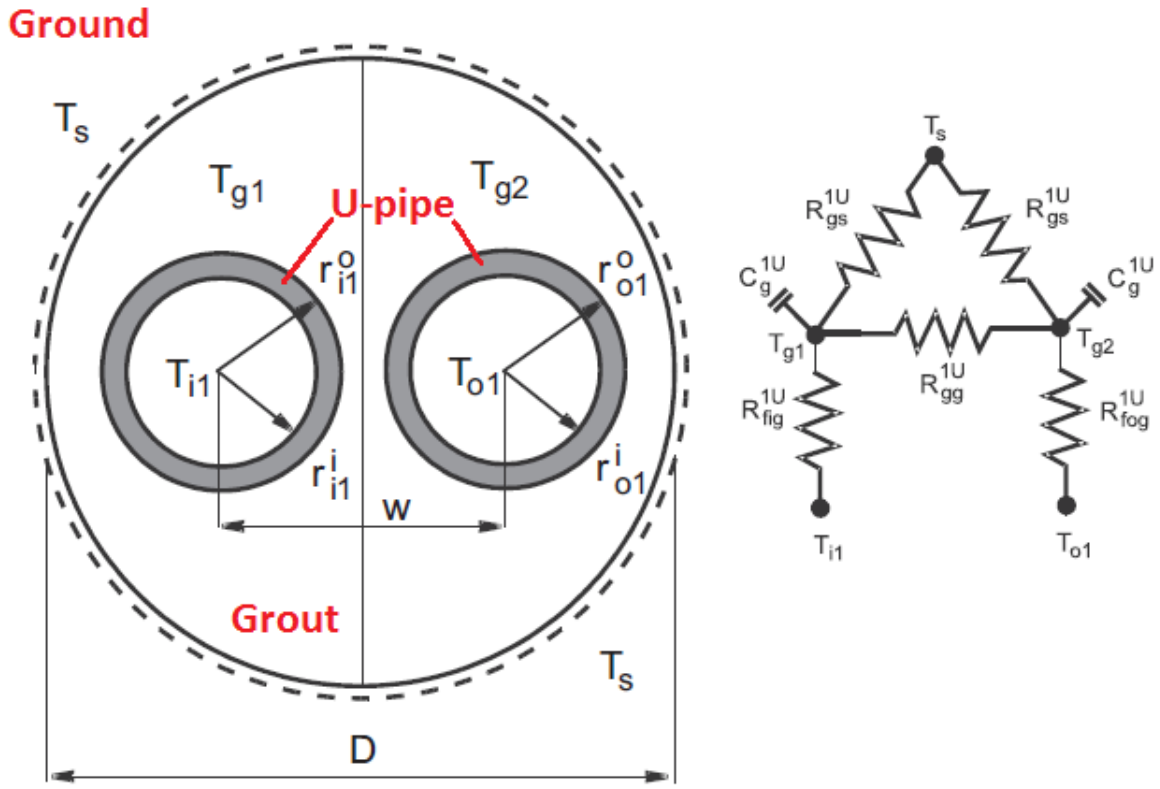

Figure 37: *RC network modeling the heat transfer between the U-pipe, the grout and the surrounding ground domain [46].*

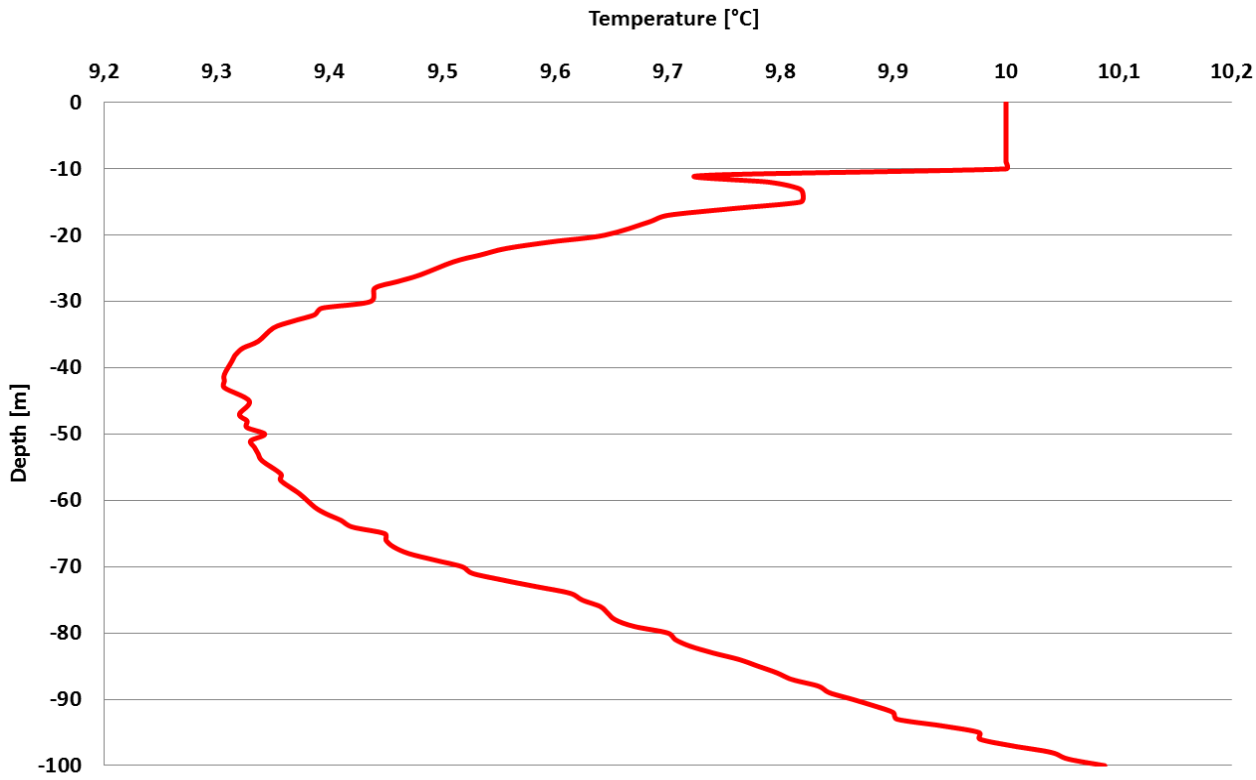

Figure 38: *Yearly temperature profile of undisturbed soil in Denmark.*

2.11. Water-Based Brines of the Hydronic Networks

In order to calculate precisely the heat transfer between the brine carrier fluid and the heat exchanger, all physical and thermal properties of 5 fluids have been modeled with polynomial correlations based on manufacturer's database. Density, thermal conductivity, specific heat capacity and dynamic viscosity are calculated in function of fluid temperature and brine product concentration for pure water, propylene glycol, ethylene glycol, ethanol or methanol. These 5 products are the most commonly used brine fluids in hydronic systems. One can see on **Figure 39 – 44** some of the polynomial correlations established from tabulated data of manufacturers and textbooks [47] [48] [49] [50] [51] [52] [53] [54] [55] [56] [57] [58] [59] [60] [61] [62] [63] [64] [65].

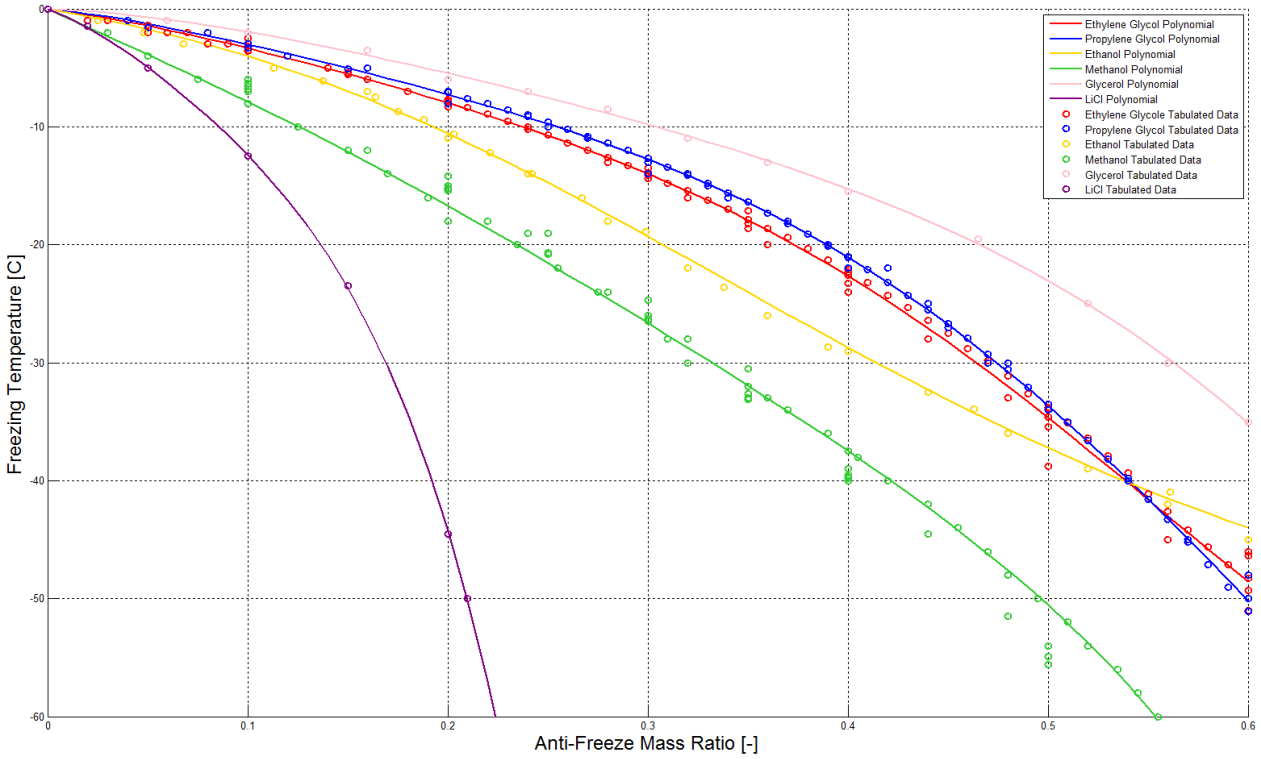

Figure 39: *Water-based brine freezing temperature in function of product concentration.*

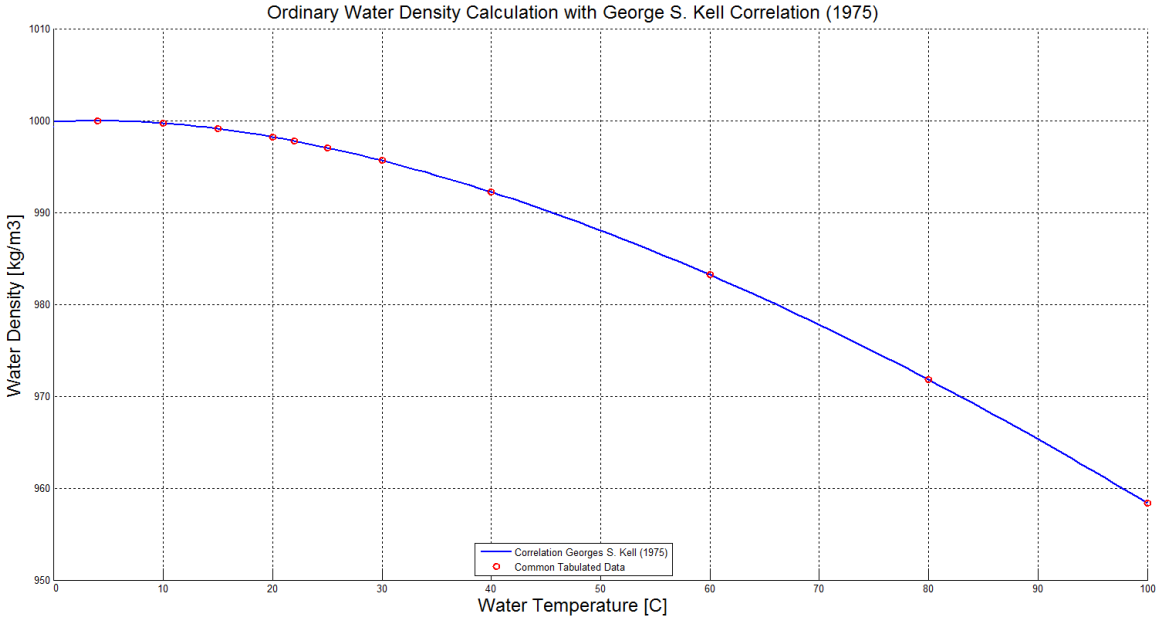

Figure 40: *Ordinary water density in function of temperature.*

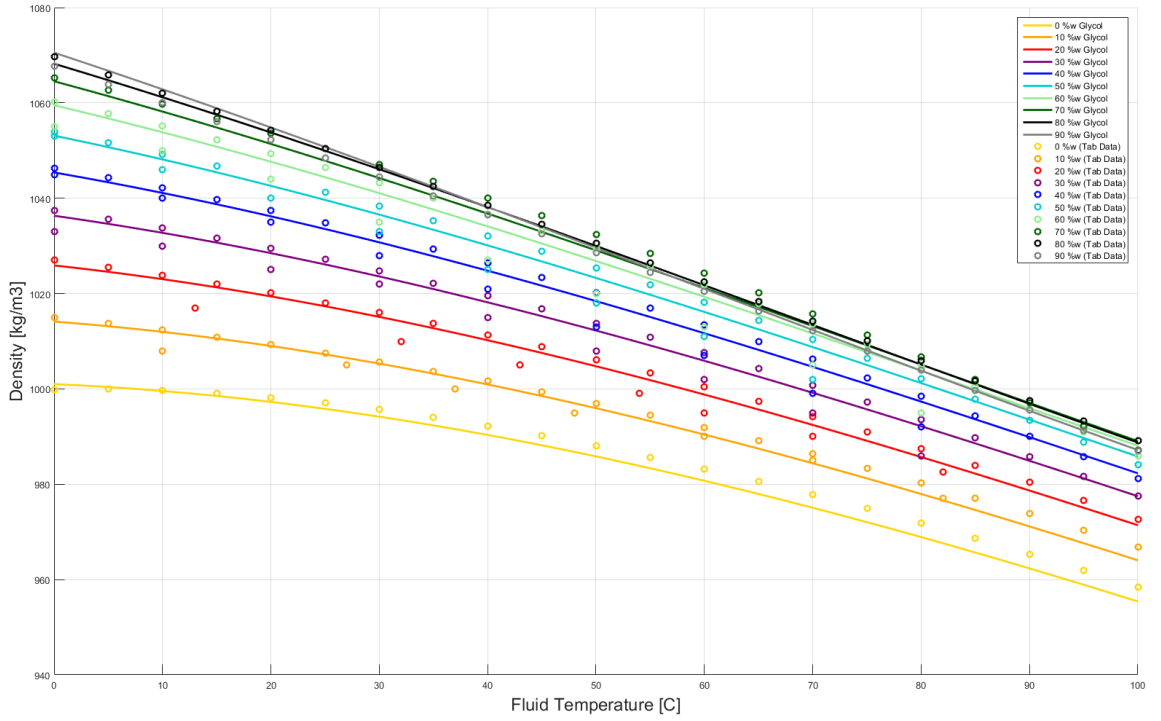

Figure 41: *Propylene glycol density in function of temperature and concentration.*

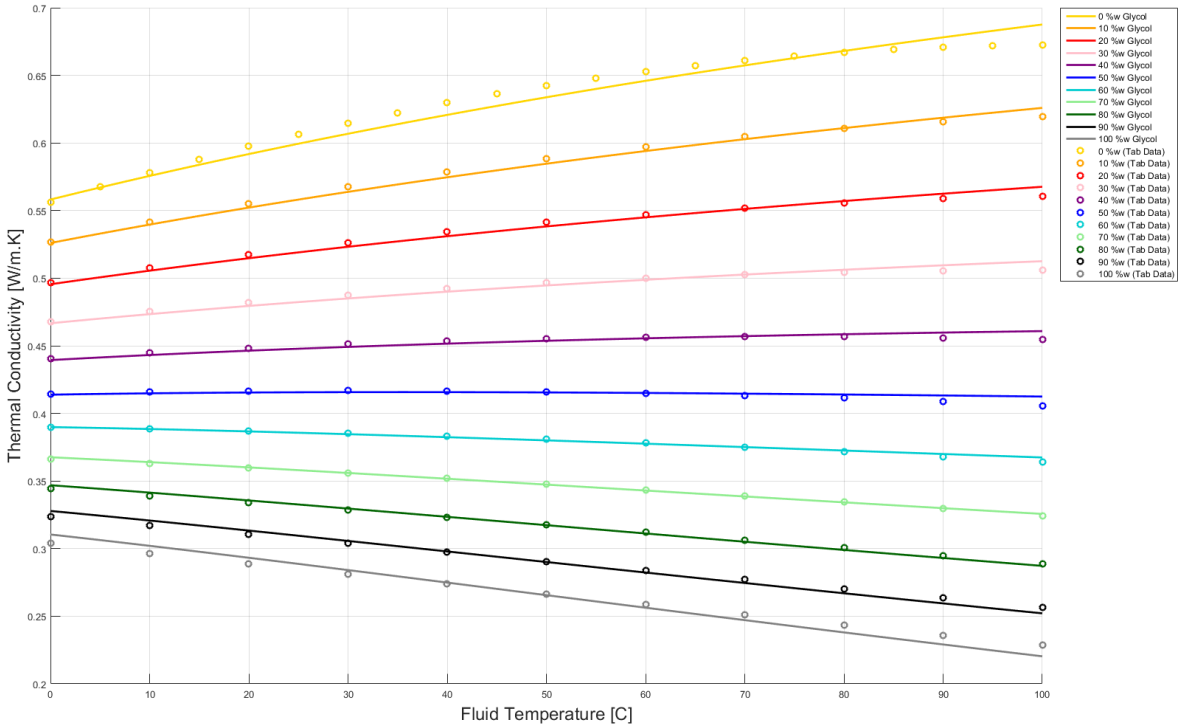

Figure 42: *Ethylene glycol thermal conductivity in function of temperature and concentration.*

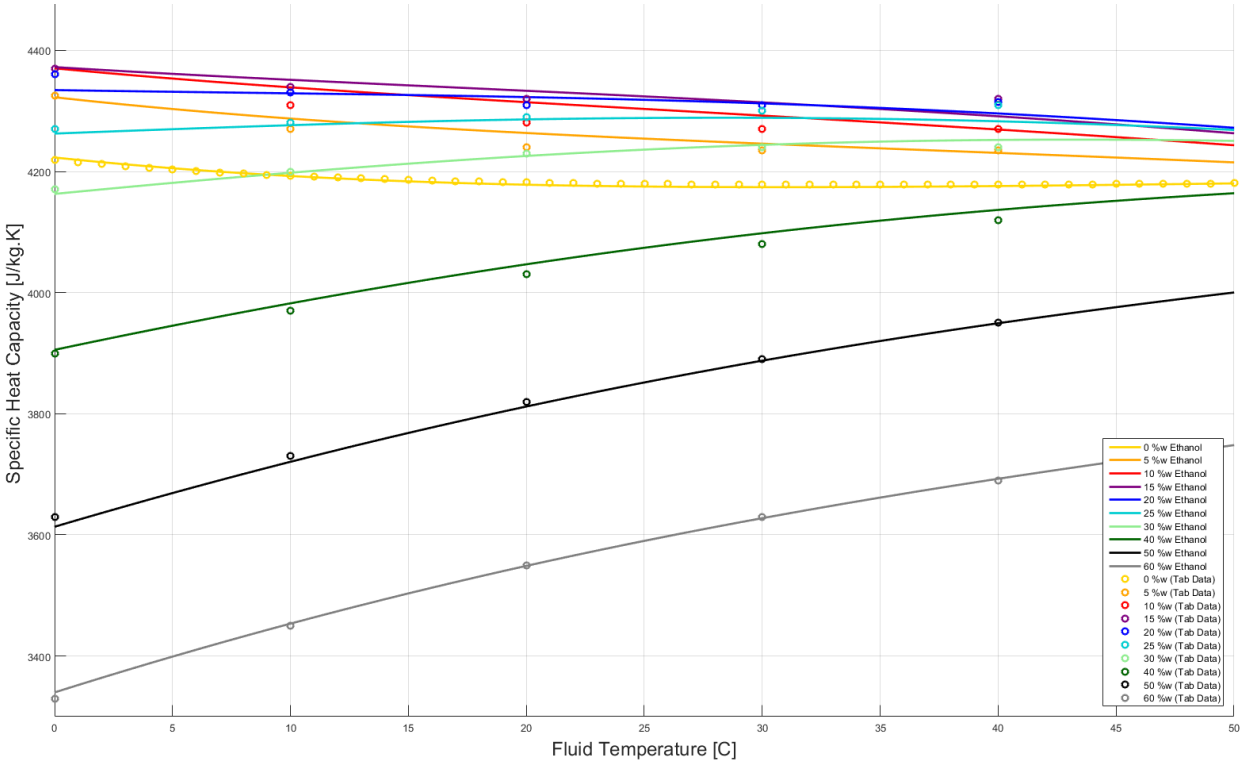

Figure 43: *Ethanol specific heat capacity in function of temperature and concentration.*

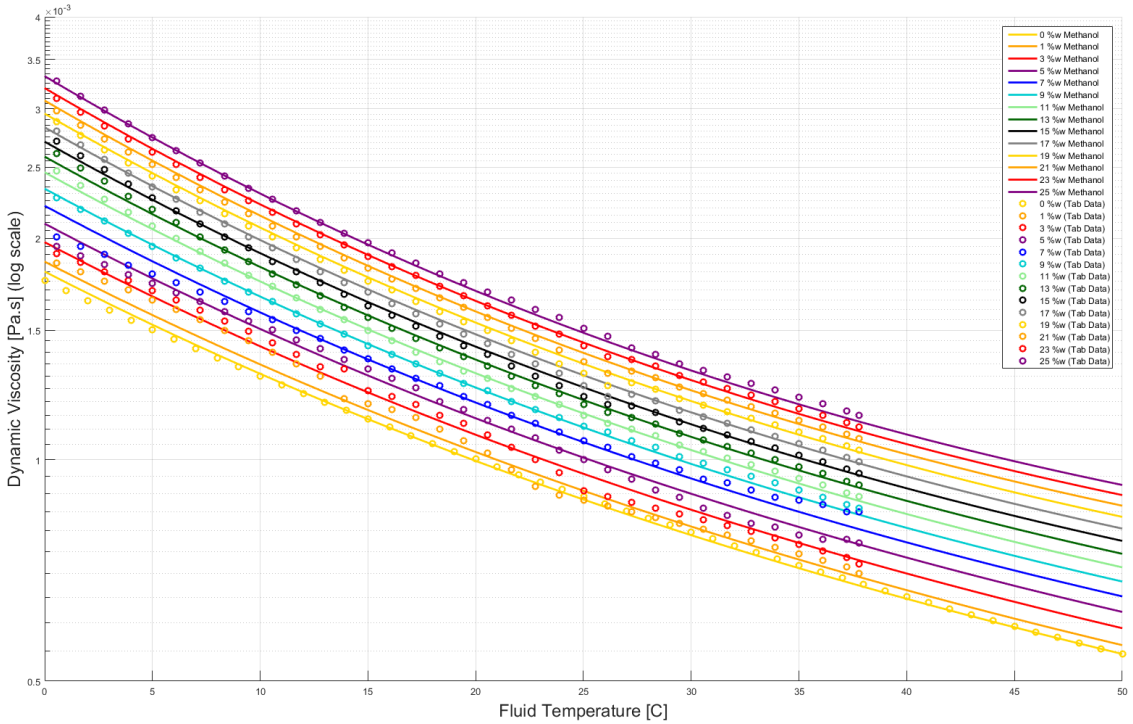

Figure 44: *Methanol dynamic viscosity in function of temperature and concentration.*

The Prandtl number, the Reynolds number, the Darcy friction factor (see **Figure 44**) and the Nusselt number are then derived from the thermo-physical properties of the brine.

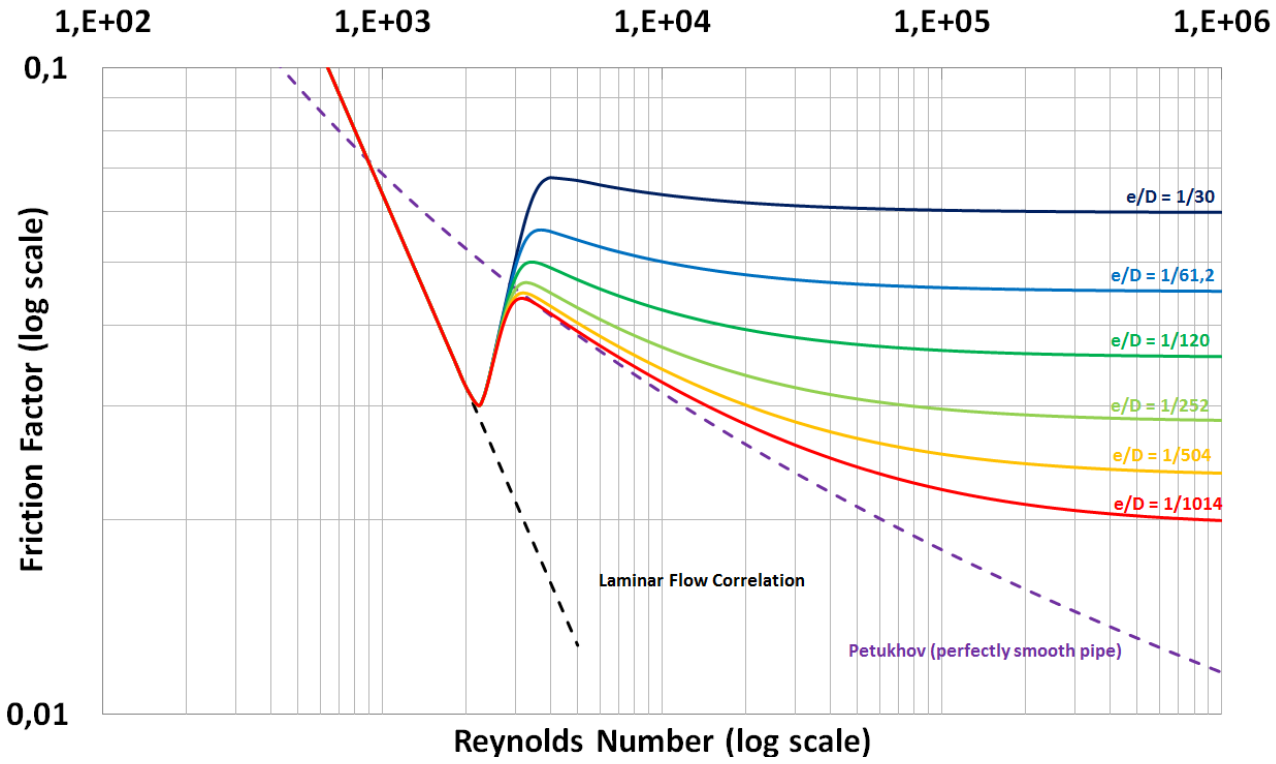

Figure 48: *Darcy friction factor (correlation Churchill 1977).*

Finally, the convective heat transfer coefficient and the convective thermal resistance are calculated for the circular pipe (See **Figure 46 – 47**).

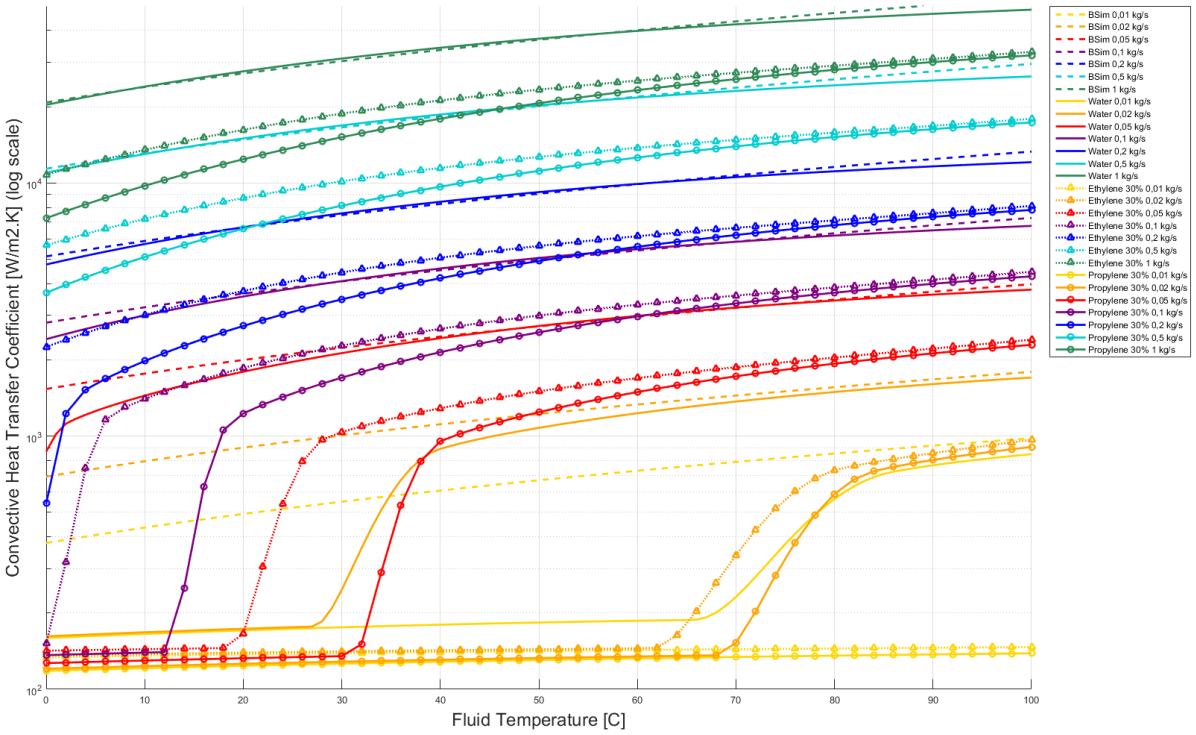

Figure 46: *Convective heat transfer coefficient in circular pipe (Di = 13 mm, e = 0.0015 mm, L = 100 m).*

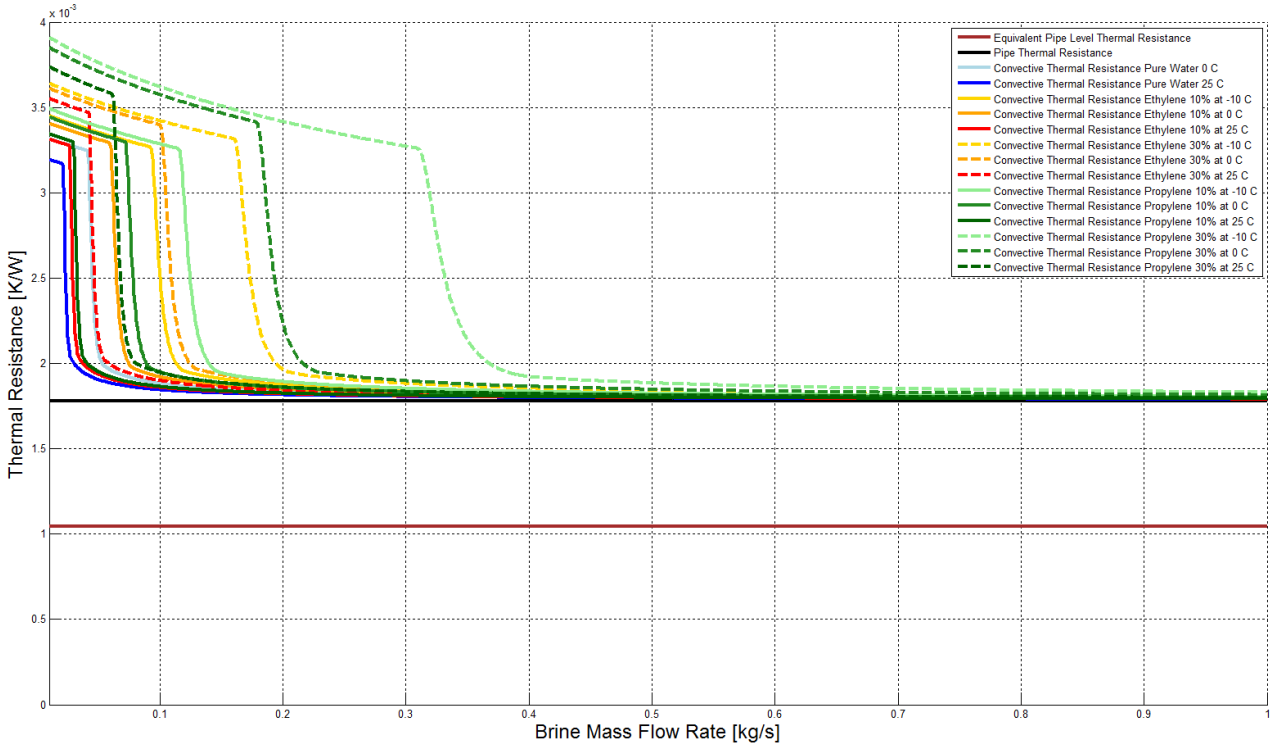

Figure 47: *Floor heating heat exchanger thermal resistance (Di = 13 mm, e = 0.0015 mm, L = 100 m).*

2.12 Pressure Loss in the Hydronic Systems

In order to evaluate the energy consumption of the entire system, the pumping workloads are assessed by calculating the total pressure drop of the whole hydronic system. The latter is obtained by adding the pressure drop across the piping loops, the manifold, the valves, the mixer the supply and return pipes. The system is a closed loop, therefore the inlet and the outlet are at the same altitude and so there is no pressure loss due to inlet and outlet height difference.

The pressure drop in straight pipes caused by fluid friction in fully developed flows of all "well-behaved" (Newtonian) fluids is described by the Darcy-Weisbach equation:

$$\Delta p = f \frac{L \rho v^2}{2D}$$

Valves and fittings cause singular pressure losses that can be greater than those caused by the pipe alone. They are expressed as:

$$\Delta p_i = K_i \frac{\rho v^2}{2}$$

5 different methods have been implemented to calculate the singular pressure drop of hydronic elements:

- Equivalent length method
- Excess head 1K method
- 2K method
- 3K method
- Babcock and Wilcox Co., 1978

2.13. Heat Pump System

The conventional water-to-water vapor-compressor heat pump system is modeled in a simple way with a collection of steady states implemented in a 4-dimensional lookup table function. The important hypothesis here (and therefore limitation of the model) is that it is assumed that the heat pump operation reaches quasi-steady state within each simulation time step of 60 sec. The data implemented in the lookup table function is obtained from documentation of the model TWM036 heat pump manufacturer [13].

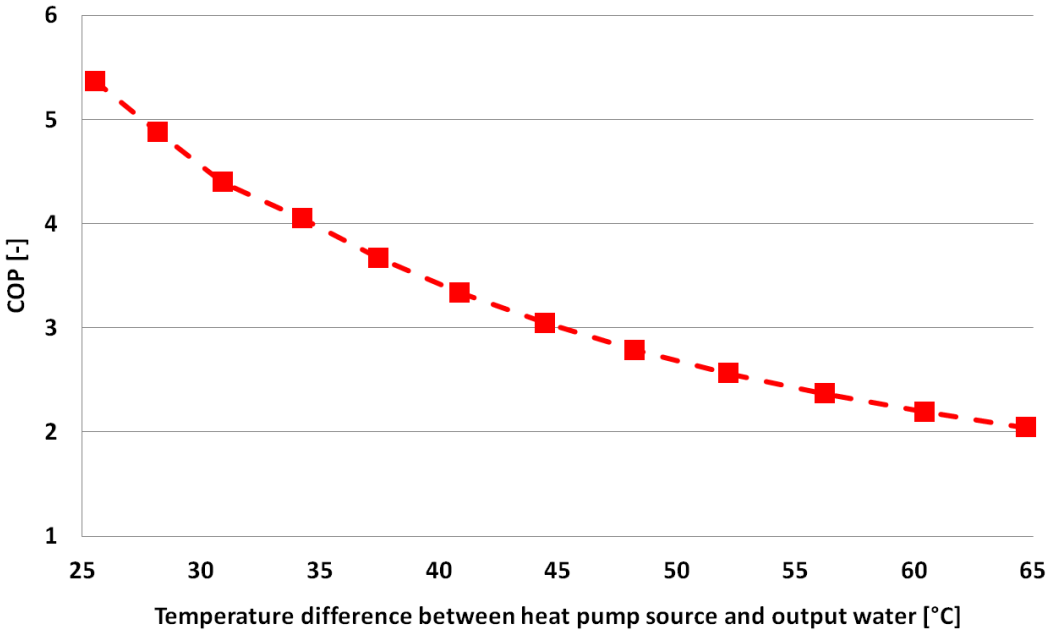

Figure 48: *Heat pump COP in function of temperature difference between evaporator inlet and condenser outlet at steady state.*

2.14. Circulation Pump for Water-Based Heating System

The modeling of the circulation pump Grundfos Alpha2 L 15-40 is made in a simple way with a second degree polynomial function fitting operation data provided by Grundfos manufacturer [14] (see **Figure 49 - 50**). The hydraulic circulation pumps are all set to constant pressure regulation (CP1) at 23 000 Pa.

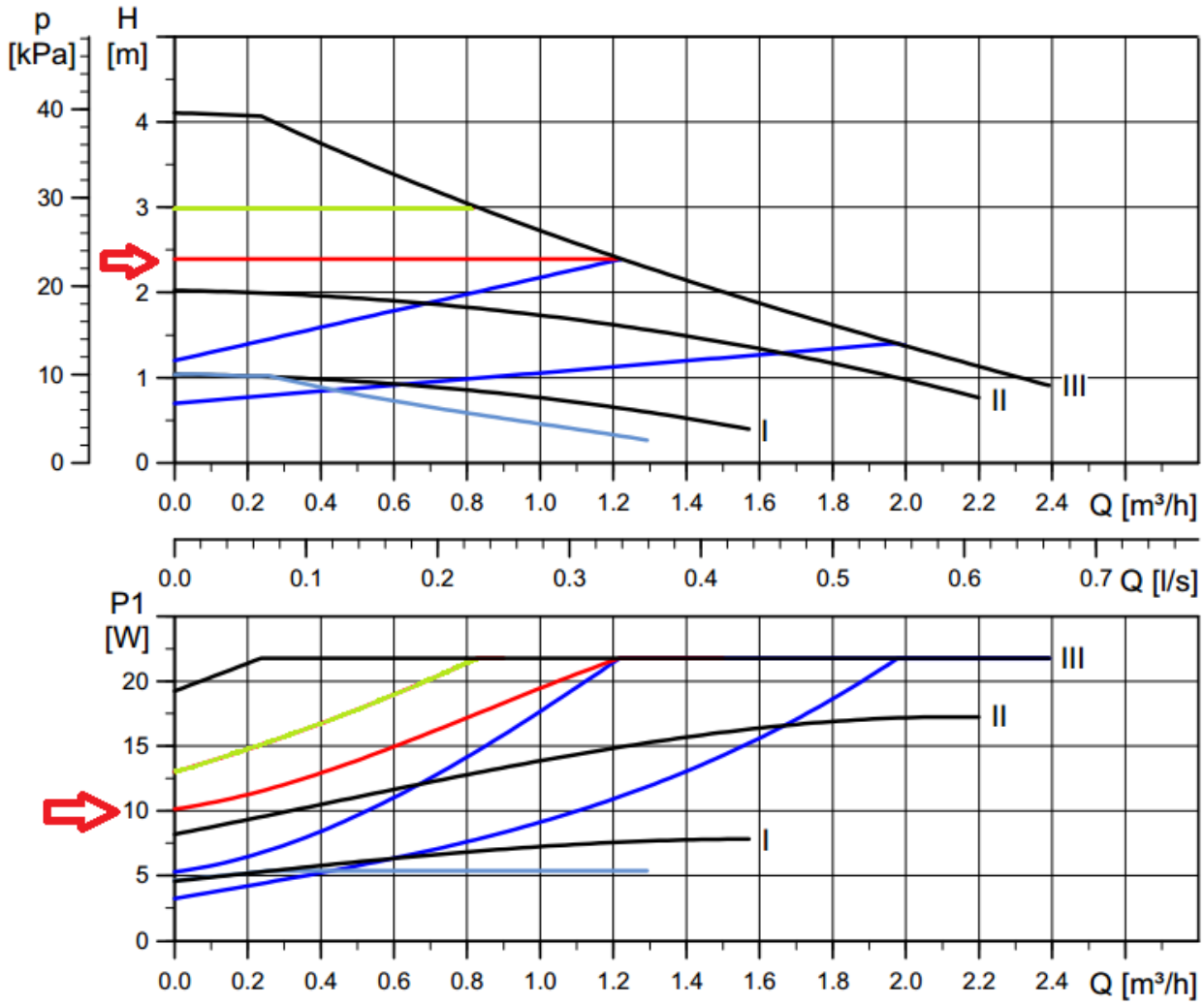

Figure 49: *Performance curves of the pump circulator Grundfos Alpha2 L 15-40.*

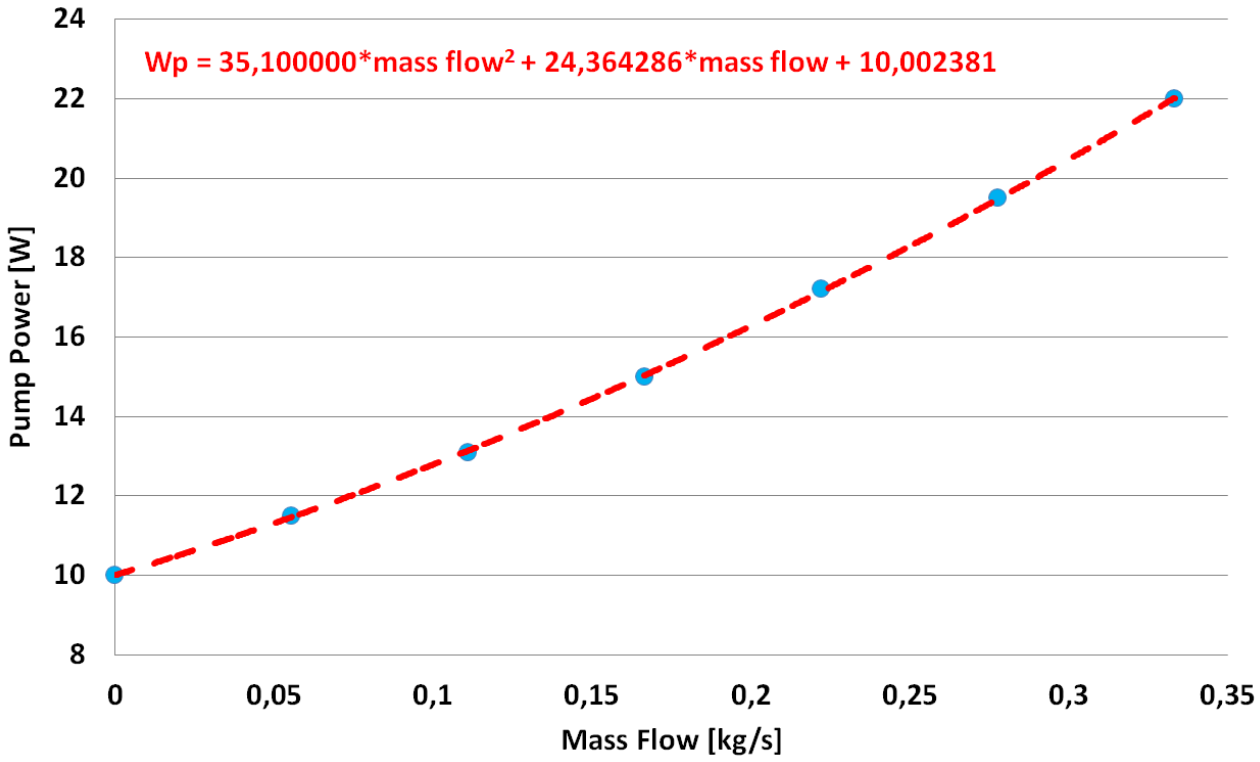

Figure 50: *Empirical model of the pump circulator Grundfos Alpha2 L 15-40.*

Similarly, the modeling of the circulation pump Grundfos CR 1-9 A-FGJ-A-E-HQQE – 96478872 is made with a second degree polynomial function fitting operation data provided by Grundfos manufacturer [15] (see **Figure 51 - 52**). The hydraulic circulation pumps is set to operate according to the power curve P2.

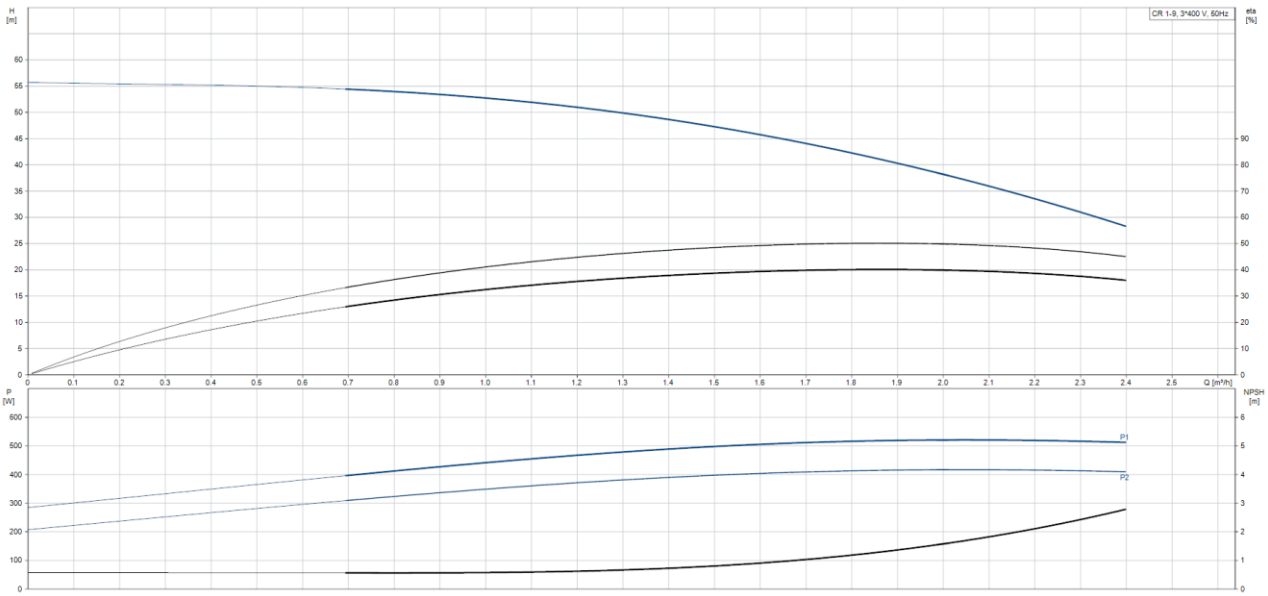

Figure 51: *Performance curves of the pump circulator Grundfos CR 1-9 A-FGJ-A-E-HQQE – 96478872.*

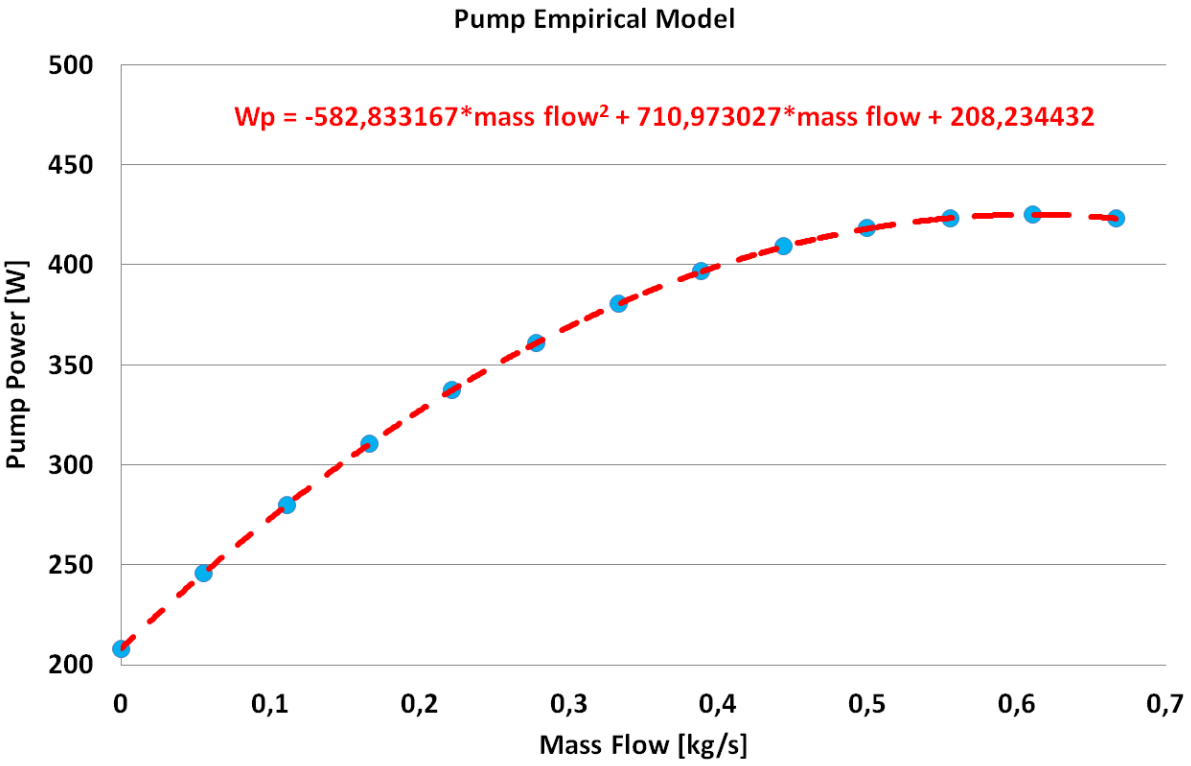

Figure 52: *Empirical model of the pump circulator Grundfos CR 1-9 A-FGJ-A-E-HQQE – 96478872.*

2.15. Hot Water Storage Tank

The 250 L stratified hot water storage tank has a cylindrical shape: radius of 29 cm and height of 95 cm. There is 5 cm of polyurethane insulation around the water tank (heat losses to the ambient are 1.356 W/K). The water tank model is a simplified version of that presented by Angrisani et al. [66]. Heat losses to the ambient are modelled with a constant heat transfer coefficient between the ambient indoor environment and the internal wall surface of the water tank. The convective and conductive heat transfer between brine circulating in cold and hot helical coil heat exchangers (heat pump condenser) and the water inside the buffer tank are calculated according to the fluid temperature and composition.

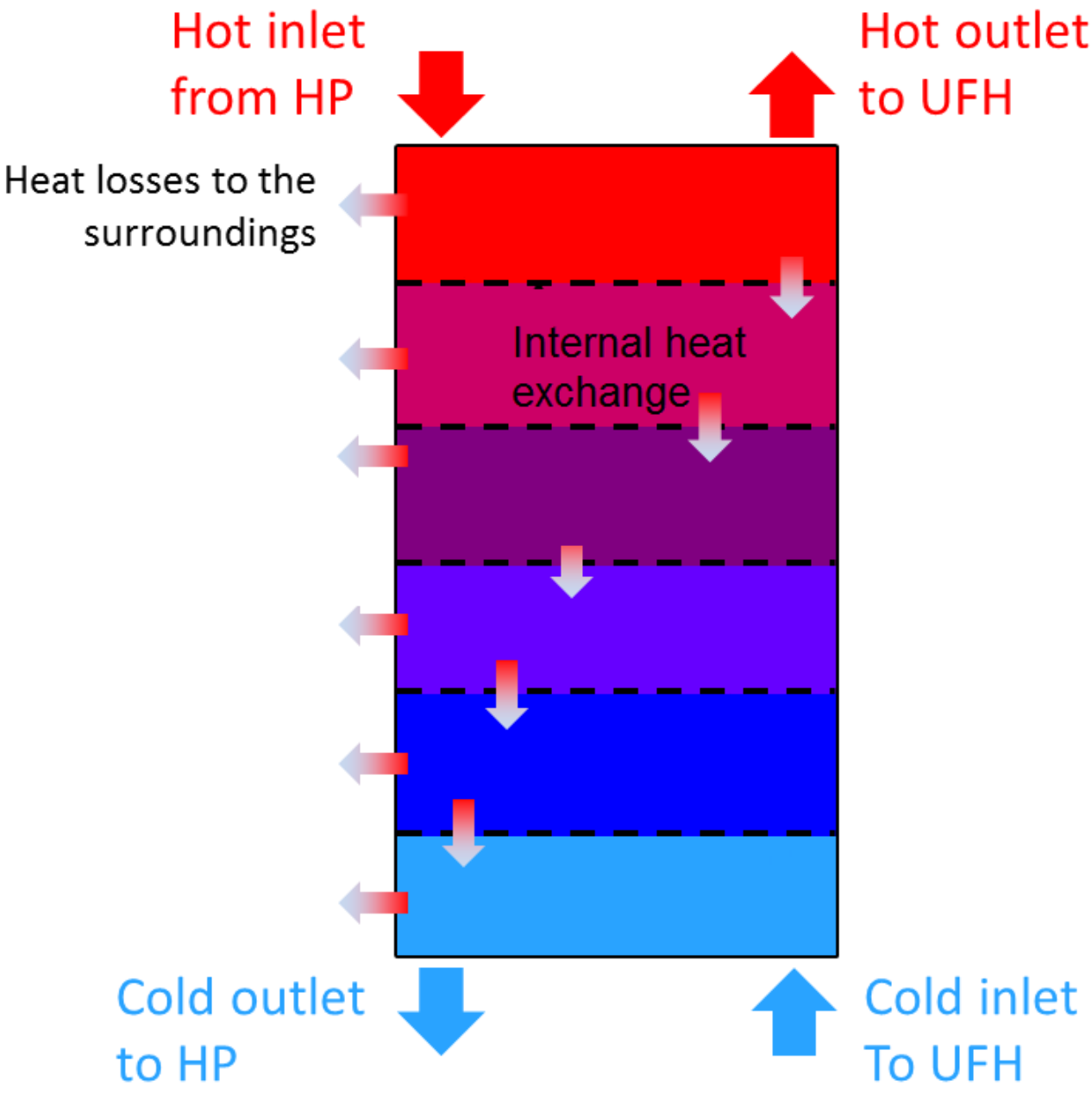

Figure 53: *Hot water storage tank model.*

2.15. Phase Change Material Wallboard

Many PCM numerical models are using an apparent heat capacity (Cp curve) formulation to take into account the latent heat of the phase transition. This variable Cp as function of temperature can be obtained from experimental tests such as differential scanning calorimetry (DSC) or T-history method. However, the apparent heat capacity modeling does not really represent the physics of the latent heat phase transition but only its apparent behavior. The shape of the Cp curve can change depending on the method used in the measurement. The size of the sample and the speed of temperature change rate are especially very sensitive parameters.

The PCM model of this study is based on an enthalpy formulation which really takes into account the phase transition process at constant temperature. The stable form PCM is considered to be a homogenous material set in thin layers so that the heat transfer can be reduced as a one-dimensional problem. The enthalpy formulation for the latent heat of the phase transition is coupled to a 1D implicit finite volume formulation to calculate the heat transfer between the PCM layers and change of internal energy. The implicit finite volume formulation is more complex to implement but has the great advantage of being unconditionally stable even with a very fine space discretization and large time step.

The density, specific heat capacity (not taking into account the latent heat) and thermal conductivity of each PCM control volume is calculated in function of its temperature based on the temperature-dependent characteristics of the PCM compounds: liquid PCM phase, solid PCM phase and non-PCM surrounding matrix. Therefore the characteristics of each compound, their proportions or the latent heat of the PCM can be changed independently and correctly taken into account in the model.

During the simulation, the PCM model calculates the heat transfers as follow: The thermo-physical properties of each PCM control volume are calculated according to the current local temperature. These properties are used to build the “stiffness matrix” for the implicit finite volume formulation. Solving the heat equation for each control volume gives the heat transfer in between each PCM layer. It is therefore possible to know what is the change of internal energy or enthalpy of each control volume.

For each PCM control volume, an enthalpy / temperature curve is built (see **Figure 54**). This function is inverted in order to find the new temperature at the next time step from the change of enthalpy and taking into account the phase transition at constant temperature. If the new temperature does not reach transition temperature, then the calculation is the same as a normal implicit FVM calculation.

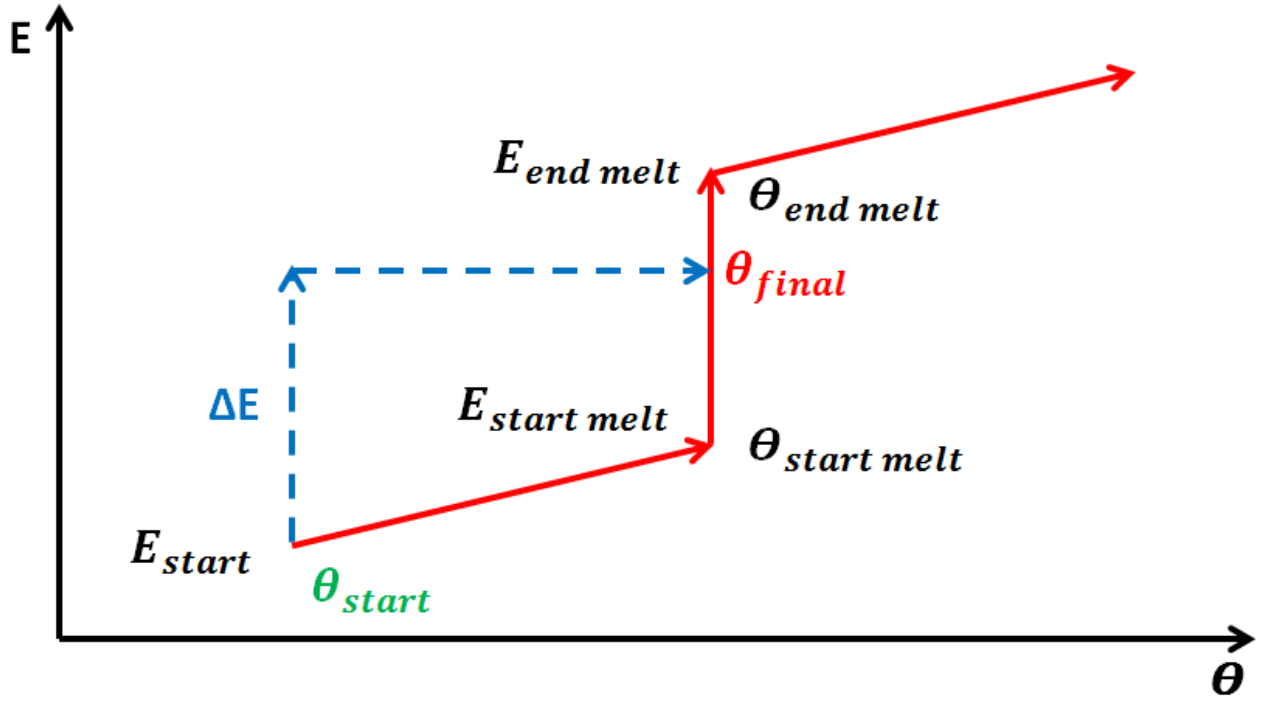

Figure 54: *Enthalpy / temperature function.*

The new temperature is then used in the next time step to re-calculate the thermo-physical material properties and the heat transfers [67] [68].

It is assumed that the PCM is pure and has only one specific melting temperature and one specific solidification temperature. These temperatures can be different to take into account hysteresis phenomena (see **Figure 55**). However, it not possible to simulate a PCM made of a mix of compounds which have different transition temperatures.

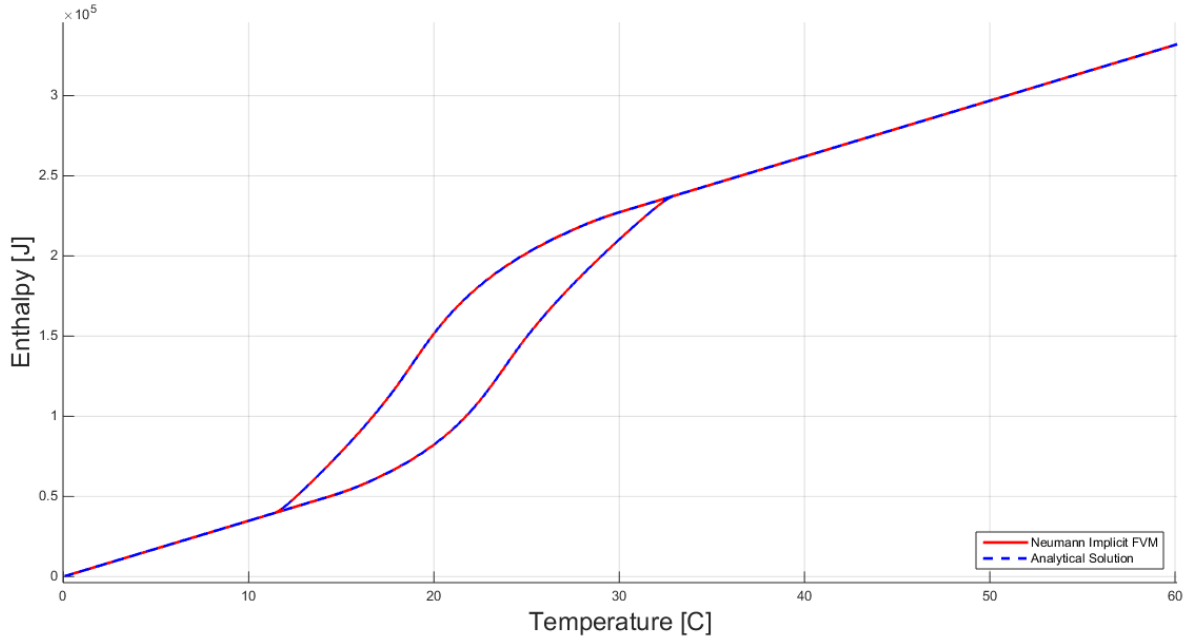

Figure 55: *Heating / cooling PCM model test with hysteresis.*

The PCM wallboard elements of the study are discretized in control volumes which are 1 mm thick.

2.15. Furniture / Indoor Content

The additional indoor thermal mass / furniture is modeled as an equivalent fictitious planar element which aggregates all indoor items into an homogenous representative material. The representative thermo-physical properties of this equivalent planar element are chosen according to a previous study about the indoor content of dwellings in Denmark [29] (see **Table 8**). The 60 kg/m² of additional indoor content are gathered in an equivalent slab which is 4.7 cm thick. The surface area of one side of the element is equal to 1.8 times the surface area of the floor in the thermal zone. The equivalent planar element does not have any real geometrical representation or position in the room. It is therefore assumed that 50% of the radiative share of the equipment, people, solar and radiator heating loads are distributed on its surfaces. The element is coupled to the rest of the thermal zone in the same way as if it was an internal wall only connected to the air node. The mixed convection/radiation surface thermal resistance coefficient t is constant and equal to 0.13 m².K/W.

	Equivalent planar element
Thickness [mm]	**47**
Density [kg/m³]	**715**
Thermal conductivity [W/m.K]	**0,3**
Specific heat capacity [J/kg.K]	**1400**
Space discretization [nodes]	**20**

Table 8: *Equivalent indoor thermal mass / furniture properties.*

In the case of PCM integrated on furniture elements, the two models for indoor thermal mass / furniture and for PCM are combined together. A 1.5 cm thick layer of stable form PCM is added on the upper part of the equivalent planar element.

3. Validation of the Building Model

This section presents different validation tests performed to demonstrate the usefulness of the models presented before.

3.1. Validation of the Construction Element with BSim Software

The first step for validating a building model is to make sure that the basic construction element blocks are calculating the heat transfer properly. One can see on **Figure 56**, the validation test in steady state of a MATLAB Simulink block modeling an external wall for the building model of the study. The 5 temperatures of the 5 thermal nodes fit perfectly with the analytical solution. Average absolute error of the model is 0.0015 °C.

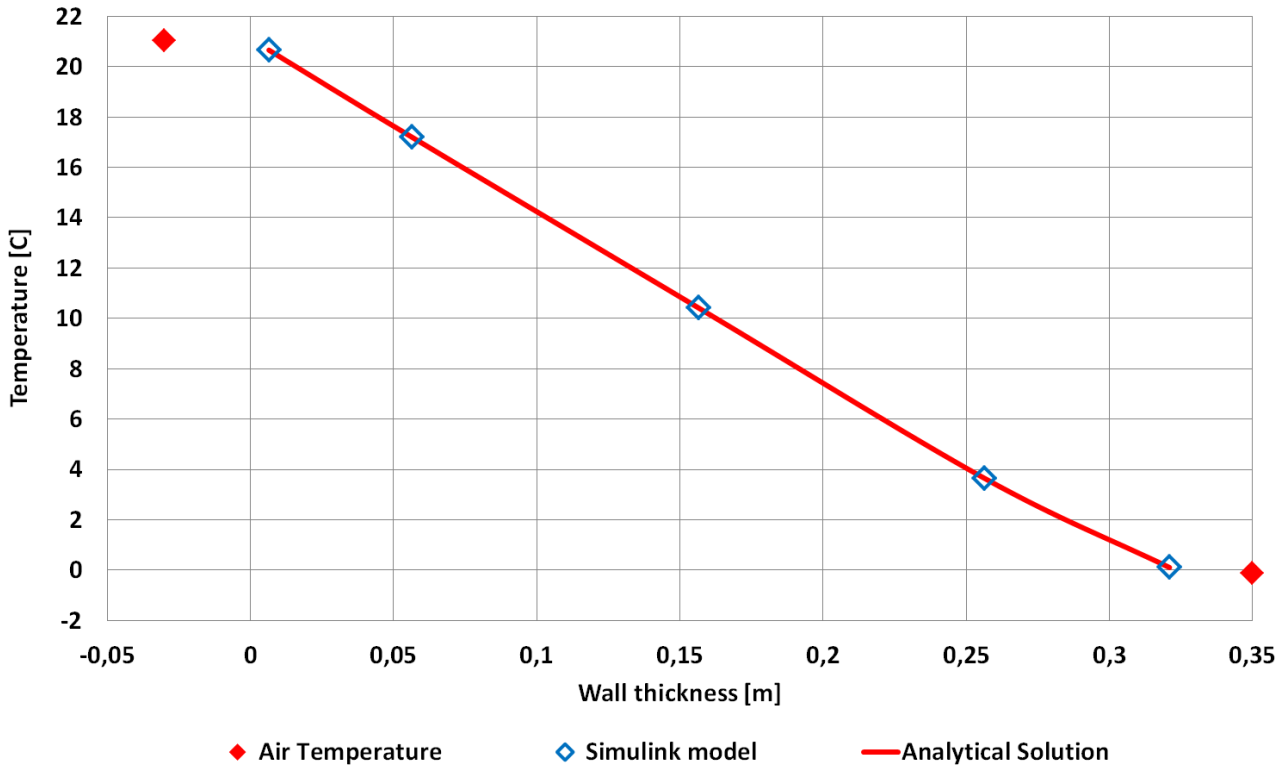

Figure 56: *Steady state temperature profile of external test wall.*

The construction element block for wall elements is then tested with dynamic boundary conditions (weather data DRY 2013) including varying outdoor temperature, solar radiation, wind, long-wave radiations to the sky and constant indoor air temperature and internal radiation loads. The temperatures of the different thermal nodes in de MATLAB – Simulink model are compared with the temperature of a BSim reference model. BSim software is a well-known and validated building energy software. One can see on

Figure 57 – 59, that the temperatures of the MATLAB –Simulink model fit very well the ones of the BSim reference model for dynamic boundary conditions.

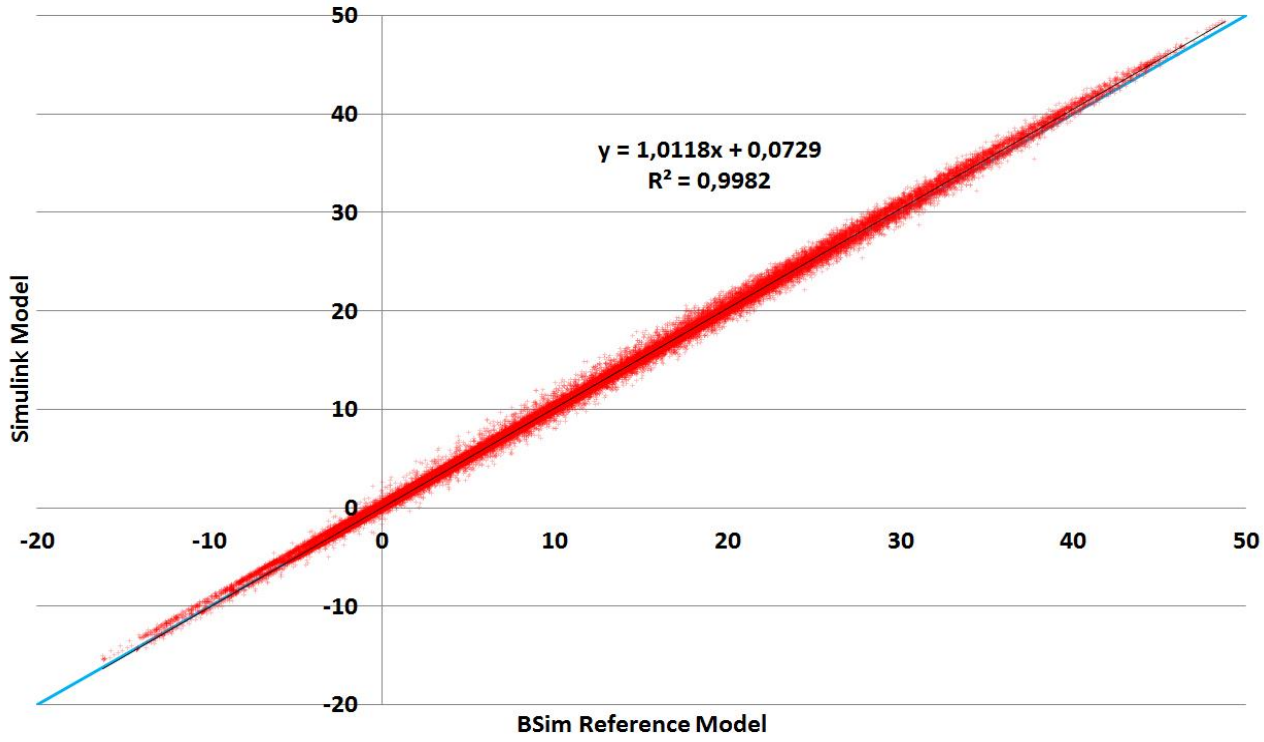

Figure 57: *Wall external surface temperature BSim reference model vs MATLAB-Simulink model.*

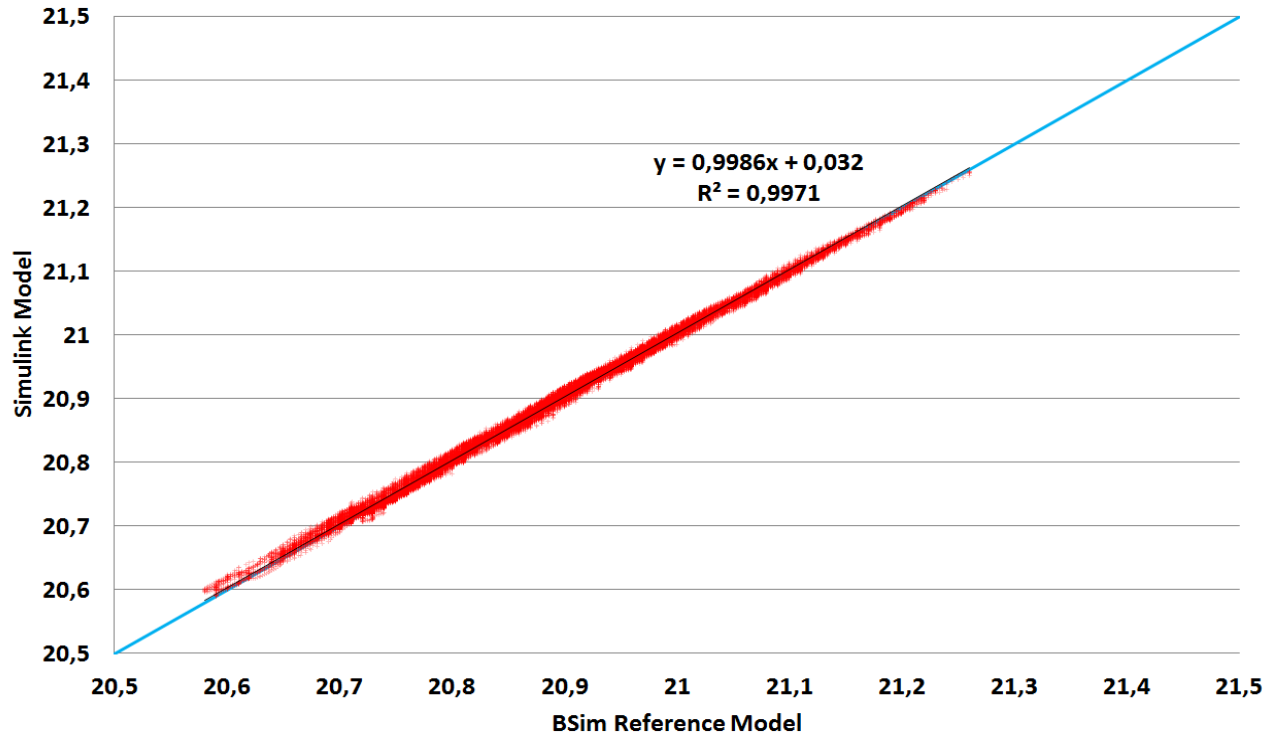

Figure 58: *Wall internal surface temperature BSim reference model vs MATLAB-Simulink model.*

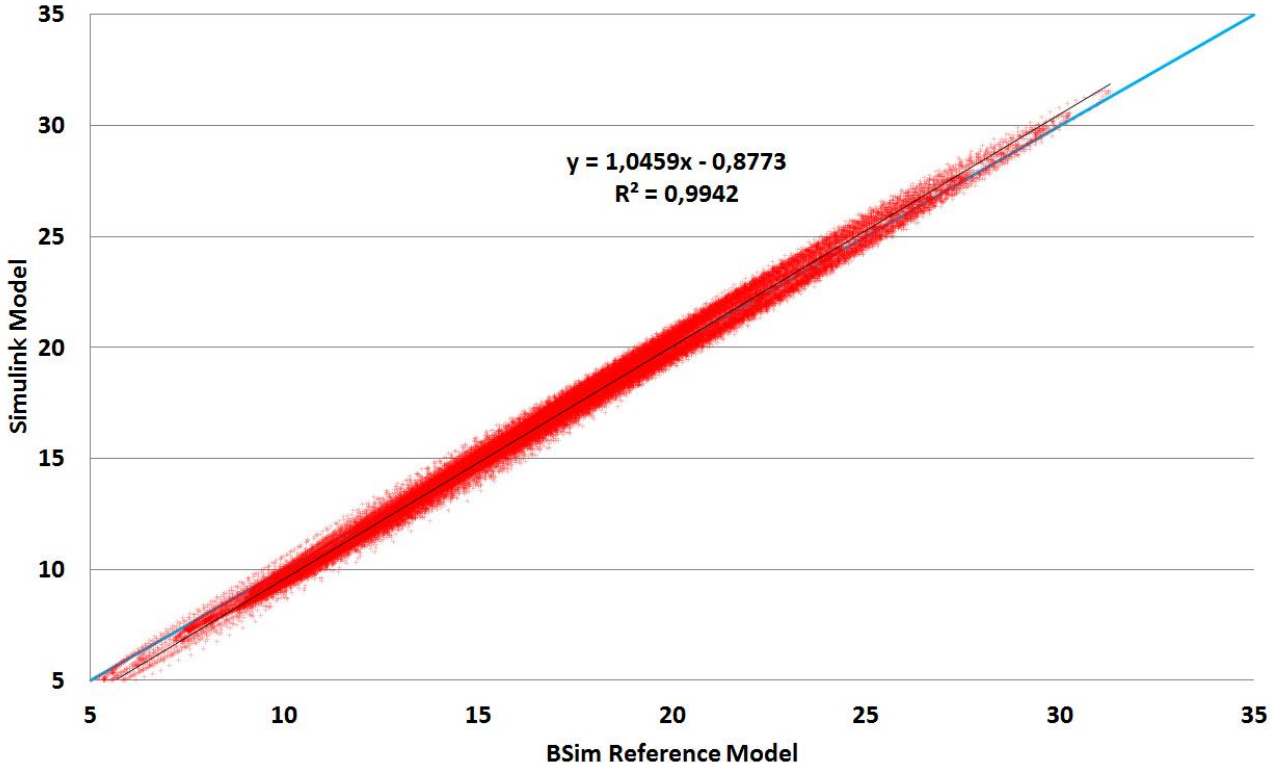

Figure 59: *Wall insulation layer temperature BSim reference model vs MATLAB-Simulink model.*

The average absolute temperature difference between the MATLAB-Simulink model and the BSim reference model is 0.3 °C.

3.2. Validation of the Multi-Zone Model with BSim Software

The full multi-zone MATLAB-Simulink building model is then tested against the BSim reference model of the same building for the same weather data and building parameters. The building type tested here is a well-insulated house (Passive House) with medium structural thermal mass and radiator heating system.

One can see on **Figure 60 – 62** that the building temperatures and heating power needs of the MATLAB-Simulink model fit very well with the ones of the BSim reference model. The average absolute building temperature difference between the MATLAB-Simulink model and the BSim reference model is 0.12 °C. The average absolute building heating power need difference between the MATLAB-Simulink model and the BSim reference model is 82 W (0.54 W/m²) which represents 3% of the maximum heating power need of the house. The difference in cumulative energy consumption over 2000 hours of heating period is 10.42 kWh, which represents a relative difference of 0.88%.

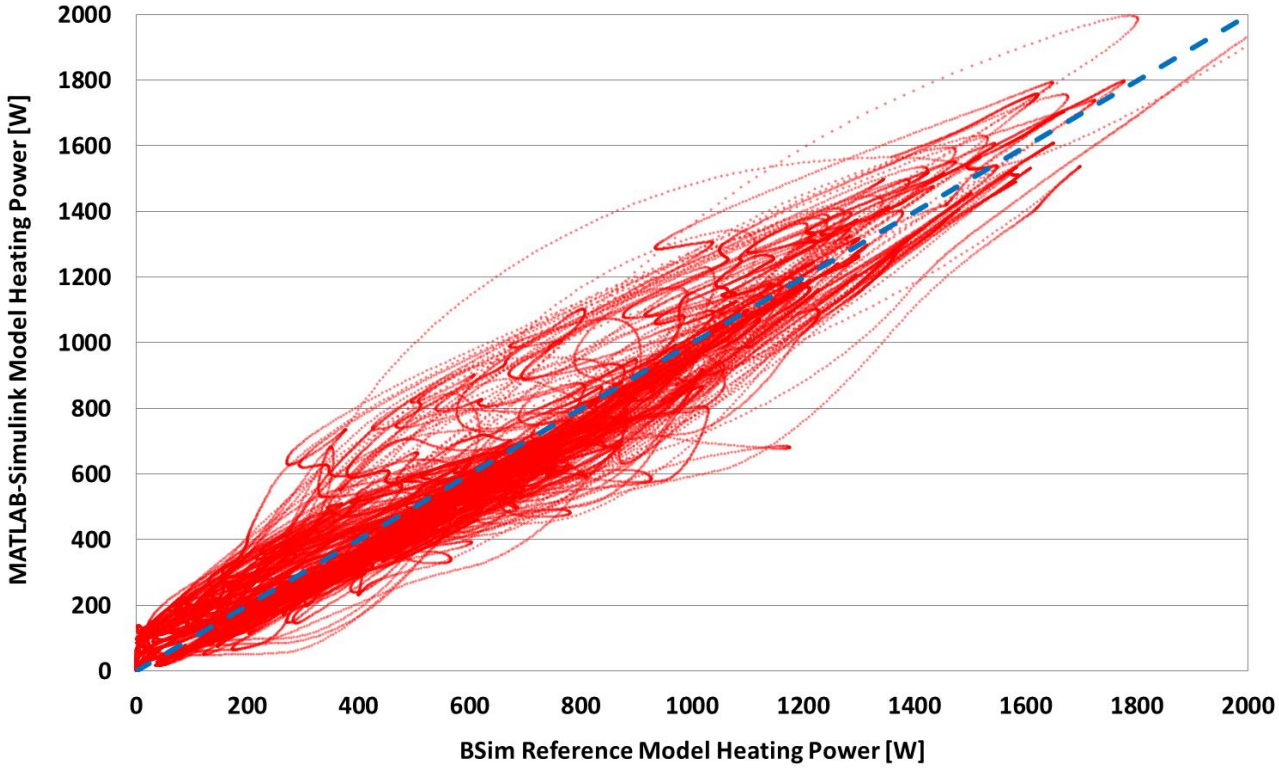

Figure 60: *Multi-zone heating power need BSim reference model vs MATLAB-Simulink model.*

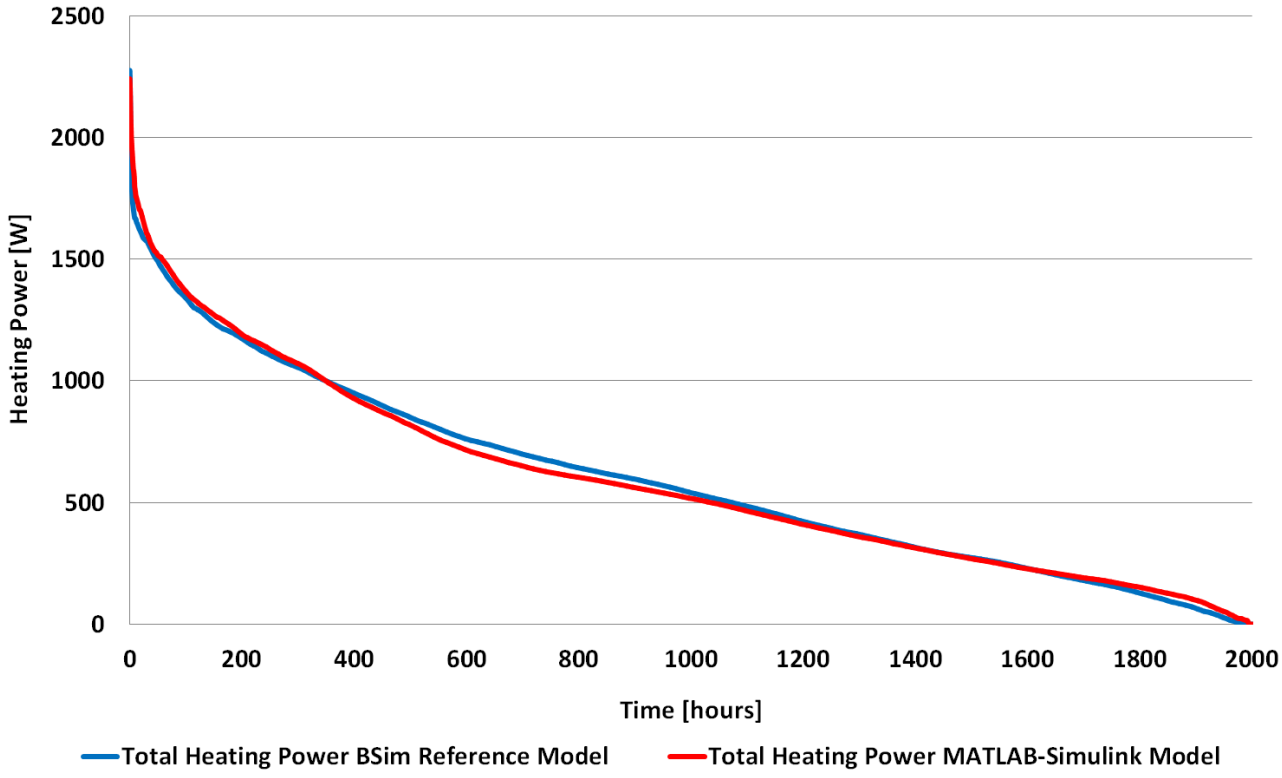

Figure 61: *Ordered heating power need of the multi-zone building models.*

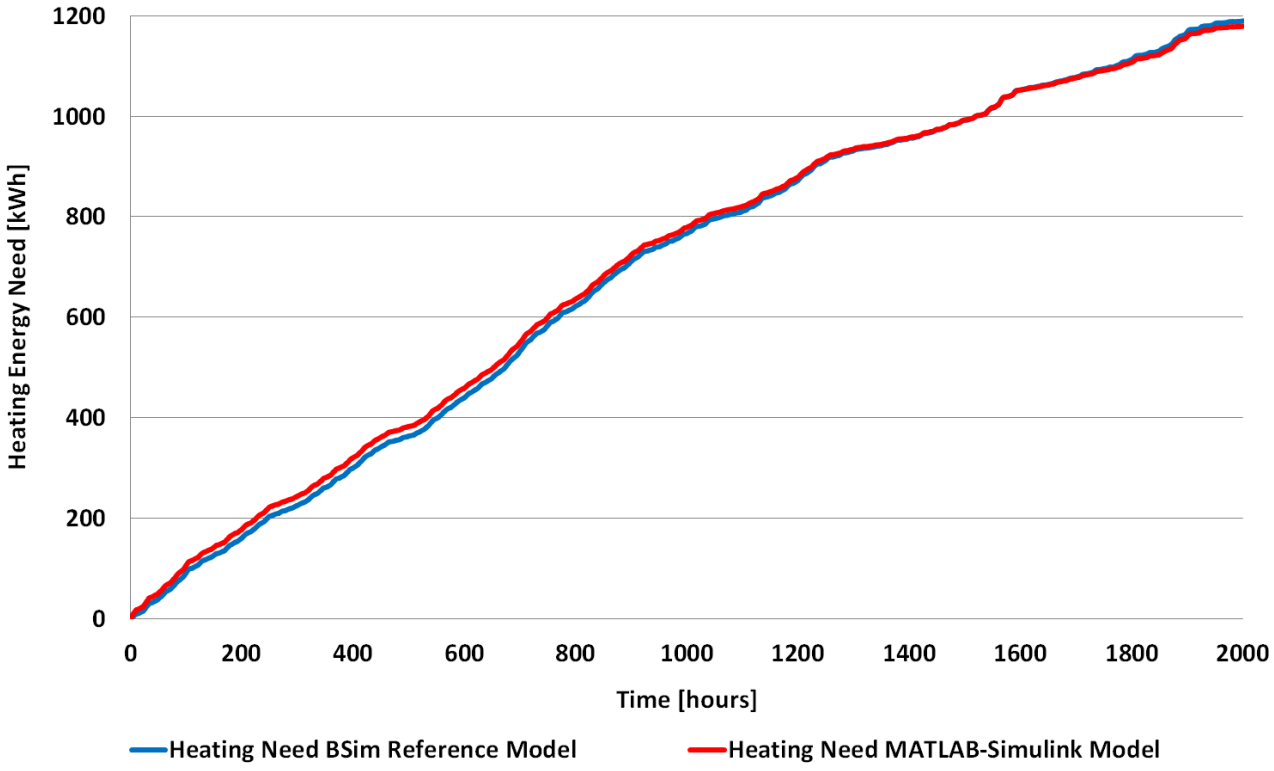

Figure 62: *Cumulative heating need of the multi-zone building models.*

3.3. Validation of the Building Model with BESTEST

In addition to the previously presented validation tests for the building numerical model used in this study, the BESTEST validation method is used to certify its correctness and consistency. The BESTEST procedure is a comparison method used to evaluate building simulation models. It is based on benchmark test cases generated by the IEA-EBC Annex 43: IEA Building Energy Simulation Test (BESTEST) [69]. The BESTEST method is described in details in ASHRAE standard [70].

6 different BESTEST cases are tested with the MATLAB-Simulink building model and presented hereafter. The basis of the different test cases is a rectangular room (see **Figure 63**).

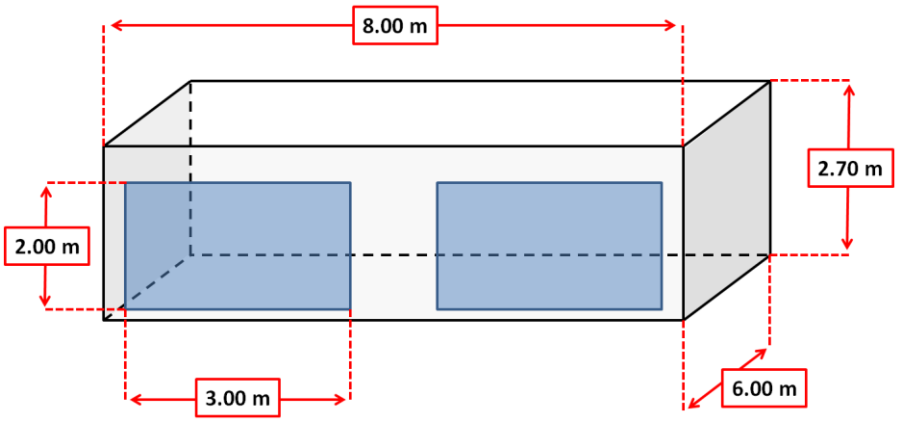

Figure 63: *BESTEST test cell.*

The envelope characteristics, orientation of windows and temperature set points vary between the different test cases. The main characteristics of the test cell are given in **Table 9** for the base test-case C600.

Test cell dimensions	**8 x 6 x 2.7 m**
Walls U-value	**0.514 W/m².K**
Roof U-value	**0.318 W/m².K**
Floor U-value	**0.039 W/m².K**
Windows dimensions	**2 x 6 m² (south oriented)**
Windows U-value	**3 W/m².K**
Windows solar factor	**0.78**
Infiltration rate	**0.5 vol/h**
Internal gains	**200 W (60% radiative, 40% convective)**
Heating / cooling system	**Perfect unlimited system (100% convective)**

Table 9: *Test cell description – C600.*

In addition to the base case C600, the case C620 (C600 with on window East oriented and one window West oriented), the case C640 (C600 with night set back to 10 °C between 23:00 and 7:00), the case C900 (C600 with heavy walls and outdoor insulation), the case C920 (C620 with heavy walls and outdoor insulation) and the case C940 (C640 with heavy walls and outdoor insulation) are also tested. These BESTEST cases are chosen to focus especially on the correctness of the calculation for solar internal gains and the proper behavior of a building with indoor temperature set point modulation and variation of envelope thermal mass.

The output results of the different test cases are presented hereafter on **Figures 64 – 72**. The MATLAB – Simulink numerical model is compared with the results of other commercial software: ESP, BLAST 3.0, DOE – 2.1 D 14, SERIRES / SUNCODE 5.7, SERIRES 1.2, S3PAS, TRNSYS 13.1 and TASE.

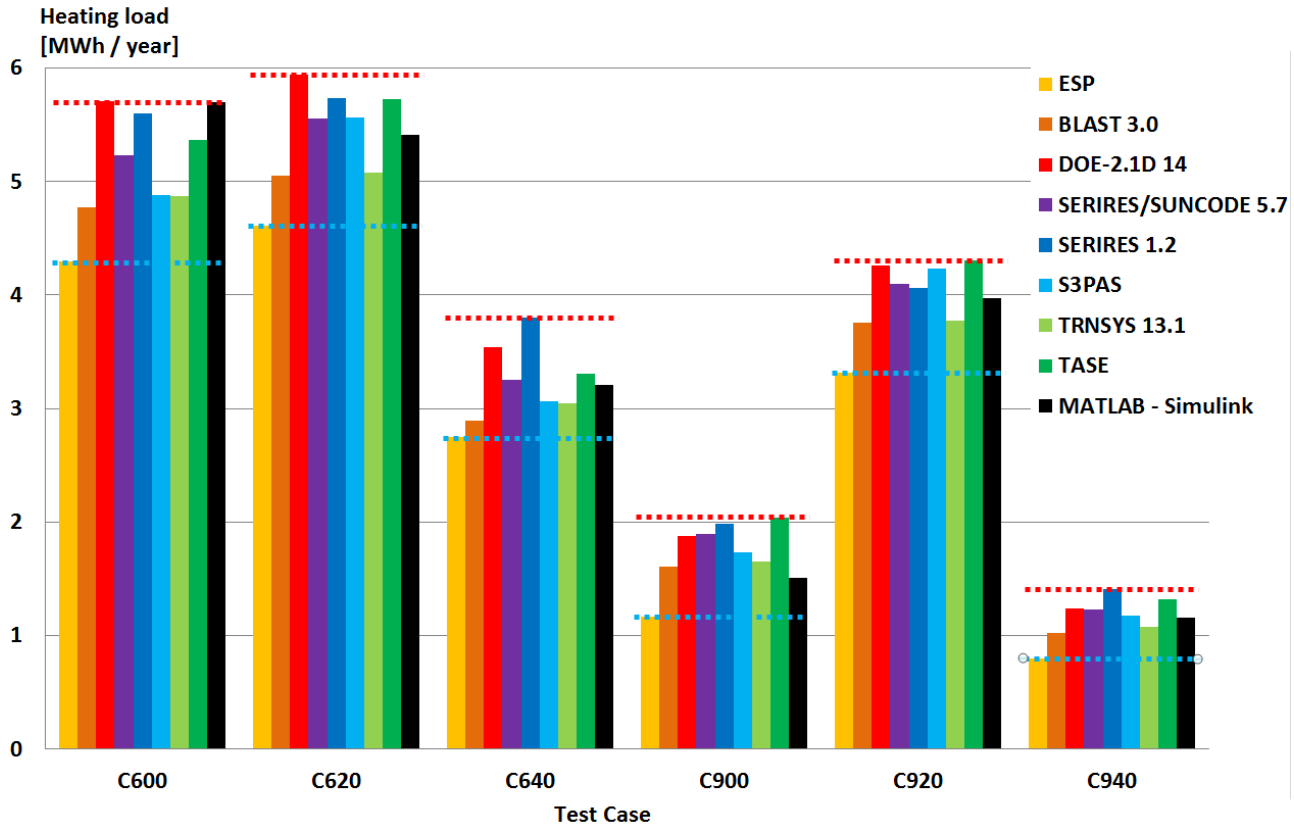

Figure 64: *BESTEST heating needs comparison.*

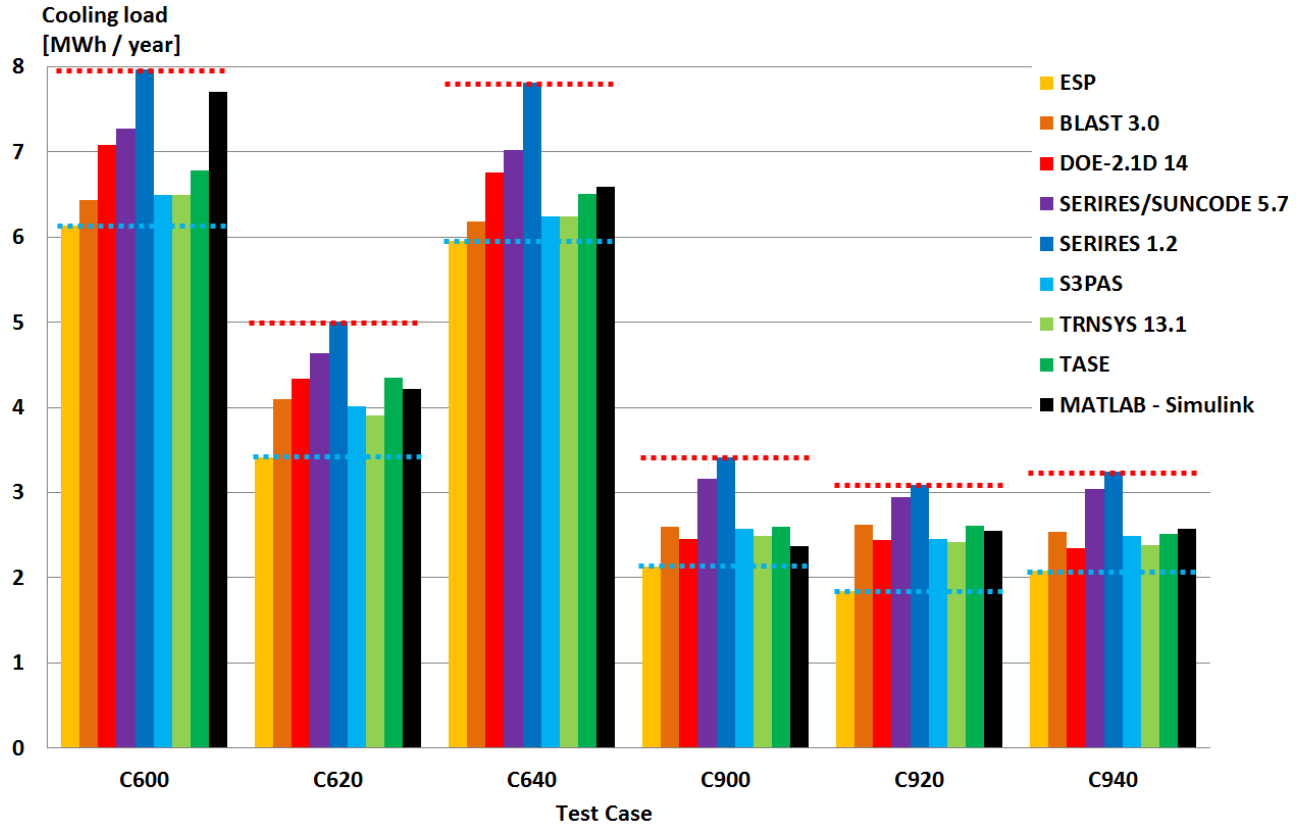

Figure 65: *BESTEST cooling needs comparison.*

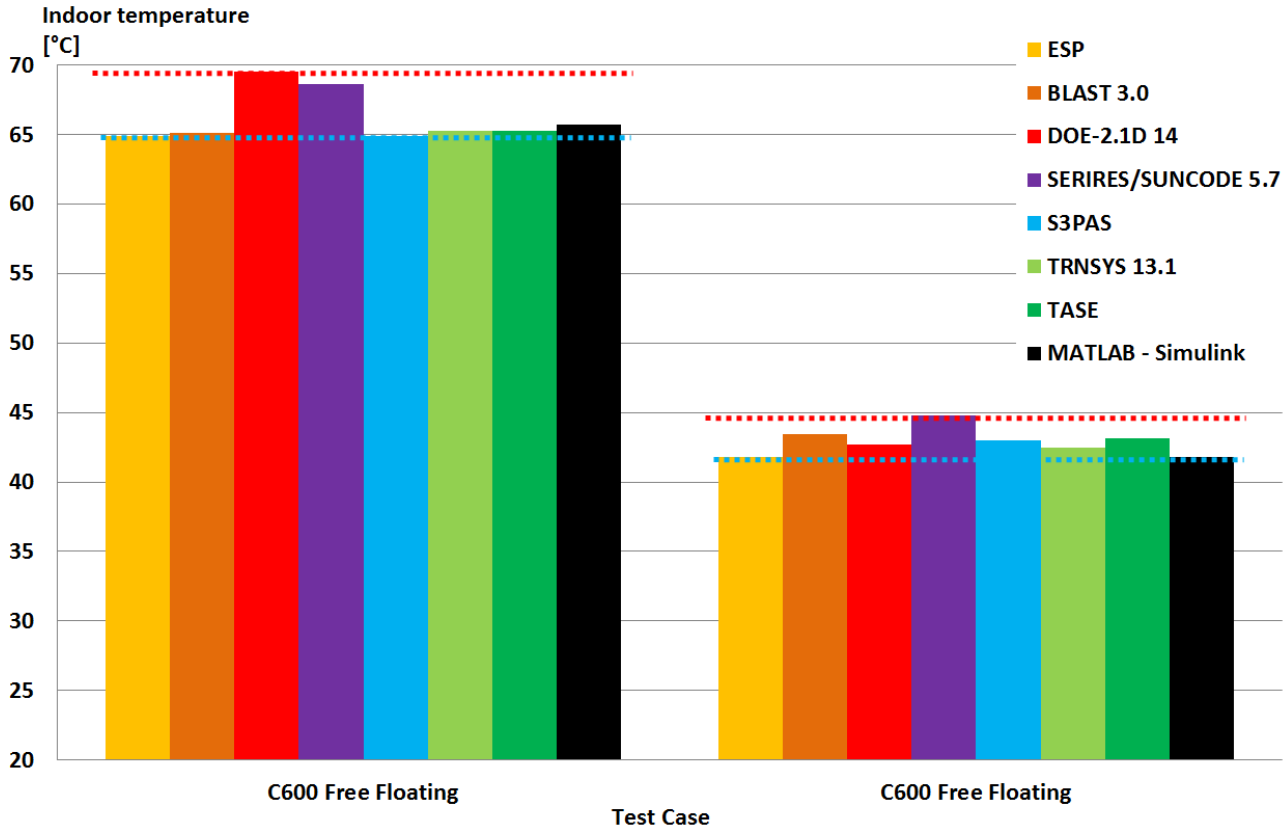

Figure 66: *BESTEST maximum indoor temperature comparison.*

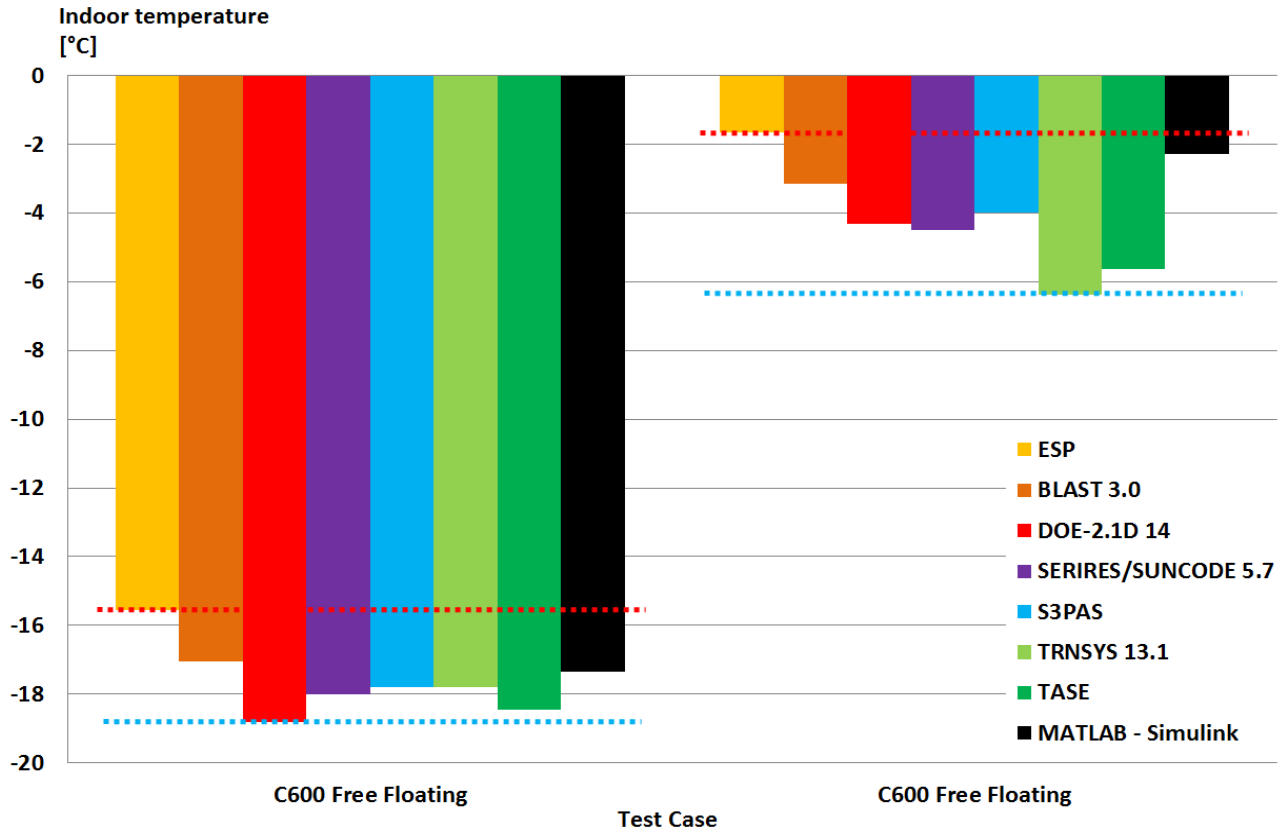

Figure 67: *BESTEST minimum indoor temperature comparison.*

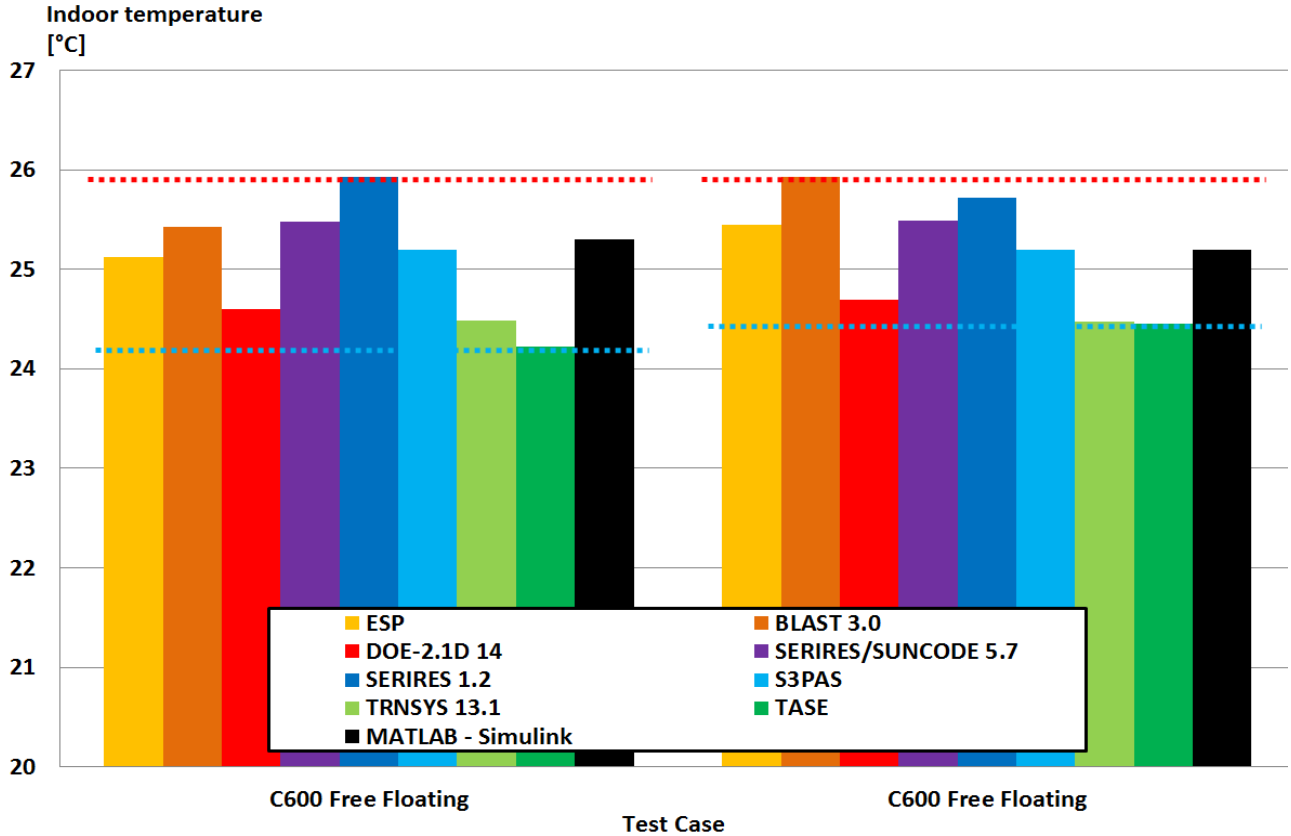

Figure 68: *BESTEST average indoor temperature comparison.*

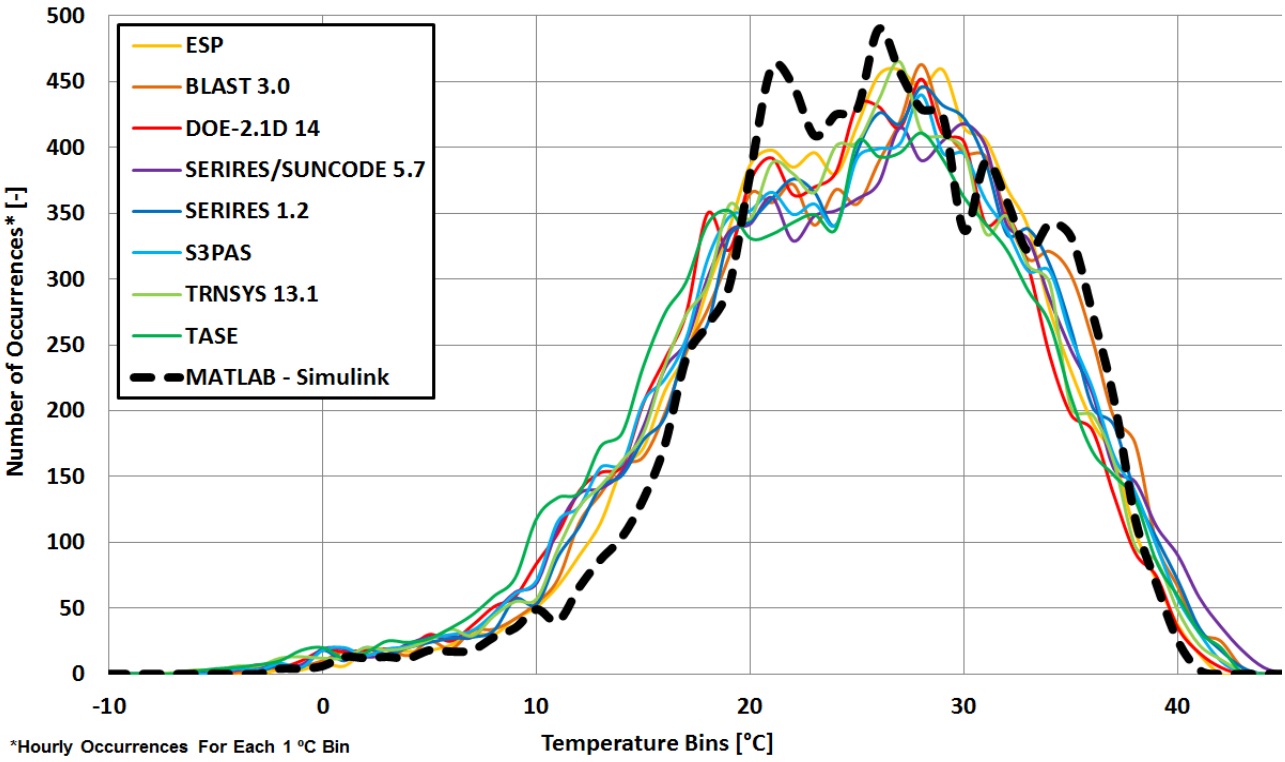

Figure 69: *BESTEST C900 Free Floating annual hourly temperature frequency comparison.*

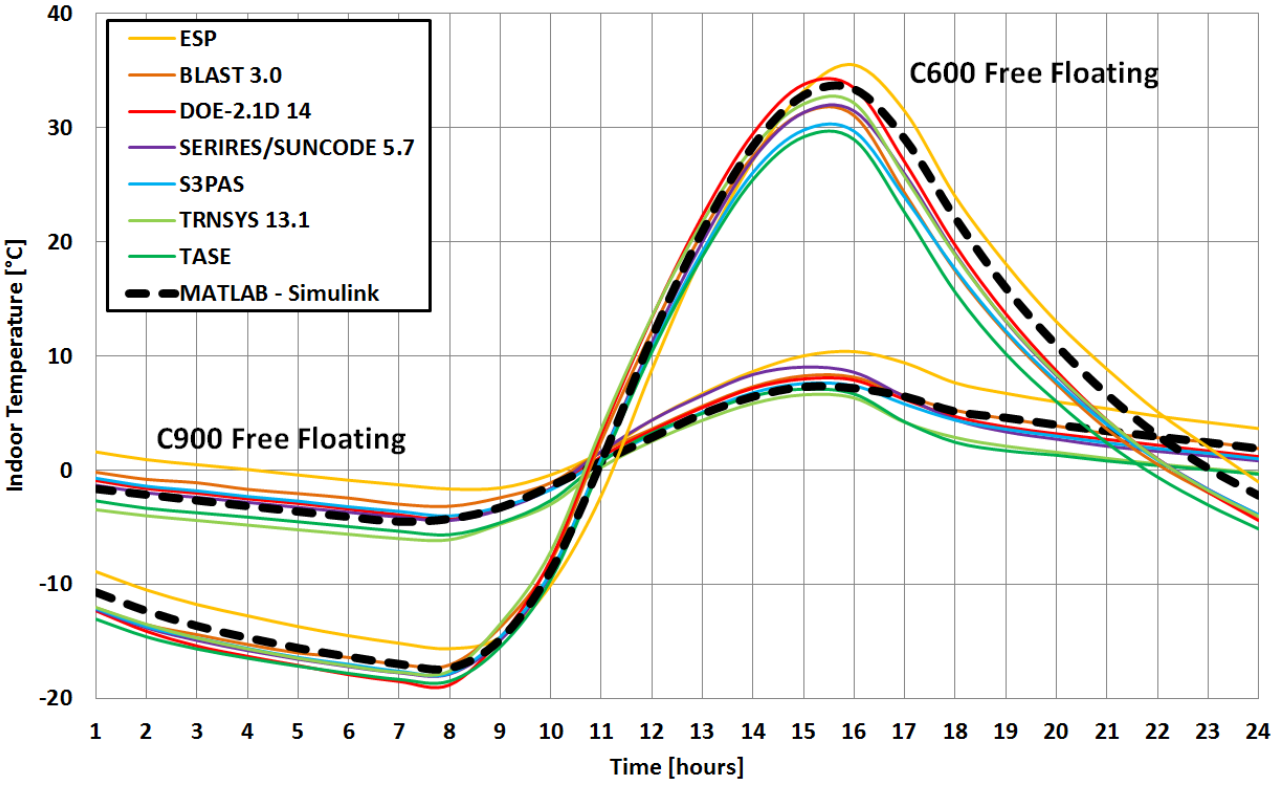

Figure 70: *BESTEST free floating temperature profiles of a clear cold day.*

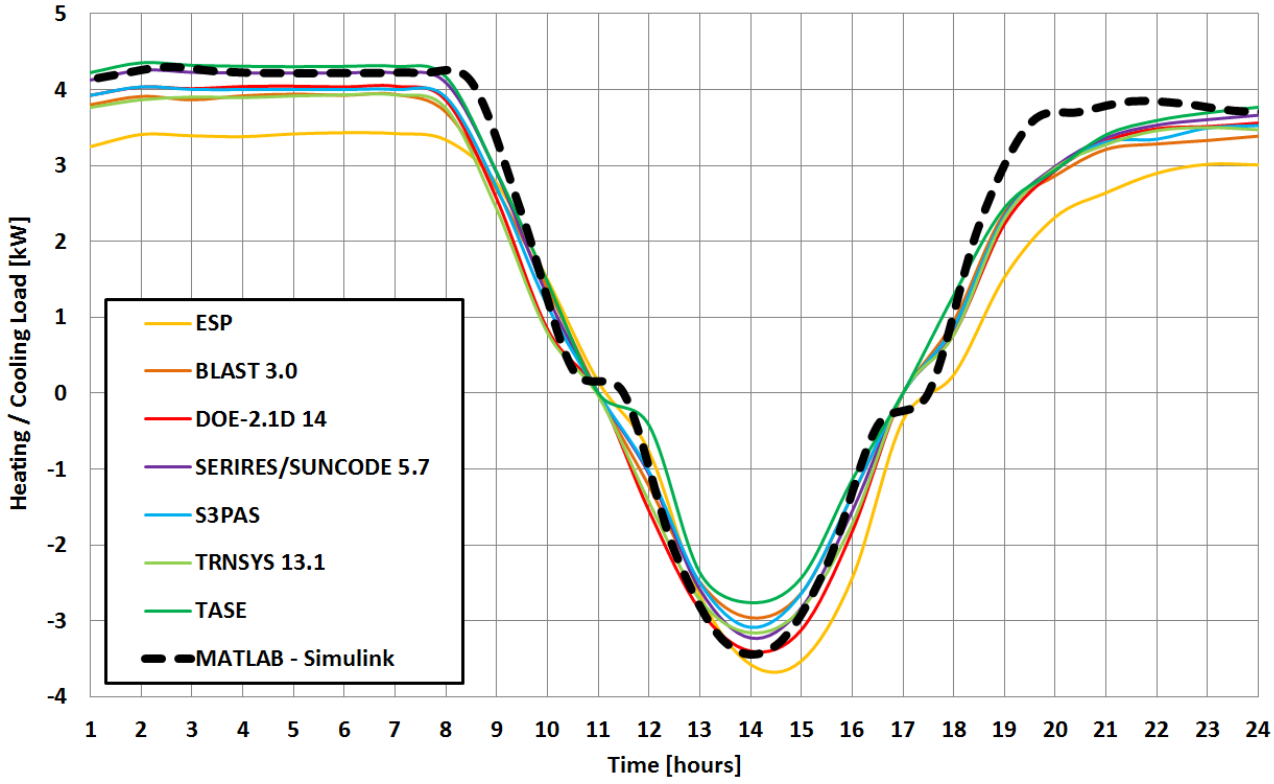

Figure 71: *BESTEST C600 heating / cooling needs during a clear cold day.*

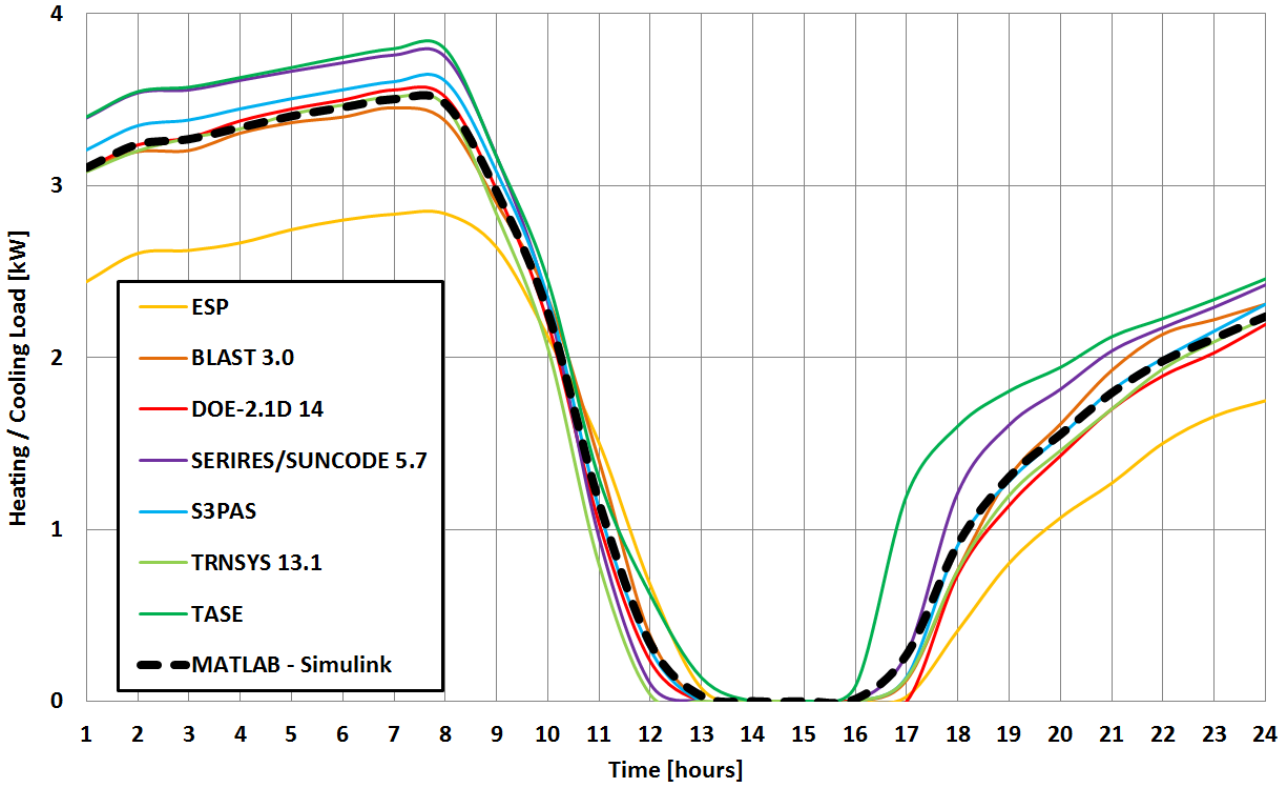

Figure 72: *BESTEST C900 heating / cooling needs during a clear cold day.*

One can see on the previous figures that the MATLAB - Simulink model gives output results which are always within the results of the other software for the different test cases. It can therefore be considered that the MATLAB – Simulink building model is validated and can be used for numerical studies.

3.4. Validation of Under Floor Heating System and Horizontal Ground Source Heat Exchanger with BSim Software

The hydronic under floor heating system and the horizontal ground source heat exchanger are modeled in the same way. In the case of the floor heating system, the bottom surface is in contact with the underground temperature of the building and the upper surface is exposed to the indoor environment of the building. In the case of horizontal ground source heat exchanger, the bottom surface is in contact with the deep ground temperature and the upper part is exposed to the outdoor conditions. Apart from the number of layers, the thermal properties of the layers and the size of the pipes, the heat exchanger model itself is the same.

The MATLAB-Simulink hydronic heat exchanger model is firstly tested in steady state conditions against the BSim reference model. One can see on **Figure 73** that the temperature profile of the MATLAB-Simulink heat exchanger's slab fits very well with the one of the BSim reference model. The average absolute temperature difference between the two models is 0.07 °C.

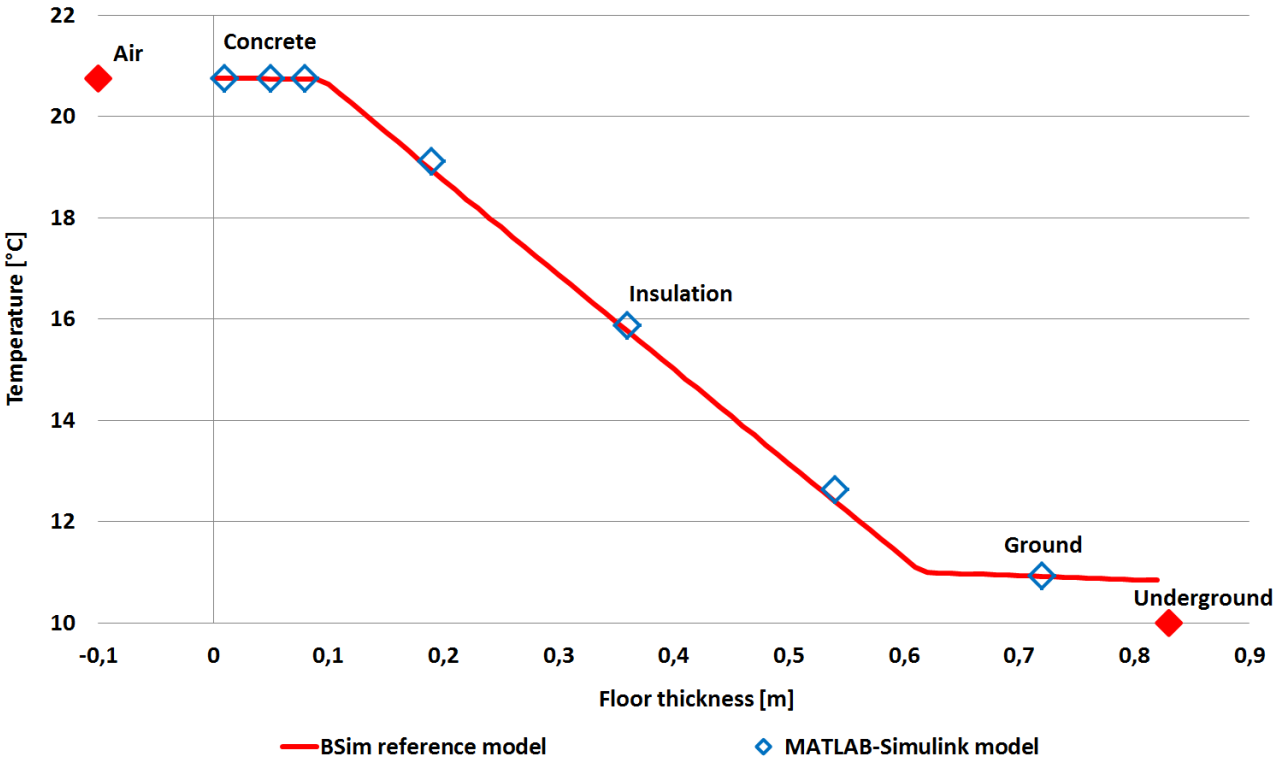

Figure 73: *Steady state temperature profile of a floor heat exchanger.*

The MATLAB-Simulink heat exchanger model is then tested in heating and cooling mode as a floor heating heat exchanger in a test room with dynamic boundary conditions. The temperatures of the different thermal nodes and the heat transfer from the fluid to the slab in de MATLAB – Simulink model are compared with ones of the BSim reference model. One can see on **Figure 74 – 76**, that the temperatures and heat transfer of the MATLAB –Simulink model fit very well the ones of the BSim reference model for dynamic boundary conditions.

The average absolute difference in heat transfer between the MATLAB – Simulink model and the BSim reference model is 3.2 W. The average absolute temperature difference in air temperature and pipe level temperature between the two models is 0.07 and 0.1 °C respectively.

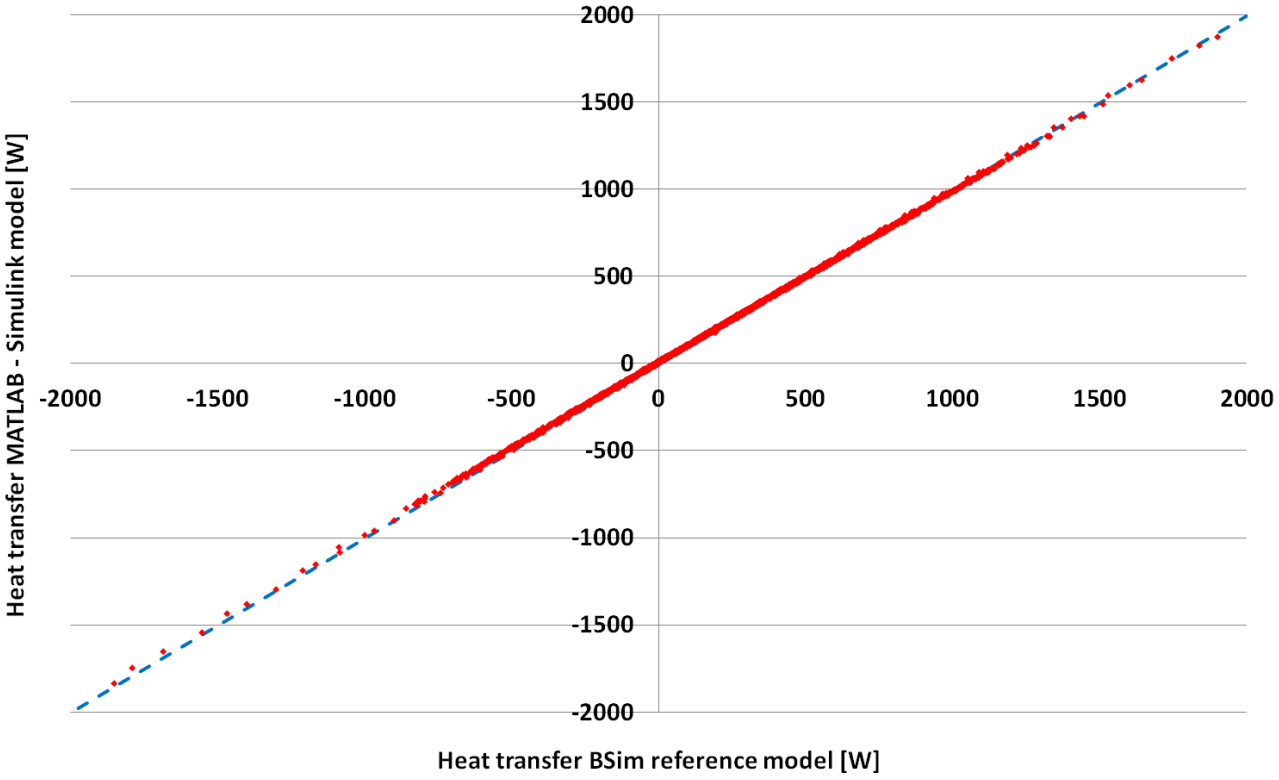

Figure 74: *Floor heat exchanger heat transfer BSim reference model vs MATLAB-Simulink model.*

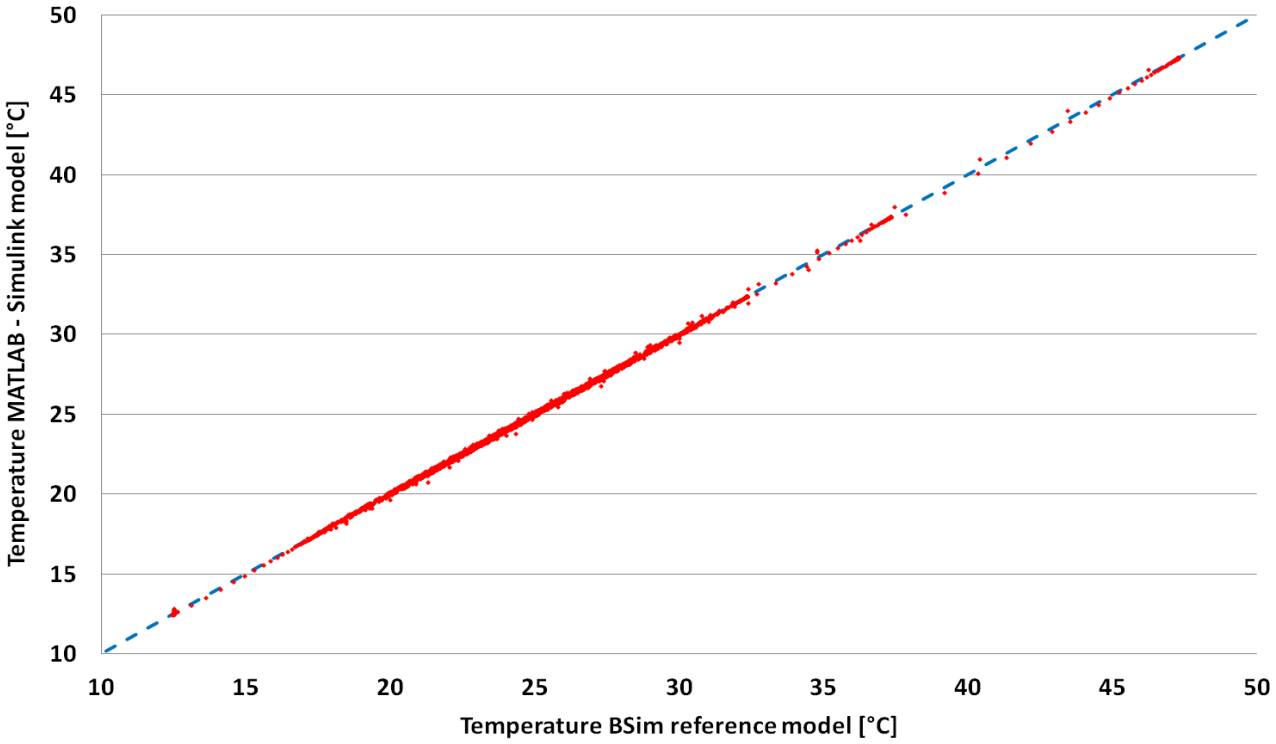

Figure 75: *Operative temperature in test room with floor heat exchanger BSim reference model vs MATLAB-Simulink model.*

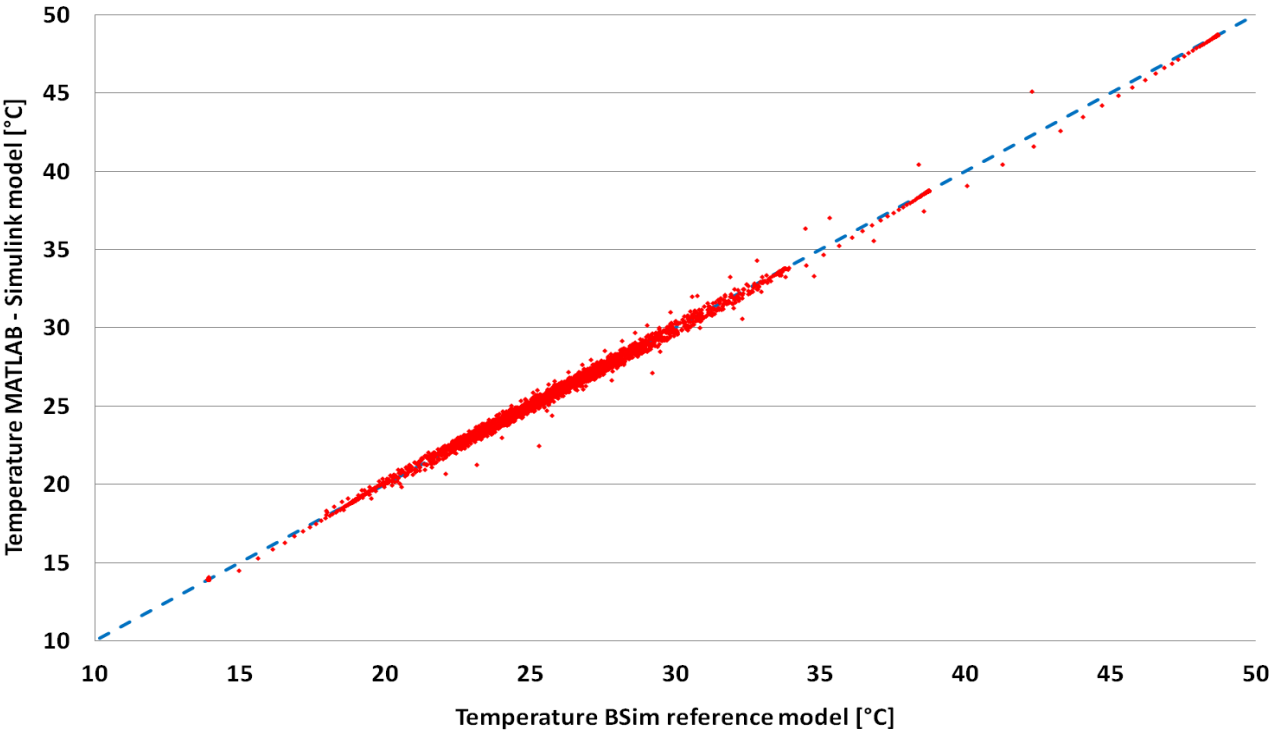

Figure 76: *Pipe level temperature in test room with floor heat exchanger BSim reference model vs MATLAB-Simulink model.*

3.5. Validation of Vertical Borehole Ground Source Heat Exchanger with Experimental Data

The vertical borehole ground source heat exchanger model is validated with the experimental data of 5 different thermal response tests performed on real borehole heat exchangers in Denmark [71][72][73]. Different geometries, length and types of brine are tested (See **Table 10**). The input data are inlet flow and inlet temperature. The outlet temperature is compared between the experiment and the MATLAB-Simulink model.

	Blaavand	Glud	Ordrupgaard	VIA 12	VIA 14
Borehole depth [m]	102	100	102	103	100
Borehole diameter [m]	0,22	0,16	0,2	0,16	1,6
Pipe external diameter [m]	0,04	0,04	0,04	0,04	0,04
Pipe internal diameter [m]	0,0326	0,0326	0,0326	0,0326	0,0326
Pipe thermal conductivity [W/m.K]	0,42	0,42	0,42	0,42	0,42
Pipe spacing [m]	0,1	0,08	0,11	0,08	0,08
Undisturbed ground temperature [C]	9,3	9,5	9,8	10,23	9,59
Ground thermal conductivity [W/m.K]	2,11	1,43	1,8029	2,04	2,14
Borehole thermal resistance [m.K/W]	0,184	0,11	0,16842	0,123	0,114
Fluid type	Water	11 % IPA Sprit (Ethanol)	Water	Water	Water

Table 10: *Validation thermal response tests parameters.*

One can see on **Figure 77 – 78** that the MATLAB-Simulink vertical borehole ground source heat exchanger model fits very well the validation experimental data. The difference between the model and the experimental data is most of the time below 0.2 °C.

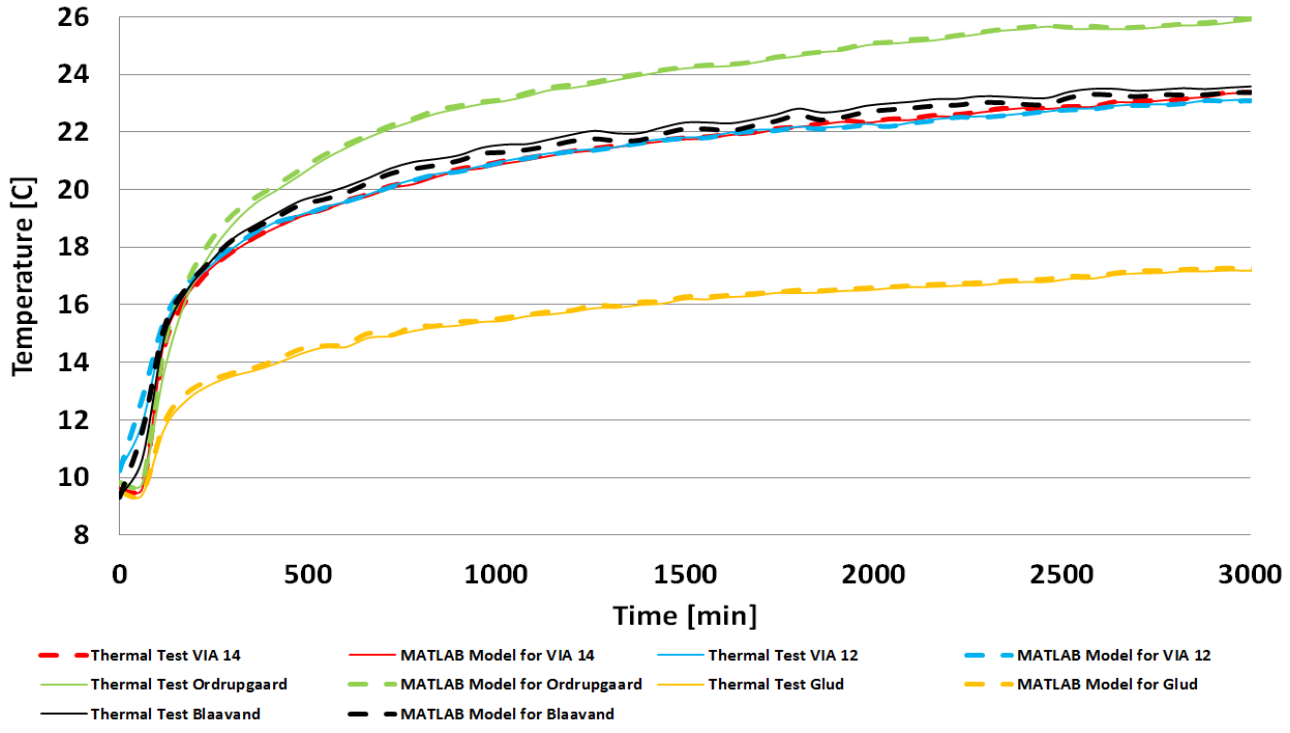

Figure 77: *Vertical borehole GSHE thermal response test temperature profiles.*

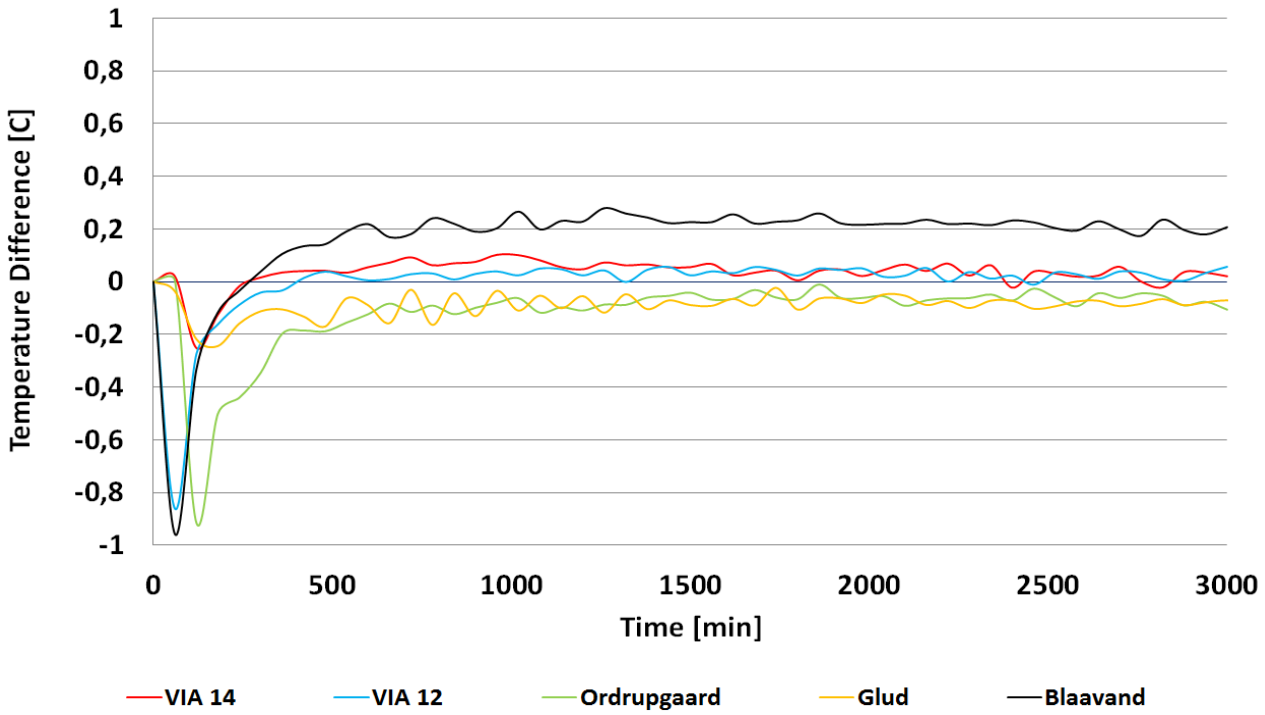

Figure 78: *Difference between MATLAB-Simulink model and validation experimental data.*

3.6. Validation of Phase Change Material Model with the COMSOL Software and the Guarded Hot Plate Apparatus Experimental Tests

First of all, the MATLAB implicit finite volume model with enthalpy formulation is tested for steady state conditions against the well-known and validated finite element method software COMSOL Multi-physics and analytical solution. The test sample is a 45 cm thick multi-layer wall made of concrete, stone wool, wood and metal. Each control volume is 1 cm thick. One can see on **Figure 79 – 80** that the MATLAB-Simulink model fits perfectly with the steady state analytical solution and the COMSOL reference model.

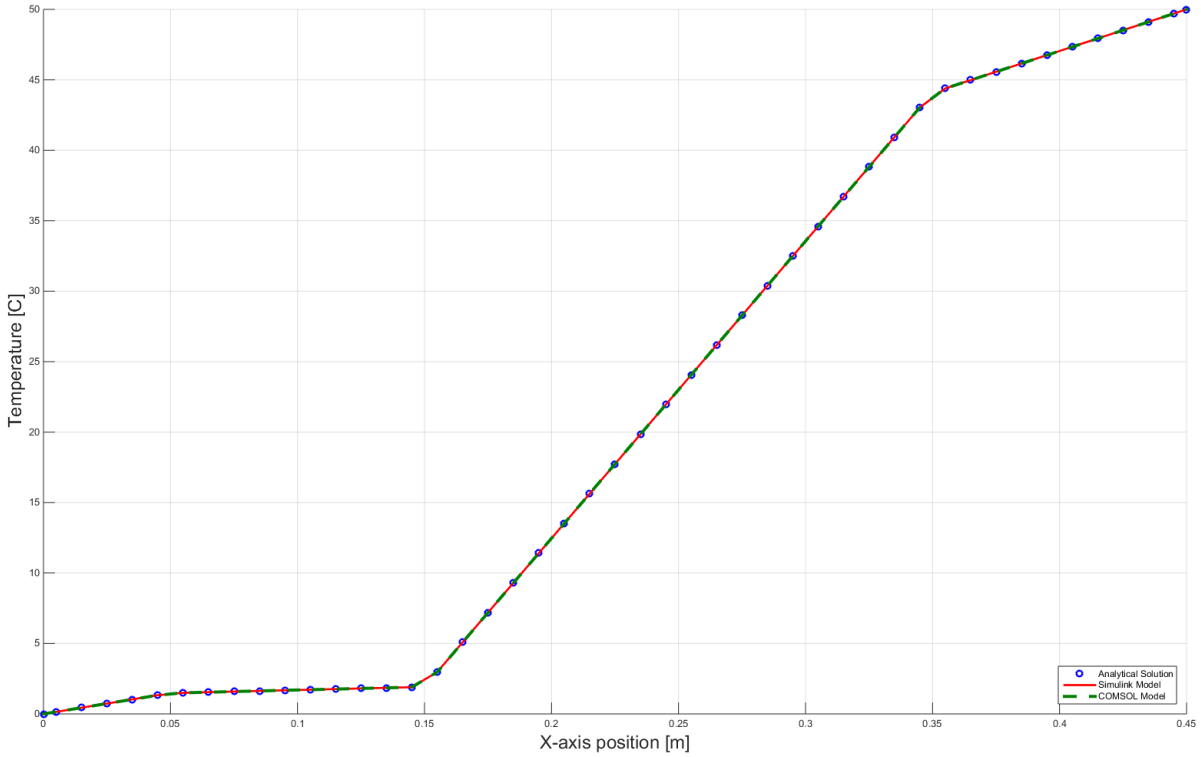

Figure 79: *Steady state multi-layer wall temperature profile.*

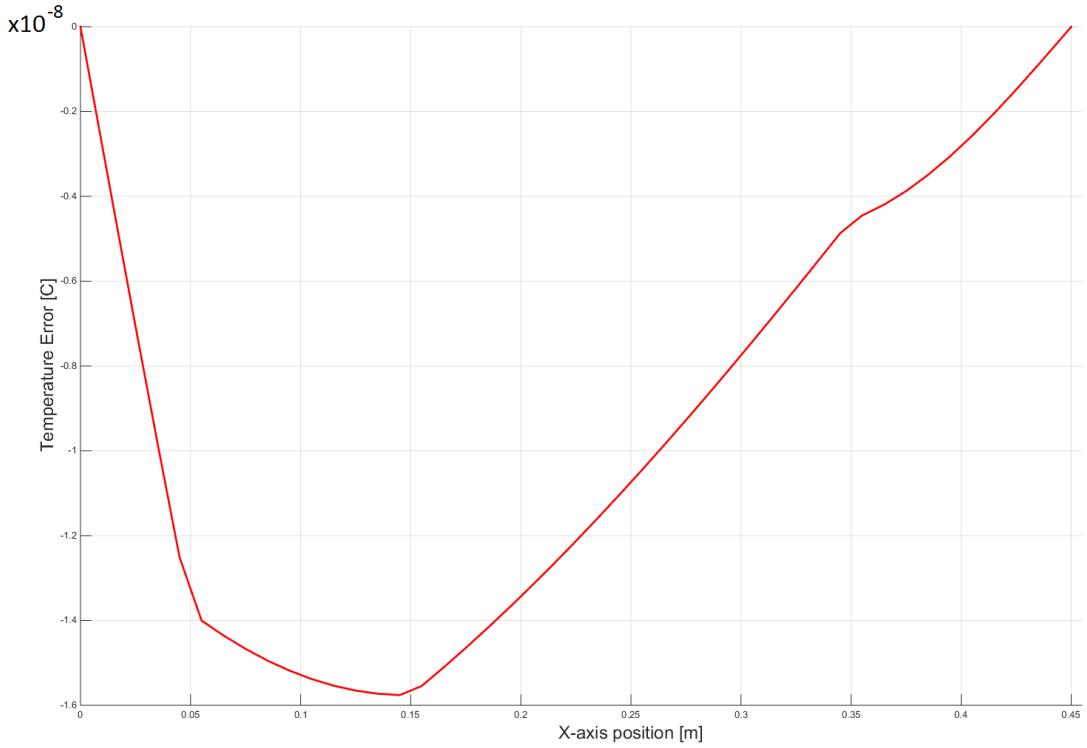

Figure 80: *Absolute temperature difference between MATLAB-Simulink model and steady state analytical solution.*

The MATLAB-Simulink model is then tested with dynamic boundary conditions against the COMSOL reference model. The surface heat transfer coefficients are kept constant while the surrounding temperatures are varying with time as sinusoidal functions. There is no phase transition in this test. One can see on **Figure 81 – 82** that the MATLAB-Simulink model fits very well to the COMSOL reference model. The temperature difference between the two models is most of the time below 0.02

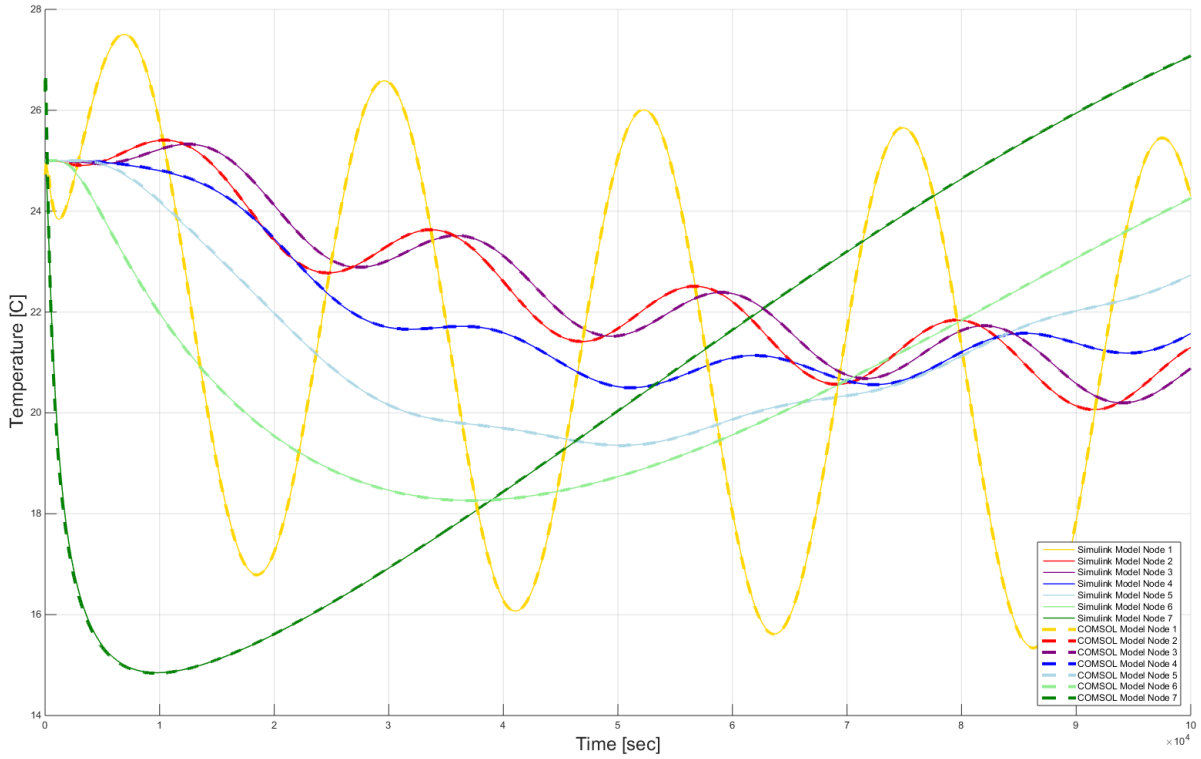

Figure 81: *Temperature of the multi-layer sample test with dynamic boundary conditions.*

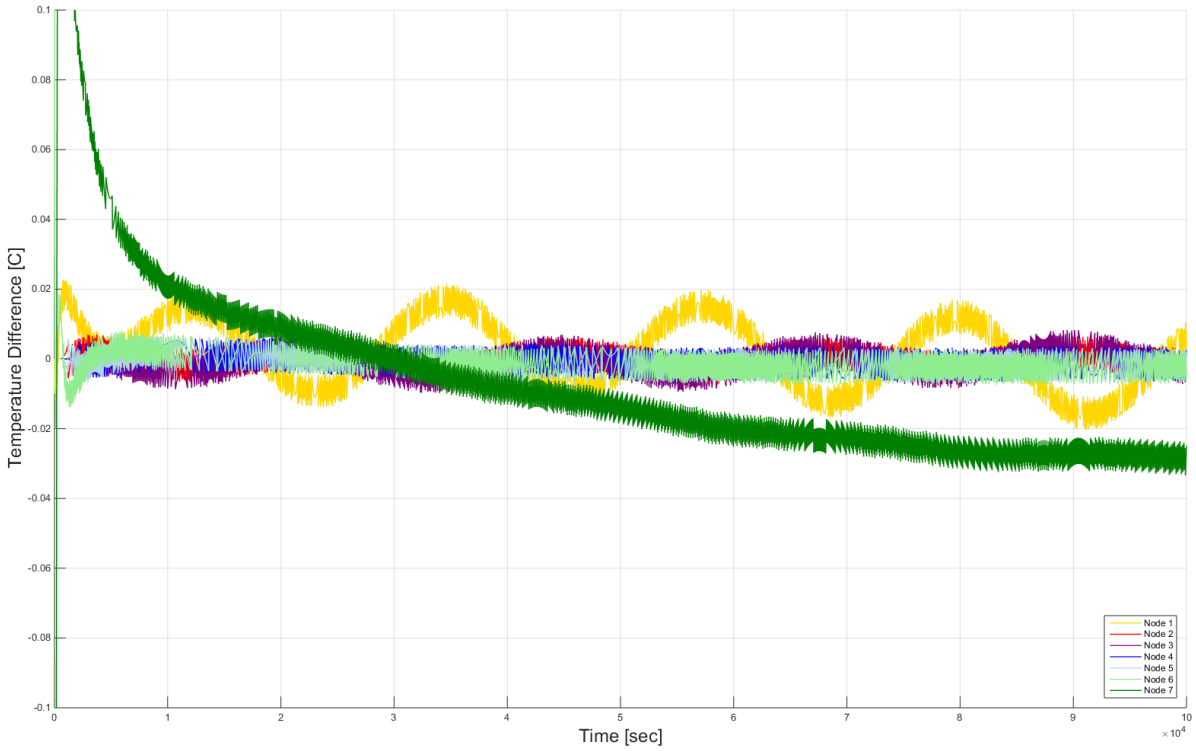

Figure 82: *Temperature difference between MATLAB-Simulink model and COMSOL reference model during the dynamic boundary conditions validation test.*

The PCM numerical model is then tested against experimental measurements performed with the hot plate apparatus in dynamic mode. 3 different PCM samples with different thickness and properties are prepared: BASF Micronal PCM paste, DuPont Energain PCM wall board and PCM plasterboard. Type K thermocouples are inserted inside the samples in order to record the temperature change in function of time. The uncertainty of the temperature measurement with the Type K Thermocouples is 0.15 °C [74].The thermal conductivity of the samples is measured with the guarded hot plate apparatus, the heat capacity is measured with a DSC and the latent heat of fusion is taken from manufacturer's documentation. The PCM samples are placed in the guarded hot plate and a temperature increase ramp is applied while recording the temperature inside the center of the sample.

One can see on **Figure 83** that the model has good agreement for the 3 different PCM samples tested with the dynamic hot plate apparatus. However, at low temperature, the model and the experimental data have some divergence. This is due to the fact that the phase transition of the organic PCMs in tested samples occurs within a certain range of temperature while the model can only account for a phase transition at a fixed temperature. Therefore, the model underestimates the apparent total heat capacity of the material at temperatures below the average phase transition temperature.

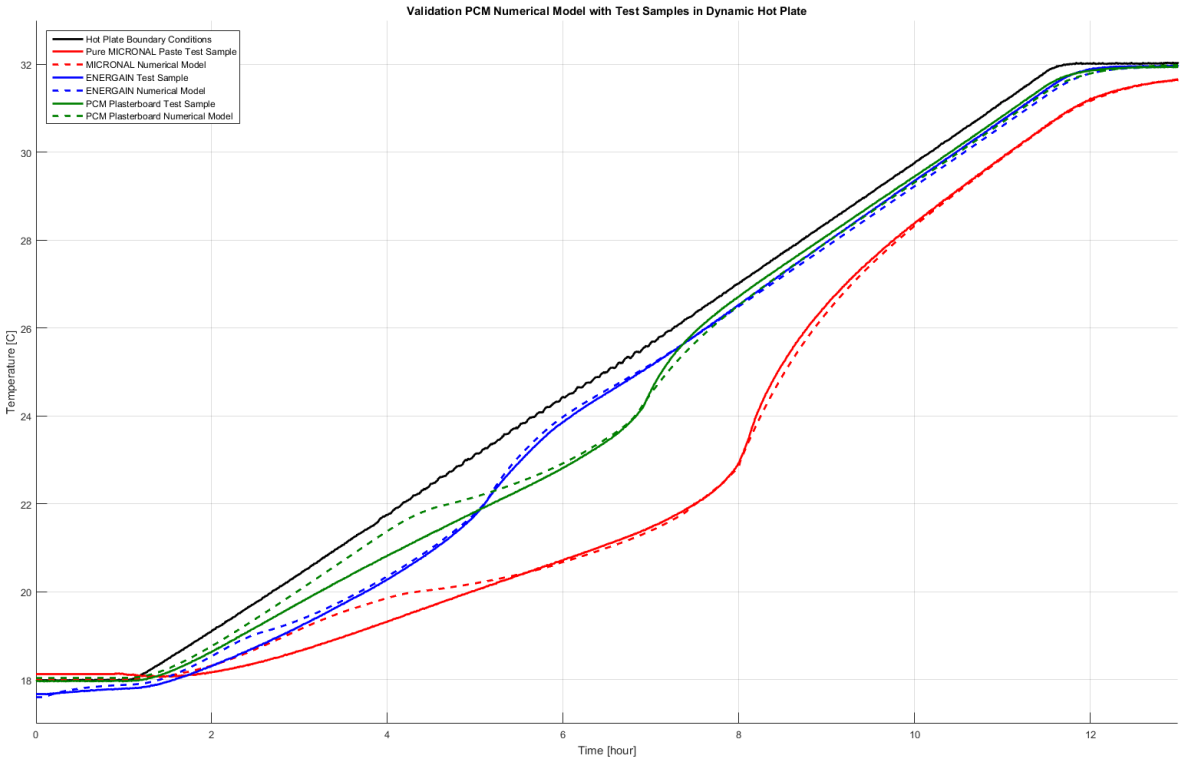

Figure 83: *Guarded hot plate validation test for PCM numerical model.*

Conclusion

This report presented in details the energy building numerical model used for the EnovHeat project, its different parameters and sub-systems. It has been demonstrated that this building model is able to simulate correctly the physics of dwellings with different levels of insulation and thermal masses, indoor content / furniture elements, phase change materials, heat pump systems with different heat sources and emitter configruations.

References

[1] H. Lund, B. Möller, B.V. Mathiesen, A. Dyrelund, The role of district heating in future renewable energy systems, Energy 35 (3) (2010) 1381-90.

[2] A. Palzer, H.M. Henning, A comprehensive model for the German electricity and heat sector in a future energy system with a dominant contribution from renewable energy technologies – Part II: Results, Renewable and Sustainable Energy Reviews 30 (2014) 1019-1034.

[3] J. Cockroft, N. Kelly, A comparative assessment of future heat and power sources for the UK domestic sector, Energy Conversion and Management 47 (2006) 2349-2360.

[4] T. Nowak, P. Westring, The European Heat Pump Association AISBL (EHPA), European heat pump market and statistics report 2015. http://www.ehpa.org/fileadmin/red/07._Market_Data/2014/EHPA_European_Heat_Pump_Market_and_Statistics_Report_2015_-_executive_Summary.pdf, 2015.

[5] C.R.H. Bahl, EnovHeat project summary: development of efficient novel magnetocaloric heat pumps, http://www.enovheat.dk/Research/ProjectSummary, 2015.

[6] H. Johra, K. Filonenko, P. Heiselberg, C. Veje, T. Lei, S. Dall'Olio, K. Engelbrecht, C. Bahl, Integration of a magnetocaloric heat pump in a low-energy residential building, Building Simulation (2017). https://doi.org/10.1007/s12273-018-0428-x

[7] J. Le Dréau, P. Heiselberg, Energy flexibility of residential buildings using short term heat storage in the thermal mass, Energy 111 (2016) 991-1002.

[8] B.V. Mathiesen, H. Lund, D. Connelly, H. Wenzel, P.A. Østergaard, B. Möller, S. Nielsen, I. Ridjan, P. Karnøe, K. Sperling, F.K. Hvelplund, Smart energy systems for coherent 100% renewable energy and transport solutions, Applied Energy 145 (2015) 139-154.

[9] H. Johra, P. Heiselberg, J. Le Dréau, Numerical Analysis of the Influence of Thermal Mass, Phase Change Materials and Furniture/Indoor Content on Building Energy Flexibility, the 15th International Conference of IBPSA, San Francisco, 2017. http://www.ibpsa.org/proceedings/BS2017/BS2017_012.pdf

[10] The Danish Ministry of Economic, Business Affairs Enterprise, and Construction Authority, Building Regulations. http://bygningsreglementet.dk/file/155699/BR10_ENGLISH.pdf, 2010.

[11] Larsen T.S, Brunsgaard C, Komfort Husene: erfaringer, viden og inspiration. Saint-Gobain Isover a/s; 2010.

[12] CSTB, French Building Energy and Thermal Regulation, 2012.

[13] ClimateMaster, Tranquility Water-to-Water (TMW) Series Submittal Data Model TMW036 – 340 50Hz - HFC-410A. http://lenergy.hu/dokuk/termekek/103/98caovp2.pdf, 2012.

[14] Grundfos Product Center, GRUNDFOS Data Booklet – ALPHA2 L 15-40 130 – 95047560, https://product-selection.grundfos.com/product-detail.product-detail.html?productnumber=95047560&qcid=323188257, 2015.

[15] Grundfos Product Center, GRUNDFOS Data Booklet – CR1-9 A-FGJ-A-E-HQQE 3x230/400 50Hz – Grundfos Pump 96478872, http://product-selection.grundfos.com/product-detail.product-detail.html?lang=ENU&productnumber=96478872&productrange=gma&qcid=233560216, 2013.

[16] European Committee for Standardization, EN 1264:2011, - Water based surface embedded heating and cooling systems, 2011.

[17] European Committee for Standardization, EN 15377:2007 - Heating systems in buildings – Design of embedded water based surface heating and cooling system, 2007.

[18] International Organization for Standardization, ISO 11855:2012 - Building environment design – Design, dimensioning, installation and control of embedded radiant heating and cooling systems, 2012.

[19] Uponor GmbH, Heating and cooling solutions - Technical guidelines, 2008.

[20] Uponor GmbH, Installation guide for underfloor heating systems - Technical information, 2013.

[21] Energiteknologisk Udviklings og Demonstrations Program (EUDP), GeoEnergi project, http://geoenergi.org/, 2014.

[22] EuroGeoSurveys, ThermoMap project, http://www.eurogeosurveys.org/projects/thermomap/, 2010.

[23] Geological Survey of Denmark and Greenland, GEUS, http://www.geus.dk/DK/Sider/default.aspx

[24] C. Ditlefsen, I. Sørensen, M. Slott, M. Hansen, Geological Survey of Denmark and Greenland, VIA University College, Estimating thermal conductivity from lithological descriptions – a new web-based tool for planning of ground-source heating and cooling, 2013.

[25] D. Bertermann (FAU), C. Bialas (FAU), M. Psyk (REHAU), L. Morper-Busch (PLUS), ThermlMap MapViewer Technical Guidelines, 2011.

[26] Verlag des Vereins Deutscher Ingenieure, VDI 4640: 2001, Thermal use of the underground - Ground source heat pump systems, 2001.

[27] Uponor GmbH, Ground Energy Technical Information, 2012.

[28] RETScreen International, Minister of Natural Resources Canada, Ground-Source Heat Pump Project Analysis, 2005.
[29] H. Johra, P. Heiselberg, Influence of internal thermal mass on the indoor thermal dynamics and integration of phase change materials in furniture for building energy storage: A review, Renewable and Sustainable Energy Reviews 69 (2017) 19-32. https://doi.org/10.1016/j.rser.2016.11.145
[30] DuPont, Energain® - Technical Datasheet.
[31] F. Kuznik,J. Virgone, J. Noel, Optimization of a phase change material wallboard for building use, Applied Thermal Engineering 28 (2008) 1291–1298.
[32] International Organization for Standardization, ISO 13786:2007 - Thermal performance of building components – Dynamic thermal characteristics – Calculation methods, 2007.
[33] P. Ma,L.S. Wang, Effective heat capacity of interior planar thermal mass (iPTM) subject to periodic heating and cooling, Energy and Buildings 47 (2012) 44-52.
[34] A.S. Kalagasidis, C. Rode, M. Woloszyn, HAM-Tools – a whole building simulation tool in Annex 41, Proceedings of the IEA ECBCS Annex 41 Closing Seminar, 2008.
[35] Danish Building Research Institute – Sbi, BSim software - User's Guide – tsbi5, 2013.
[36] P.G. Wang, M. Scharling, K.P. Nielsen, K.B. Wittchen, C. Kern-Hansen, DMI Technical Report 13-19: 2001-2010 Danish Design Reference Year – Reference Climate Dataset for Technical Dimensioning in Building, Construction and other Sectors, 2013.
[37] R.L. Jensen, J. Nørgaard, O. Daniels, R.O. Justesen, Person- og forbrugsprofiler: bygningsintegreret energiforsyning, DCE Technical Reports 69, http://vbn.aau.dk/da/publications/person-og-forbrugsprofiler(8c95574a-5bc0-4d41-9363-19932b7d9394).html, 2011.
[38] S. Adams, M. Holmes, Determining time constants for heating and cooling coils, Building Services Research & Information Association, UK, 1977.
[39] B. Glück, Strahlungsheizung – Theorie und Praxis, Verlag C.F Müller, Karlsruhe, 1982.
[40] B. Glück, Wärmeübertragung, Wärmeabgabe von Raumheizflächen und Rohren, VED Verlag für Bauwesen, Berlin, 1989.
[41] M. Koschenz, B. Lehmann, Thermoaktive Bauteilsysteme, EMPA, Dübendorf (CH), 2000.
[42] B. Lehmann, V. Dorer, M. Koschenz, Application range of thermally activated building systems TABS, Energy and Buildings 39 (2007) 593-598.
[43] M. Scarpa, K. Grau, B.W. Olesen, Development and validation of a versatile method for the calculation of heat transfer in water-based radiant systems, 11th International IBPSA Conference, Glasgow, Scotland, July 27-30, 2009.
[44] Energy Plus Engineering Reference Manual.
[45] University of Wisconsin-Madison Solar Energy Laboratory, TRANSSOLAR Energietechnik GmbH, CSTB, TESS, Type 31: Pipe Or Duct, in: TRNSYS 17 - Mathematical Reference, 2012, pp. 186-188.
[46] H.J.G. Diersch, D. Bauer, W. Heidemann, W. Rühaak, P. Schätzl, Finite element modeling of borehole heat exchanger systems - Part 1.Fundamentals, Computers & Geosciences 37 (2011) 1122-1135.
[47] G.S. Kell, Density, thermal expansivity, and compressibility of liquid water from 0 to 150 C: correlations and tables for atmospheric pressure and saturation reviewed and expressed on 1968 temperature scale", J Chem Eng Data 1975 (20) 97-105.
[48] J.B. Patterson, E.C. Morris, Measurement of absolute water density, 1–40 C, Metrologia 31 (1994) 277-288.
[49] M. Tanaka, G. Girard, R. Davis, A. Peuto, N. Bignell, Recommended table for the density of water between 0 and 40 C based on recent experimental reports, Metrologia 38 (2001) 301-309.
[50] Engineering tool box, http://www.engineeringtoolbox.com/ethylene-glycol-d_146.html
[51] J.V. Sengers, J.T.R. Watson, Improved international formulations for he viscosity and thermal conductivity of water substance, J. Phys. Chem. Ref. Data, 15 (1986) 1291.
[52] American Institute of Physics and American Chemical Society (IUPAC), Standard Reference Data for the Thermal Conductivity of Water, 1995.
[53] M. Conde Engineering, Thermophysical properties of brines – Models, 2011.
[54] K.N. Marsh, Recommended Reference Materials for the Realization of Physicochemical Properties, Blackwell Scientific Publications, Oxford, 1987.
[55] Incropera, DeWitt, Bergman, Lavine, Fundamentals of Heat and Mass Transfer", seventh edition.
[56] Lange's Handbook of Chemistry, 10th ed.
[57] DOW Chemical Company, Guide to Glycols (Propylene Glycols).
[58] DOW Chemical Company, Engineering and Operating Guide for DOWFROST, Inhibited Propylene Glycol-based Heat Transfer Fluid.
[59] DOW Chemical Company, Engineering and Operating Guide for DOWTHERM, Inhibited Ethylene Glycol-based Heat Transfer Fluid.
[60] MEGlobal Company, Ethylene Glycol Product Guide.
[61] Dow Chemical Database, 2001.
[62] ASHRAE Handbook Fundamentals, 2005.
[63] Freezing points of methanol solutions, novosolution.ca

[64] Å. Melinder, Thermophysical properties of aqueous solutions used as secondary working fluids, PhD Thesis, Royal Institute of Technology, Stockholm, Sweden, 2007.
[65] GeoPro. Inc, Borehole Heat Exchanger Head Loss Calculation Excel Sheet.
[66] G. Angrisani, M. Canelli, C. Roselli, M. Sasso, Calibration and validation of a thermal energy storage model: influence on simulation results, Applied Thermal Engineering 67 (2014) 190-200.
[67] R. Prapainop, K. Maneeratana, Simulation of ice formation by the finite volume method, Songklanakarin J. Sci. Technol., 26(1) (2004) 55-70.
[68] Verma P, Varun, Singal S.K. Review of mathematical modeling on latent heat thermal energy storage systems using phase-change material. Renewable and Sustainable Energy Reviews 12 (2008) 999-1031.
[69] IEA-EBC Annex 43 Project, http://www.ecbcs.org/annexes/annex43.htm
[70] ANSI/ASHRAE Standard 140-2011. Standard method of test for the evaluation of building energy analysis computer programs, 2011.
[71] S.E. Poulsen, M. Alberdi-Pagola, Thermal Response Test and temperature profiles at Kongestien 45, Virum (Denmark), Research output report, http://vbn.aau.dk/en/publications/thermal-response-test-and-temperature-profiles-at-kongestien-45-virum-denmark(243a4fef-e879-47db-9246-99b3cb487e8a).html, 2015.
[72] S.E. Poulsen, M. Alberdi-Pagola, Thermal Response Test at Ordrupgaard Museum, Ordrupgaard (Denmark), http://vbn.aau.dk/en/publications/thermal-response-test-at-ordrupgaard-museum-ordrupgaard-denmark(490330c0-790e-4a38-9c37-43c1bd85ec7a).html, 2015.
[73] S.E. Poulsen, M. Alberdi-Pagola, Interpretation of ongoing thermal response tests of vertical (BHE) borehole heat exchangers with predictive uncertainty based stopping criterion, Energy 88 (2015) 157-167.
https://doi.org/10.1016/j.energy.2015.03.133
[74] J. Le Dreau, P. Heiselberg, R.L. Jensen, Experimental data from a full-scale facility investigating radiant and convective terminals: Uncertainty and sensitivity analysis, Description of the experimental data, DCE Technical Reports 168, http://vbn.aau.dk/da/publications/experimental-data-from-a-fullscale-facility-investigating-radiant-and-convective-terminals(1ce46b33-cfa8-4979-b112-cd9ab487f9c7).html, 2014.

ISSN 1901-726X

DCE Technical Report No. 238